ORNL-3006
UC-80 - Reactors-General

HFIR PRELIMINARY PHYSICS REPORT

R. D. Cheverton

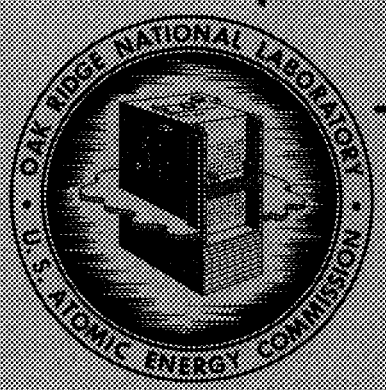

OAK RIDGE NATIONAL LABORATORY
operated by
UNION CARBIDE CORPORATION
for the
U.S. ATOMIC ENERGY COMMISSION

Printed in USA. Price $2.50. Available from the
Office of Technical Services
Department of Commerce
Washington 25, D.C.

ORNL-3006
UC-80 - Reactors-General
TID-4500 (15th ed.)

Contract No. W-7405-eng-26

REACTOR EXPERIMENTAL ENGINEERING DIVISION

HFIR PRELIMINARY PHYSICS REPORT

R. D. Cheverton

DATE ISSUED

OCT 4 1960

OAK RIDGE NATIONAL LABORATORY
Oak Ridge, Tennessee
operated by
UNION CARBIDE CORPORATION
for the
U. S. ATOMIC ENERGY COMMISSION

ABSTRACT

High Flux Isotope Reactor physics studies were conducted to establish a core design that would permit the attainment of about 5×10^{15} neutrons/cm^2-sec unperturbed thermal flux at a power level of 100 Mw. The proposed reactor is a cylindrical flux-trap reactor, having a light-water island surrounded by a fuel annulus containing fully enriched uranium, water, and aluminum. A vertical-plate control system separates the fuel region from the water-cooled beryllium side reflector. The island diameter is 14 cm, the fuel-annulus outer diameter 38 cm, and the active core length 45.7 cm. It is estimated that this core, with enough fuel for 10 days of operation at 100 Mw, will produce a maximum unperturbed thermal flux of 6.6×10^{15} neutrons/cm^2-sec and an average thermal flux of 3.7×10^{15} in a 200-g sample of Pu-242. The corresponding maximum heat flux was estimated to be 1.6×10^6 Btu/hr-ft^2 for a fuel element containing 0.050-in.-thick plates and 0.050-in.-thick coolant channels.

CONTENTS

LIST OF TABLES

LIST OF FIGURES

ACKNOWLEDGMENTS

The studies reported herein have extended over a period of nearly two years, during which time many people have been involved to varying degrees in the design and analysis of the HFIR and thus to some extent in the physics studies. The author is particularly grateful for the many helpful suggestions and guidance provided by P. R. Kasten, J. A. Lane, and C. E. Winters.

In the process of conducting the HFIR studies, hundreds of machine calculations were made. Those responsible for expediting these calculations were Marjorie Lietzke, T. B. Fowler, and C. D. Griffies. The author also wishes to express graditude to N. Hilvety and D. W. Vroom who helped extensively in preparing problems for machine calculation and in reducing much of the output data.

HFIR PRELIMINARY PHYSICS REPORT

R. D. Cheverton

SUMMARY

Specifications for the High Flux Isotope Reactor (HFIR) call for a maximum unperturbed thermal-neutron flux of 5×10^{15} neutrons/cm^2-sec at a nominal operating power level of 100 Mw. The reactor proposed to meet these specifications is a cylindrical flux-trap type consisting of a light-water island that is surrounded by an annular fuel region containing fully enriched uranium, aluminum fuel plates, and light-water coolant and moderator. A light-water-cooled beryllium side reflector is separated from the fuel region by an annular control region.

The purpose of the preliminary physics studies was to determine a combination of reactor parameters that would result in the attainment of the desired neutron flux level without exceeding the permissible heat flux. Parameters considered in the studies were island diameter, length and thickness of the fuel annulus, fuel loading, radial distribution of fuel in the fuel annulus, burnable poison concentration in the fuel, control surface effects, metal-to-water ratio, weight and size of a Pu-242 feed-material target to be inserted in the water island, and a few others. The studies also included fuel-cycle analysis, investigation of xenon instability, and the calculation of reactivity coefficients and neutron lifetime.

The results of the studies indicate that a core having a 14-cm-diameter island, a fuel annulus 45.7 cm long and 12 cm thick containing radially graded fuel and burnable poison, and containing enough fuel for a 10-day cycle can achieve a maximum thermal flux in the island of 6.6×10^{15} neutrons/cm^2-sec at a power level of 100 Mw. The corresponding maximum heat flux is estimated to be 1.6×10^6 Btu/hr-ft^2 for a fuel element containing 0.050-in.-thick coolant channels and 0.050-in.-thick fuel plates. During the fuel cycle the maximum power density is essentially constant, while the thermal flux in the island decreases by about 2%.

For several calculations a quantity of Pu-242, which is to be irradiated in the HFIR for the purpose of producing transplutonium isotopes, was included in the island region in order to determine the weight of Pu-242 and the size of the target that would result in the maximum production of Cf-252 in a one-year period. Using a homogenized target consisting of water, aluminum matrix and cladding material, and plutonium, the optimum weight and diameter (for a core-length target) were determined to be about 300 g and 10.6 cm, respectively. The corresponding volume-averaged thermal flux and the maximum heat generation rate in the target were 3.3×10^{15} neutrons/cm^2-sec and 740 kw, respectively. A 200-g target, having a corresponding flux of 3.7×10^{15} and a heat generation rate of 540 kw, is tentatively being proposed for the HFIR.

The control system selected for the HFIR is a mechanical system consisting of two thin (approximately 1 cm thick) concentric cylinders located in the annular space between the fuel annulus and side reflector. Both cylinders are three core lengths long, being made up of three equal-length vertical sections: a "black" section for emergency shutdown, a "gray" region for shim and regulation, and a "white" region. As a fuel cycle progresses, the control cylinders are withdrawn in opposite directions so as to maintain

symmetry about the longitudinal axis and the horizontal midplane. At no time during the fuel cycle does this method of control result in excessive power-density peaking.

Temperature coefficients of reactivity were calculated for the composite core, assuming all regions to be at the same temperature, and also for the water island and fuel region separately. The calculational and limited experimental results indicate that below about 110°F the over-all coefficient (all regions at the same temperature) is positive with a maximum positive reactivity addition of about 0.2% when the temperature is increased above 70°F. The calculated room-temperature coefficients for the island and fuel region separately are $+1.0 \times 10^{-4}$ and -0.8×10^{-4} $\Delta k/k/°F$, respectively. At an average operating temperature of about 150°F, the over-all coefficient is approximately -1.0×10^{-4} $\Delta k/k/°F$ at the beginning of the fuel cycle and -0.2×10^{-4} $\Delta k/k/°F$ near the end of the cycle.

Void coefficients of reactivity were calculated for the composite core, assuming all regions to contain the same void fraction, and for the all-water island region and the fuel region separately. Void coefficients were also calculated for cylindrical voids in the center of the island. For the case of a cylindrical void in the island equal to the active length of the core and reflected on the ends by water the coefficient was positive up to a cylindrical void diameter of about 9 cm in a 14-cm-diameter island. The corresponding maximum change in k was about +1.2%. In the case of uniform voids the over-all and fuel-region coefficients were negative, while the all-water island coefficient was positive up to 45% voids with a maximum positive reactivity addition of 2.5%.

The prompt-neutron lifetime was calculated for the beginning of the fuel cycle with the shim control plates fully inserted, and for the end of the fuel cycle with the shim control plates completely withdrawn. The lifetimes were 50 and 100 μsec, respectively.

Xenon instability was investigated by both digital and analogue computer techniques. Step changes in reactivity up to 2% were introduced in the form of local perturbations, and these did not cause significant oscillations in power distribution.

Figure 1 is a schematic representation of the HFIR showing typical flux distributions. Pertinent characteristics of the core are listed in Table 1.

Table 1. HFIR Characteristics

Nuclear	
Reactor power, Mw	100
Neutron fluxes, neutrons/cm^2-sec	
Maximum unperturbed thermal flux in the island	6.6×10^{15}
Maximum total fast flux in fuel region	5.7×10^{15}
Maximum unperturbed thermal flux in beryllium side reflector	
Beginning of cycle	1.0×10^{15}
End of cycle	2.0×10^{15}

Table 1. (Continued)

Average thermal flux in island target (200 g of Pu-242)		3.7×10^{15}
Temperature coefficient of reactivity (no target in island), $\Delta k/k/°F$		
Average core temperature, °F	70	150
Beginning of cycle		
Water island	$+1.0 \times 10^{-4}$	$+1.1 \times 10^{-4}$
Fuel annulus	-0.8×10^{-4}	-2.0×10^{-4}
Over-all	$\sim +0.8 \times 10^{-4}$	-1.0×10^{-4}
End of cycle		
Over-all	-	-0.3×10^{-4}
Void coefficient of reactivity (no target in island; voids confined to volume within active core length)		
Cylindrical void in island, $(\Delta k/k)/(R_V/R_I)$	$< +0.002$ at $R_V/R_I = 0$	
	Max $\Delta k/k = +0.012$ at $R_V/R_I = 0.6$	
Uniform voids (beginning of cycle), $(\Delta k/k)/(\Delta \rho/\rho)$		
Island	$+0.08$ at $\Delta \rho/\rho = 0$	
	Max $\Delta k/k = +0.025$ at $\Delta \rho/\rho = 0.45$	
Fuel	-0.4 at $\Delta \rho/\rho = 0$	
Over-all	-0.3 at $\Delta \rho/\rho = 0$	
Prompt-neutron lifetime, μsec		
Beginning of cycle		50
End of cycle		100
Length of fuel cycle, days		10
Heat Removal		
Fuel-plate thickness, in.	0.040	0.050
Power density (97.5 Mw in core), Mw/liter		
Average	2.18	2.18
Maximum	3.90	3.90
Heat flux (97.5 Mw removed from plates), $Btu/hr\text{-}ft^2$		
Average	7.89×10^5	8.77×10^5
Maximum	1.41×10^6	1.57×10^6
Ratio of maximum-to-average power density	1.79	1.79

Table 1. (Continued)

Burnout heat flux, Btu/hr-ft^2		
Nominal	3.5×10^6	3.5×10^6
Minimum	3.0×10^6	3.0×10^6
Burnout-heat-flux reduction factor	0.86	0.86
Temperatures, °F		
Coolant inlet	120	120
Coolant outlet	184	192
Maximum surface	343	365
Drop across aluminum oxide film	47	52
Maximum metal	399	430
Coolant velocity, ft/sec	40	40
Pressure drop across core, psi	67	67
System pressure at pump discharge, psi	500	500
Core Design and Size		
Type of core	Cylindrical annulus, flux trap	
Type of fuel elements	Aluminum plates, involute geometry	
Fuel-plate thickness, in.	0.040 or 0.050	
Coolant-channel thickness, in.	0.050	
Length of fuel plates, in.	24	
Length of active core, in.	18	
Inside diameter of fuel annulus, in.	5.5	
Outside diameter of fuel annulus, in.	14.9	
Volume in fuel annulus (active portion), liters	44.8	
Outside diameter of side reflector, in.	41	
Core Materials		
Fuel	Enriched uranium (~90%)	
Fuel loading, kg of U^{235}	~6	
Coolant	H_2O	
Island moderator-reflector	H_2O	
Side reflector	Be + 5% H_2O	

PREFACE TABLE FOR FIG. 1

Code calculation, GNU
Cross-section set, GNU 34 groups (ORNL revised set)
Thermal temperature, 80°C

Active core length, 45.72 cm
Axial buckling, 0.002591 cm^{-2}
k_{eff}, 0.992

Region No.	Outer Radius (cm)	Composition	$N^{25} \times 10^5$ (atom/barn-cm)	$N^{B} \times 10^5$ (atom/barn-cm)
1	7	H_2O		
2	7.5	U-235 + Al + H_2O, M/W = 1	15	
3	8		18.03	
4	8.5		21.60	
5	9		25.53	
6	9.5		29.91	
7	10		34.43	
8	11		39.12	
9	12		47.75	
10	13		54.50	
11	15		60.00	
12	16		57.72	
13	17		50.88	
14	17.5		46.02	
15	18		41.13	
16	18.5		35.97	
17	19		31.13	
18	21	Be + 5% H_2O + Exp + B		200
19	51	Be + 5% H_2O + Exp		

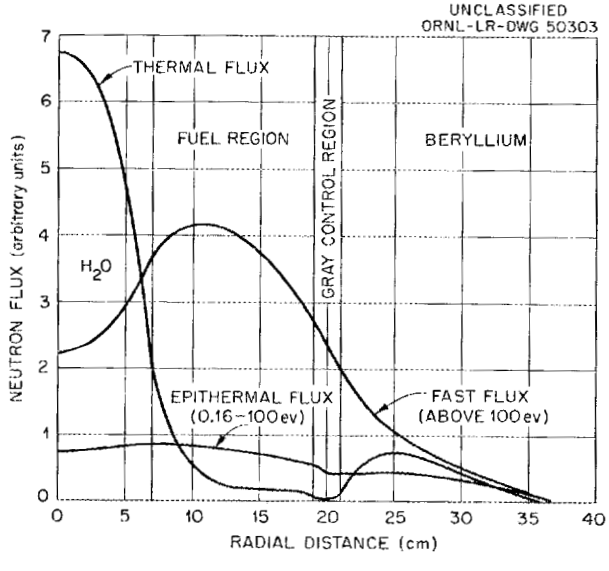

Fig. 1. Radial Flux Distribution at Horizontal Midplane of Clean HFIR Core.

INTRODUCTION

The primary purpose of the High Flux Isotope Reactor (HFIR) is to produce milligram quantities of americium, curium, berkelium, and californium by 1965, the quantities and date being consistent with projected needs for basic research. Considering the time required for design and construction of the reactor, the time available for irradiation of the feed material and the subsequent production of the transplutonium isotopes is about one year. A secondary purpose of the HFIR is to produce an unperturbed thermal-neutron flux of about 5×10^{15} neutrons/cm^2-sec that can be used for irradiation and production of other special isotopes.

The possible feed materials to be used for the production of the transplutonium elements are Pu-242, americium, and curium, their use depending on how much of each one is available and what end product is desired. For these studies Pu-242 was specified as the feed material and Cf-252 as the desired end product.* (Californium is probably the highest-atomic-number element and Cf-252 its heaviest isotope that can be produced in significant quantity in reactors operating at flux levels less than 10^{17} nv because of the very short half lives of the heavier nuclides.) As shown by the isotope chain in Fig. 2, ten successive neutron captures are required to transmute Pu-242 to Cf-252, indicating that for a specified irradiation period Cf-252 production has a strong dependence on thermal flux. Solution of the isotope equations indicates that the total production for a one-year period is proportional to about the third power of the thermal flux for flux levels between 1×10^{15} and 5×10^{15} neutrons/cm^2-sec; and at a flux level of 3×10^{15} about 30 mg of Cf-252 would be produced in a one-year period for each 100 g of Pu-242 feed material. Assuming that a 100-g quantity of feed material

*The results of the parameter studies reported herein indicate that the basic optimum core design would not be significantly different with different heavy-isotope feed materials yielding the desired end products.

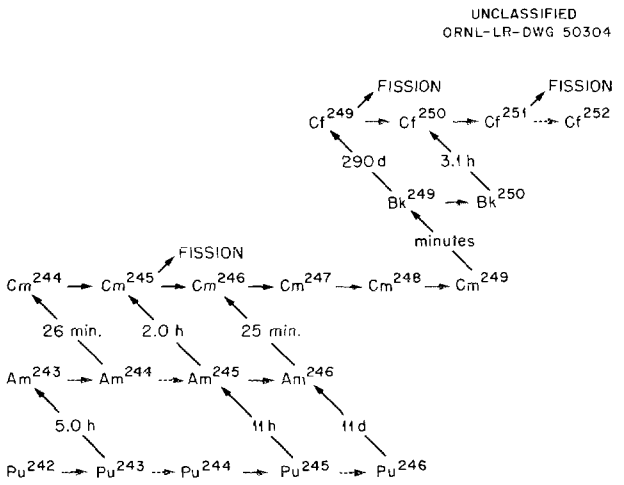

Fig. 2. Reaction Paths in the Production of Cf^{252} from Pu^{242}.

would depress the thermal flux by no more than about 40%, it was concluded that a maximum unperturbed thermal flux of 5×10^{15} would be adequate for the HFIR.

The HFIR requirement of high thermal flux but small irradiation space in the high-flux region (by comparison to general research and materials testing reactors) suggested the use of a flux-trap-type reactor which provides a high thermal flux in a central moderator-reflector region outside of the fuel region. A review of previous flux-trap core designs[1] indicated that a maximum thermal flux per unit of power equal to about 2.5×10^{13} neutrons/cm^2-sec-Mw could be achieved in a cylindrical D_2O flux-trap reactor;[2,3,4] the same type of reactor, containing H_2O instead of D_2O in the island, could produce a maximum thermal flux of about 5×10^{13} neutrons/cm^2-sec-Mw.[5,6] Corresponding flux values for the Materials Testing Reactor (MTR), Engineering Test Reactor (ETR), and Oak Ridge Research Reactor (ORR) are 1.25×10^{13}, 0.40×10^{13}, and 2.0×10^{13}, respectively. A further comparison between flux-trap peaking and side-reflector peaking was made in the course of the HFIR studies (refer to Appendix 2). The results indicated that for the same power and average power density a flux-trap reactor could produce a thermal flux in a light-water island three times greater than in the beryllium side reflector of a similar core without the central water island. Thus, in the interest of minimizing capital and operating costs, it was concluded that the HFIR should be a light-water-island, flux-trap-type reactor.

Cylindrical geometry as opposed to rectangular geometry was selected for the HFIR on the basis of experimental work done by Feinberg,[6] which indicated that the cylindrical geometry would result in a 35% lower maximum power density for the same maximum neutron flux and total power. For the fuel annulus, aluminum fuel plates and light-water coolant were selected in keeping with the desire to minimize costs. Light-water-cooled beryllium was selected for the side reflector to eliminate the need for D_2O anywhere in the reactor. (Light water alone is not a satisfactory side reflector because of its comparatively large absorption cross section.) As indicated by Fowler,[7] the use of H_2O instead of D_2O as the coolant-moderator in a fuel annulus containing a solution fuel results in a peak thermal-flux loss of about 14%, when the comparison is made on the basis of equal power densities. This loss, which would be even less with about 50% of the fuel annulus volume occupied with cladding material, was considered insufficient to warrant the use of D_2O and the additional separate cooling system.

The previous flux-trap-reactor design studies referred to above indicated that a power level of 100 Mw would be required to achieve the desired thermal-flux level of 5×10^{15} neutrons/cm^2-sec. Since the estimated cost of such a reactor was consistent with the amount of funds expected to be available, 100 Mw was specified as the maximum normal operating power level for the HFIR.

With this much of the HFIR design tentatively specified, the preliminary physics studies reported herein were conducted to determine a suitable combination of dimensions and materials that would result in satisfactory values of neutron flux and heat flux. The neutron fluxes of greatest interest were the maximum unperturbed thermal flux in the water island, ϕ_m, and the volume-averaged thermal flux, ϕ_E, in the homogenized heavy-isotope target located in the center of the water island. The first part of the parameter study was concerned with determining the optimum diameter of the water island. Once this was done, the length and thickness of the fuel annulus were adjusted to obtain the minimum power density for given values of maximum thermal flux and total reactor power. (These calculations were made with and without the plutonium feed material in the central experimental region.) On the basis of these studies a typical HFIR core design was selected for further detailed analysis. Some of the parameters considered in the detailed analysis were radial and axial power distribution, control-surface configurations, fuel loading, burnable-poison concentrations, metal-to-water ratio, plutonium feed-material weight, and size of plutonium target.

The HFIR studies also included the analysis of different types of control systems in order to determine their reactivity worth and effect on maximum power density. After the control scheme was selected, fuel-cycle-time calculations were made to determine the core life for a particular loading and to determine how neutron flux and maximum power density varied with time.

Calculations were made to determine the temperature and void coefficients of reactivity and the prompt neutron lifetime. A study was also made of xenon instability.

In the process of making the numerous HFIR calculations, several simplifying assumptions were made regarding the island and side reflector, targets, and experiments. Assuming that the beryllium side-reflector rabbit tubes, beam holes, and associated experiments would represent about -2% in reactivity, an approximately equivalent amount of thermal absorber (absorption cross section of 0.002 cm^{-1}) was added to the beryllium cross section for all calculations. For the island region it was necessary to know how production, cross section, and heat generation varied with neutron flux, time, and type of feed material in order to include the heavy-isotope-bearing target in the reactor study. The results of studies made by Claiborne,[8,9,10] Ergen,[11] and Chetham-Strode[12] indicated that heavy-isotope experiments could be adequately represented by considering only thermal irradiation of Pu-242, having Cf-252 as a final product. Claiborne's estimate of the thermal cross section of the heavy-isotope feed material as a function of thermal-neutron exposure (assuming constant flux level) was used to obtain time-averaged and flux-time-product averaged cross sections. (The time-averaged cross sections were somewhat dependent on the absolute flux level, whereas the cross sections averaged over products of flux and time were essentially independent of flux. Actually, the differences in the two types of cross sections for the range of exposure times and fluxes considered were small enough to be considered negligible. Therefore only one value of the feed-material cross section was used in the parameter studies.)

Another simplifying condition imposed on many of the parametric calculations was the omission of control surfaces. Most of the cores were compared on the basis of $k_{eff} = 1.20$ with the core clean and at 80°C. (This included enough reactivity for a proposed fuel cycle of about ten days.) After a typical core design was selected, the effects of control surfaces and fuel burnup were considered.

It should be emphasized that the studies reported herein are of a preliminary nature, having been made to demonstrate the feasibility of the HFIR and to establish a typical core design. The majority of the calculations were made using two-group, one-dimensional, multiregion, diffusion-theory reactor codes in order to reduce to practical proportions the time and money required for the very extensive parameter study that was undertaken. At various times the results for particular cases were checked with more sophisticated methods such as two-group, two-dimensional, multiregion, diffusion theory; thirty-four-group, one-dimensional, multiregion, diffusion theory employing the Selengut-Goertzel term for neutron slowing-down by hydrogen; thirty-four-group, one-dimensional, multiregion, consistent P_1 theory employing hydrogen-like slowing-down for four elements; and multigroup, one-dimensional, multiregion, transport theory. Provided that spectrum-averaged fast-group constants were used, the two-group results compared favorably with multigroup diffusion- and transport-theory results. Therefore most of the results reported are considered to be satisfactory for at least the preliminary analysis. The final HFIR nuclear design will be based on the calculational model that most nearly reproduces the results obtained from HFIR criticality experiments.

GENERAL PARAMETER STUDIES

In the initial parameter studies, it was assumed that the maximum neutron flux was limited only by the maximum permissible power density and by the specified nominal power level. Thus the quantities of particular interest were the flux per unit of maximum power density, $\phi/(P/V)_m$, and flux per unit of power, ϕ/P, where the flux in this case was either the maximum unperturbed thermal flux in the island, ϕ_m, or the volume-averaged thermal flux in the island target (Pu-242 target), ϕ_E. Within core-volume limits of interest for the HFIR, decreasing the size of the fuel annulus (while maintaining a constant island diameter) to increase ϕ/P results in a decrease in $\phi/(P/V)_m$ since the decrease in volume more than offsets the increase in ϕ/P. Thus, in the design of the HFIR core, it was necessary to compromise between the maximum achievable values of ϕ/P and $\phi/(P/V)_m$, taking into consideration all the practical aspects of reactor design.

The general parameter studies dealt mainly with the optimization of the island diameter, the investigation of beryllium as an alternate or supplementary moderating material for the island, and the selection of appropriate thickness and height dimensions for the fuel annulus. All cores used in the calculations here contained enough fuel for $k_{eff} = 1.20$ with the core clean and at 80°C, the fuel being distributed uniformly throughout the fuel annulus; no control poisons were included in any of the regions. Results from a lesser number of calculations, which included sufficient control poison to make $k_{eff} = 1.0$, indicated that the exclusion of the control surfaces would not significantly change the optimum core dimensions.

A schematic representation of a typical cylindrical core used in the general parameter studies is presented in Fig. 3. The figure also includes two-group neutron flux distributions for a core containing no island target and no control surfaces.

Island Diameter

The function of the central water island is to slow down to thermal energies nonthermal neutrons leaking from the fuel annulus into the island and to retain them for some time so as to build up their density. Such a scheme provides thermal fluxes in a non-fuel-bearing region significantly higher than in the fuel region and the side-reflector region. For a given current and spectrum of neutrons into the island region, the magnitude of the peak thermal flux is determined by the moderating properties of the island and therefore the size of the island, and the neutron slowing-down and absorbing characteristics of the material in the island. If the island diameter is too small, insufficient moderation will take place, thus resulting in a thermal-neutron density that is less than the maximum achievable for the particular entering current. If the island diameter is too large, absorption in the moderator and the increased ratio of volume to neutrom-emitting surface area will depress the thermal flux. The effect of changing core parameters outside the island region, such as thickness and height of the fuel annulus, is to change the energy spectrum of the nonthermal current entering the island, and to change the distance a neutron must travel through the fuel to reach the island. Changes in the energy spectrum change the effective neutron slowing-down and absorption properties of the island moderator, and also change the probability of a neutron leaking out of the fuel region into the island. Thus, in optimizing the island diameter on the basis of ϕ/P, several fuel-annulus thicknesses were considered.

PREFACE TABLE FOR FIG. 3

Code calculation, Wanda
Cross-section set, No. 2 (GNU averaged two-group)
Thermal temperature, 80°C

Active core length, 45.72 cm
Axial buckling, 0.002591 cm^{-2}
k_{eff}, 1.20

Region No.	Outer Radius (cm)	Composition	$N^{25} \times 10^5$ (atom/barn-cm)
1	7	H_2O	
2	19	U-235 + H_2O + Al, M/W = 1	25
3	49	Be + 5% H_2O + Exp	

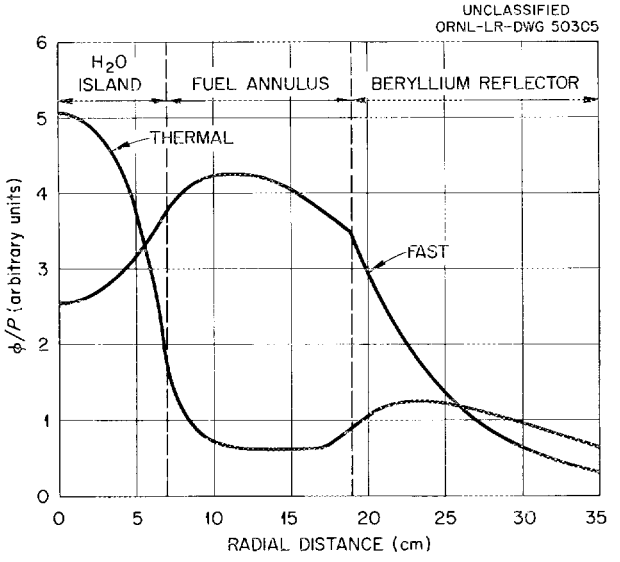

Fig. 3. One-Dimensional Schematic Representation of the HFIR Cylindrical Core Showing Typical Two-Group Flux Distributions.

Figures 4 and 5 show the results of the calculations made to determine the optimum radius of a water island containing a 2-cm-radius Pu-242 target. As indicated, the optimum island radius was essentially independent of fuel-annulus thickness for the particular cores investigated and it was assumed to also be essentially independent of core heights considered for the HFIR. The optimum radius based on $\phi/(P/V)_m$ was greater than that based on ϕ/P, because increasing the island radius of a fixed-thickness fuel annulus increases the annulus volume sufficiently, over a small range of radii, to more than offset the decrease in ϕ/P and the increase in the ratio of maximum to average radial power density, $(q_{max}/q_{av})_R$. When both the power and average power density and therefore the volume of the reactor are specified, a curve of flux vs island radius should be plotted with fuel-annulus volume rather than fuel-annulus thickness as a constant. As shown in Fig. 6, such a plot produces an optimum island

PREFACE TABLES FOR FIGS. 4, 5, 6, AND 8

Code calculation, Wanda
Cross-section set, No. 1 (two-group)
Thermal temperature, 80°C

Active core length, 30.5 cm
Axial buckling, 0.004568 cm^{-2}
k_{eff}, 1.10

Region No.	Outer Radius (cm)	Composition
1	2	100 g Pu-242, Al, H_2O, M/W = 1
2*		Be + 5% H_2O
3		H_2O
4		U-235, Al, H_2O, Equilib. Xe and Sm, M/W = 1
5	r_4 + 50	Be + 5% H_2O + Exp

*The dashed curves in Figs. 4 and 5 represent cores containing the optimum amount of beryllium in region 2 (as determined from Fig. 8.) The cores represented by the solid curves in Figs. 4 and 5 used H_2O in regions 2 and 3.

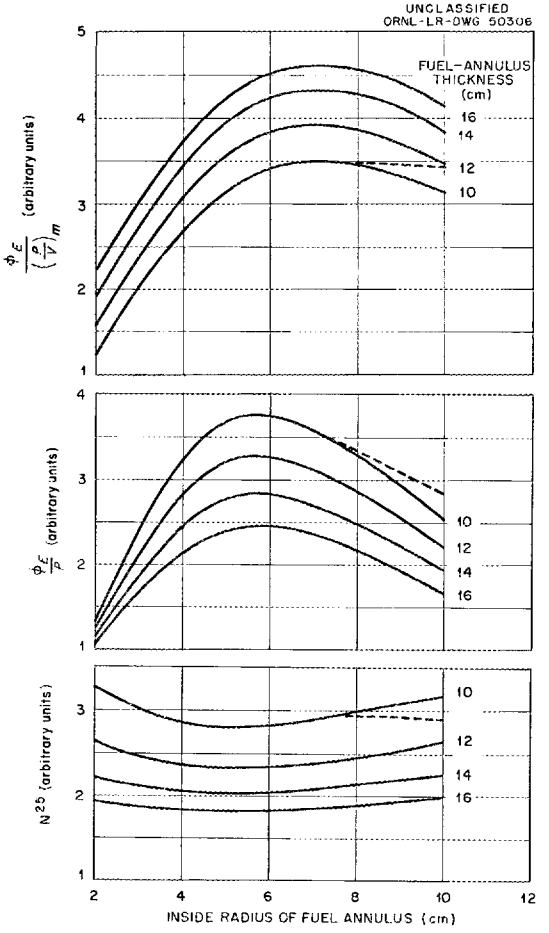

Fig. 4. Average Thermal Flux in Target per Unit Maximum Power Density and per Unit Power, and U^{235} Concentration vs Inside Radius and Thickness of Fuel Annulus.

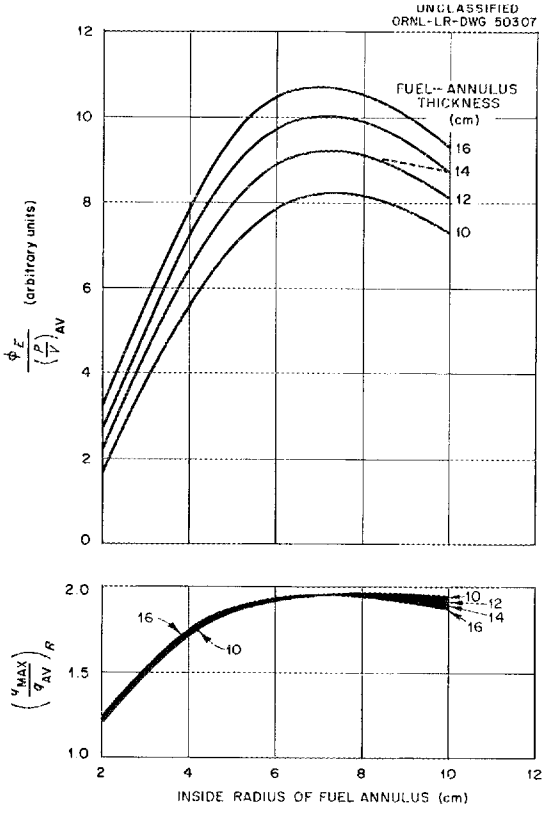

Fig. 5. Average Thermal Flux in Target per Unit Average Power Density, and Ratio of Radial Maximum-to-Average Power Density vs Inside Radius and Thickness of Fuel Annulus.

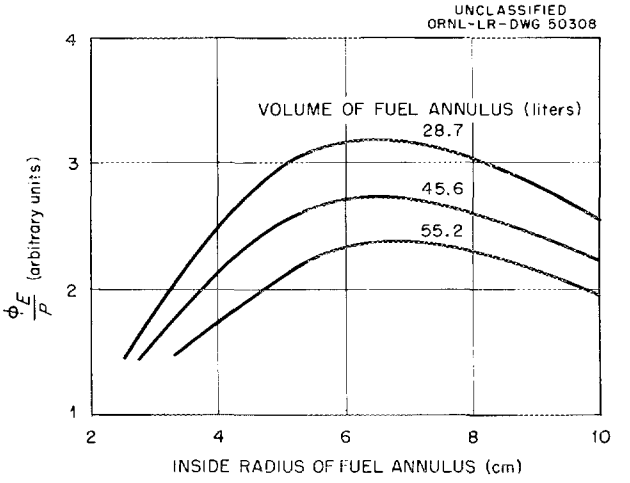

Fig. 6. Average Thermal Flux in Experiment per Unit Power vs Inside Radius and Volume of Fuel Annulus.

radius equal to about 6.5 cm* as compared to values of 5.7 and 7.0 cm obtained by plotting Φ_E/P and $\Phi_E/(P/V)_m$, respectively, using constant-fuel-annulus thickness as a parameter. If the maximum power density instead of the average power density is specified, the optimum radius could be different yet. However, as indicated by the curves in Fig. 5, $(q_{max}/q_{av})_R$ is very nearly constant for island radii in the range of 6 to 10 cm and for the fuel-region volumes considered. Therefore the optimum radii based on average and maximum power densities would be essentially the same.

In selecting the island radius for the HFIR, two other factors were considered: effect of the Pu-242 target size, and the effects of nonuniform fuel burnup and initial radial fuel distribution. Increasing the amount of Pu-242 in the target increases the volume of the associated aluminum matrix and cladding material and decreases the volume of water in the island. The resultant decrease in island moderation and thermal flux can be partially compensated for by increasing the diameter of the island as the size of the target is increased, although this would result in a lower unperturbed island thermal flux.

Variations in $(q_{max}/q_{av})_R$ also have an effect on the optimum diameter of the island, thus requiring consideration of the initial fuel distribution and uniformity of fuel burnup. Since neutrons born close to the island have a greater probability of entering the island than those born farther out in the fuel annulus, increasing $(q_{max}\ q_{av})_R$ increases ϕ/P, provided that the maximum power density always remains at the island-fuel

---

* The validity of this value was substantiated to some extent by critical experiments conducted on flux-trap-type cores by Feinberg et al.[6] The cores consisted of a square water island surrounded by a square fuel annulus that was 14 cm thick and contained fully enriched U-235 (U_3O_8), hydrogen (polyethylene), and aluminum. The fuel annulus was 25 cm long and was surrounded by a beryllium oxide reflector. Of all the variations of uranium-water cores investigated, a water cavity 10.6 by 10.6 cm proved to be the best from the viewpoint of critical dimensions and relative neutron density in the center of the island. Assuming that an equivalent circular radius can be derived solely on the basis of equivalent areas, an optimum cylindrical island radius would be 6.0 cm. This agrees very well with the HFIR calculations from the standpoint of both peak flux and minimum critical mass.

interface. Therefore, with reference to Fig. 5, it might be suspected that the increasing value of $(q_{max}/q_{av})_R$ with increasing island diameter had the effect of making the optimum island radius larger than that which would have been obtained with all the radial power distributions the same. For reasons that are discussed later, an essentially uniform initial radial power distribution is desirable in the HFIR. Thus the optimum island diameter associated with the beginning of the fuel cycle is somewhat smaller than predicted by Fig. 6. Even if the initial values of $(q_{max}/q_{av})_R$ are as shown in Fig. 5, the optimum diameter associated with a time-averaged value of $(q_{max}/q_{av})_R$ will be less, since nonuniform burnup of the fuel tends to flatten the power distribution for all cores.

The above qualitative analysis implies that in order to obtain the maximum unperturbed thermal flux per unit of power the island diameter should be less than that indicated in Fig. 6, whereas larger diameters are required for maximum Cf-252 production. Considering californium production to be of greatest importance initially, the inside diameter selected for the actual fuel-bearing annular area was 14 cm. Allowing about 1 cm for a non-fuel-bearing inner cylindrical side plate, the water-island diameter was 13 cm.

Island Composition

In comparison with other moderators, H_2O has a large absorption cross section and short neutron-slowing-down distance, thus resulting in a comparatively small optimum island diameter. Should the water island be smaller than desirable, the optimum diameter can be increased by replacing some or all of the water with a different moderator such as beryllium. To investigate this aspect, calculations were performed to determine the optimum diameter of a solid beryllium cylinder inserted in the middle of a fixed-diameter water island. This was done for several island radii and a fixed fuel-annulus thickness. As shown in Fig. 7, the optimum ratio of beryllium-cylinder diameter to island diameter ranges from zero for island radii less than about 7 cm to unity for island radii in excess of about 16 cm. The greatest thermal flux was obtained with the optimum-diameter island that contained no beryllium. However, the results in Fig. 7 indicate that the use of beryllium in the water island tends to broaden the range of essentially optimum island radii. To further illustrate this point, beryllium cylinders of varying diameters were placed in the center of one of the cores associated with Figs. 4 and 5. As shown in Fig. 8, the optimum radius for a beryllium cylinder placed in the center of a 10-cm-radius water island was about 6 cm. The results of these calculations determined the dashed curves in Figs. 4 and 5 and illustrated that by making use of beryllium in the island, it is possible to increase the island radius from say 7 cm to 10 cm with only about a 5% decrease in $\phi/(P/V)_m$, although there is a 20% decrease in ϕ/P. This assumes that the same fuel-annulus thickness is retained. Decreasing the fuel-annulus thickness in order to maintain approximately the same fuel volume will decrease $\phi/(P/V)_m$ some more but will increase ϕ/P.

The results presented in Fig. 9 indicate that all cores containing the optimum-size beryllium insert have approximately the same value of $(q_{max}/q_{av})_R$. The presence of the beryllium apparently is not responsible for this since, as shown in Fig. 5, cores containing no beryllium and having water-island radii in excess of 6 cm, also have nearly equal values of $(q_{max}/q_{av})_R$. It is concluded, therefore, that the optimum beryllium-cylinder diameters determined using uniform fuel distribution in the fuel annulus are the same as would be obtained using essentially uniform radial power distribution, as proposed for the HFIR.

PREFACE TABLE FOR FIGS. 7 AND 9

Code calculation, Wanda
Cross-section set, No. 1 (two-group)
Thermal temperature, 80°C in fuel, 100°C elsewhere

Active core length, 45.72 cm
Axial buckling, 0.002591 cm^{-2}
k_{eff}, 1.20

Region No.	Outer Radius (cm)	Composition
1		Be + 5% H_2O
2		H_2O
3	r_2 + 10	U-235 + Al + H_2O, M/W = 1
4	r_3 + 50	Be + 5% H_2O + Exp

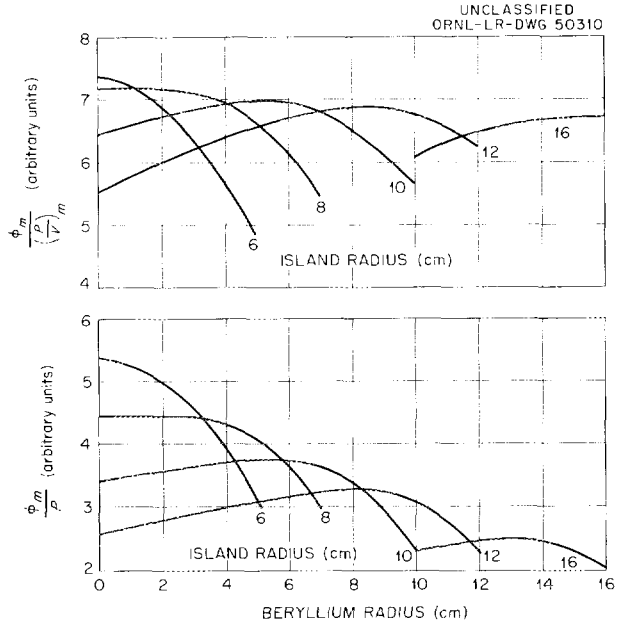

Fig. 7. Maximum Thermal Flux in Island per Unit Maximum Power Density and per Unit Power vs Island Radius and Radius of Cylindrical Beryllium Insert in Water Island.

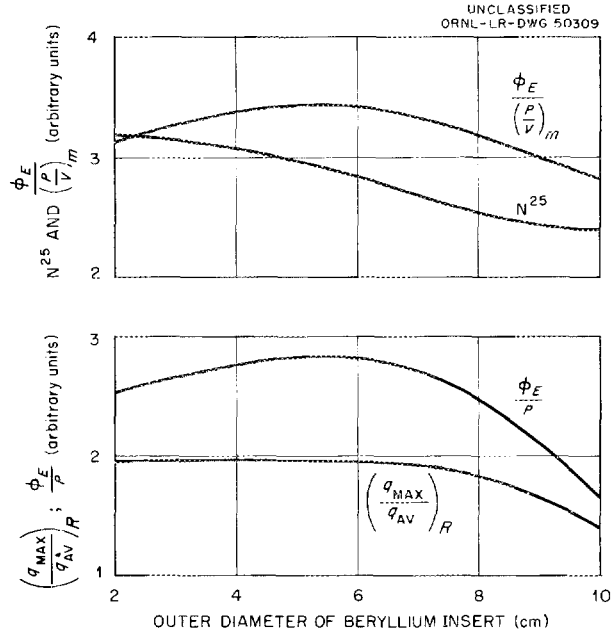

Fig. 8. Average Thermal Flux in Target per Unit Maximum Power Density and per Unit Power; Ratio of Maximum-to-Average Power Density in Radial Direction; and U^{235} Concentration vs Outer Diameter of Beryllium Insert in Island. (Preface table same as for Fig. 4.)

Fuel-Annulus Thickness and Length

For fixed values of power and power density, variations in the thickness and length of the fuel annulus affect the number of neutrons leaking into the island. If only the power density is fixed, the maximum leak rate into the island per unit length of the core is obtained with an annulus infinite in height and outer diameter and with uniform power distribution. The power, of course, would be infinite.

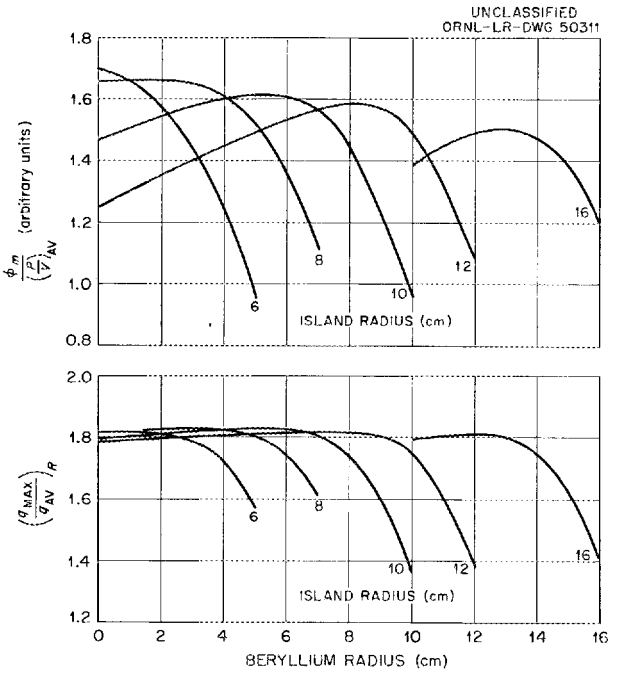

Fig. 9. Maximum Thermal Flux in Island per Unit Average Power Density, and Ratio of Maximum-to-Average Power Density in Radial Direction vs Island Radius and Radius of Cylindrical Beryllium Insert in Water Island. (Preface table same as for Fig. 7.)

Neutrons that are born more than a few migration lengths from the island make a relatively small contribution to the island flux, and therefore ϕ/P can be increased without significantly decreasing $\phi/(P/V)$ by reducing the thickness of the fuel annulus from many to a few migration lengths. As the annulus thickness is reduced further, ϕ/P continues to increase, primarily as a result of an increase in the fuel-region nonthermal flux. (For some flux-trap core designs a maximum value for ϕ/P is eventually achieved;[3,7] however, as shown in Fig. 10, if a maximum exists for the HFIR-type cores, the corresponding fuel-annulus thickness is probably less than $\frac{1}{2}$ cm.) For a given annulus thickness, decreasing the length of the core will also increase ϕ/P until the increase in fuel concentration and the increase in neutron leakage from the ends of the core offset the decrease in volume. The lengths and thicknesses that result in maximum values for ϕ/P are generally too small for practical consideration, requiring extremely high fuel concentrations and resulting in very low values for $\phi/(P/V)$. Therefore, it is necessary to compromise between ϕ/P and $\phi/(P/V)$.

When values for both ϕ and P are specified, the desirable combination of fuel-annulus thickness and height is that which results in the lowest power density. Suppose that both length and thickness of the fuel annulus are varied simultaneously so that the same values of ϕ and P, and therefore ϕ/P, are obtained for each core. If it were also possible for the power density to be the same in each core, then the volume of each core would be the same, and the integrated neutron source per unit length of the core would increase with decreasing core length. However, the neutron source in a very short, large-radius core is, on the average, farther from the island so that by comparison to a longer, equal-volume core the probability of a neutron leaking out the ends before reaching the island is greater. To obtain the same ϕ and

PREFACE TABLE FOR FIG. 10

Code calculation, GNU
Cross-section set, GNU 34 group (ORNL revised set)
Thermal temperature, 80°C

Active core length, 45.72 cm
Axial buckling, 0.002591 cm^{-2}
k_{eff}, 1.00

Region No.	Outer Radius (cm)	Composition
1	7	H_2O
2		H_2O + Al + U-235, M/W = 1
3	20	Be
4	40	Be

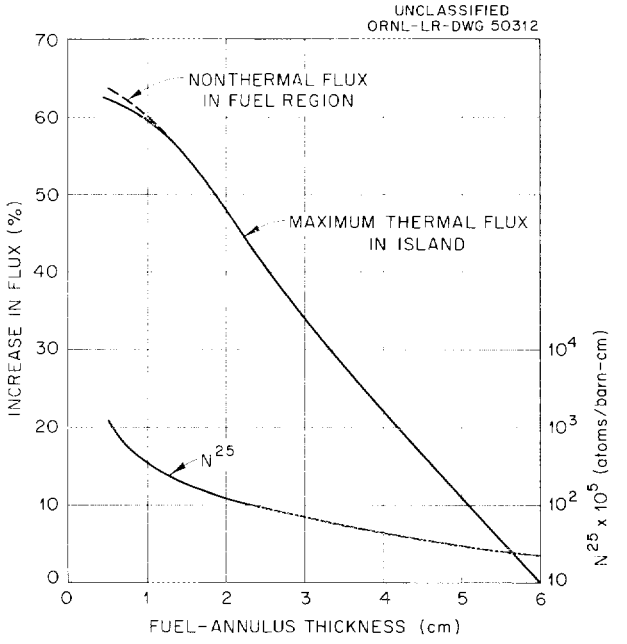

Fig. 10. Increase in Neutron Fluxes and Fuel Concentration with Decrease in Fuel Annulus Thickness.

P as in the longer core, it is necessary to increase the power density and, for a given length core, decrease the thickness of the fuel annulus. Thus, if ϕ/P is maintained constant as the length of the core is increased from a very short core, $\phi/(P/V)$ will increase and the fuel concentration will decrease. For a very long, thin annular core the neutron path length to the island is short. However, by comparison to a shorter, equal-volume core, the fuel concentration is high, and, for the same power density, volume, and power, the integrated neutron source per unit length of the core is less. Therefore the peak thermal flux in the horizontal midplane is less but can be increased by increasing the power density, although the volume must be reduced to keep the power the same. Thus, if ϕ/P is maintained constant as the length of the core is decreased from a very long core, $\phi/(P/V)$ and the volume will increase and the fuel concentration will decrease. On the basis of this qualitative argument it was concluded that there must be an optimum combination of length and thickness of the fuel annulus that results in a maximum value of $\phi/(P/V)$ for a given ϕ/P or a maximum value of ϕ/P for a given $\phi/(P/V)$.

To determine the proper dimensions of the fuel region, a study was conducted on a core with a fixed water-island radius, considering the core length and outer radius, target weight, target diameter and length, and fuel concentration as parameters. The length of the target was in all cases equal to the length of the core, and the fuel concentration (which was uniform throughout the annulus) was adjusted so that k_{eff} = 1.20. Three basic cases were considered: a core with no target, a 100-g target, or a 200-g target in the center of the water island. The ratio of aluminum matrix material to plutonium feed material was maintained constant, and for comparison purposes the target diameter was adjusted in each core to produce the maximum thermal flux. The inclusion of a target in the island in the manner described above introduced another variable affecting the optimum combination of core length and width, since increasing the length of the target region decreased the macroscopic absorption cross section, thus resulting in less flux perturbation within the target. The resultant greater integrated flux would tend to increase the length of the optimum core as the target weight increased.

The results of the calculations for the no-target and 200-g target cases are presented in Fig. 11. As indicated by the dashed curves, which represent the locus of points for $\phi/P = 5 \times 10^{13}$ nv/Mw (5×10^{15} at 100 Mw) in the core with no target, there is a combination of length and fuel-annulus thickness that results in a maximum value of $\phi/(P/V)_m$ for the core with no target, and another combination that yields a maximum $\phi/(P/V)_m$ for the core with the 200-g target. The core length for the no-target case appears to be a little over 46 cm; for the 200-g target case it is about 60 cm. If one chooses to specify a particular value of ϕ/P for the 200-g target case (or values of $\phi/(P/V)_m$ for either case), the optimum combination of dimensions comes out to be about the same, although the lower the required value of ϕ/P, the longer and thicker the fuel annulus will be. Since it was desired to obtain an unperturbed maximum thermal flux of at least 5×10^{15} in the HFIR, and since the corresponding $\phi/(P/V)_m$ curves are nearly flat between 46 and 60 cm, 45.72 cm (18 in.) and 12 cm (4.72 in.) were selected for the fuel-annulus length and thickness, respectively. (The shorter length core was in part selected because it would result in a smaller pressure drop across the core.)

If it is desired to use uniform power distribution rather than uniform fuel distribution in the fuel annulus, the results would be slightly different from those presented in Fig. 11. For the case of uniform fuel concentration the ratio of radial maximum-to-average power density decreases as the core length is increased for all cores represented by the dashed curves. Therefore, if the power distribution were the same for all cores, the optimum-length core would be expected to be somewhat shorter than predicted by Fig. 11. However, there is a decrease in ϕ/P associated with a decrease in $(q_{max}/q_{av})_R$ which tends to increase the optimum core length. Since these latter effects appeared to be small, it was assumed that the results in Fig. 11 were adequate for determining the optimum core dimensions for both the uniform-fuel-distribution core and the uniform-power-distribution core.

PREFACE TABLE FOR FIG. 11

Code calculation, Wanda
Cross-section set, No. 2 (GNU averaged two-group)
Thermal temperature, 80°C

Active core length, variable
Extrapolated core length, active core length + 16 cm
k_{eff}, 1.20

Region No.	Outer Radius (cm)	Composition
1*	Optimum	200 g Pu-242 + Al + H_2O, M/W varies, (g Al)/(g Pu) = 5
2	7	H_2O
3		U-235 + Al + H_2O, M/W = 1
4	r_3 + 30	Be + 5% H_2O + Exp

*Cores represented by solid curves contained only H_2O in region 1.

Note: Fluxes normalized assuming 3.3×10^{10} fissions/w-sec.

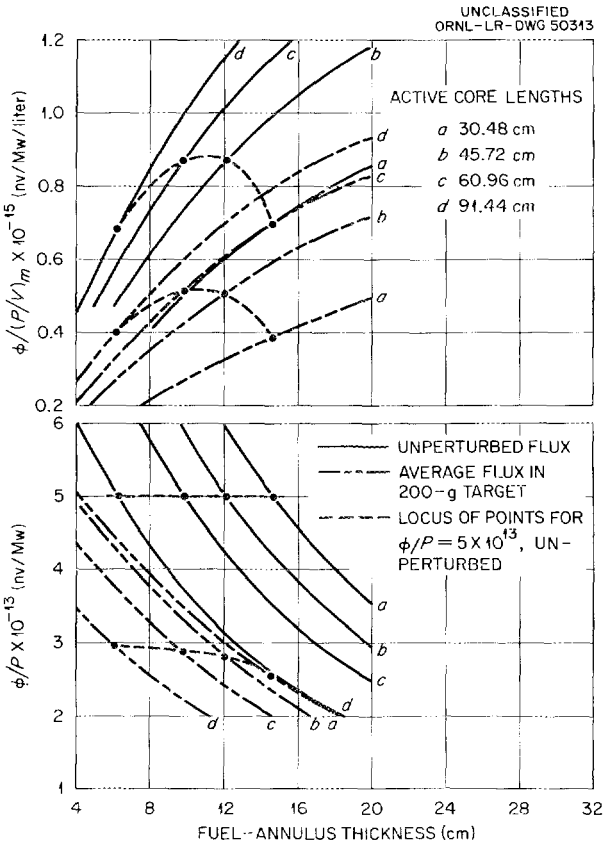

Fig. 11. Thermal Flux in Island per Unit Maximum Power Density and per Unit Power vs Length and Thickness of Fuel Annulus for a Particular Island Radius.

FURTHER STUDIES OF A CLEAN CORE

Several parameters that were assumed to have small and/or predictable effects on the selection of the HFIR core dimensions were considered in detail in the study of only a limited number of cores. The parameters treated in this manner included radial and axial power distributions, control-surface effects, fuel concentration and burnable poisons as related to power-distribution control and fuel cycle time, metal-to-water ratio in the fuel region, Pu-242 target size, and others. Some of the parameters considered here in detail were discussed very briefly in the preceding section in connection with the selection of the core dimensions. In this section the parameters are discussed in a specific order, although it is necessary, at times, to include one or more parameters in the discussion of another related parameter. The results of these studies indicated that no major changes were required in the previously selected core dimensions.

Radial Power Distribution (Radial Fuel Distribution)

Typical two-group flux and power distributions in a fuel annulus containing a uniform fuel distribution are shown in Fig. 12. If the maximum permissible power density is the main limitation on island neutron flux, it is apparent that flattening of the power distribution in the radial direction so as to make the average power density essentially equal to the maximum power density will increase $\phi/(P/V)_m$. However, the increased number of neutrons being born farther from the island do not contribute to the island proportionately as much as those closer to the island because of their reduced probability of leakage into the island. Therefore it would be expected that flattening of the power distribution would reduce ϕ/P. The effect is offset somewhat by an increase in the leakage probability for neutrons near the inner edge of the fuel annulus. This is a result of reducing the fuel concentration near the edges of the fuel annulus in order to obtain the uniform radial power distribution. (As a first approximation the distribution of fuel for producing uniform radial power is the mirror image of the power distribution curve obtained with uniform radial fuel distribution because the shape of the flux causing fission changes very little with changes in fuel distribution.) To simulate varying degrees of uniformity in radial power distribution, the fuel annulus was divided into one, two, five, twelve, and seventeen radial fuel regions, the fuel concentrations being adjusted so as to make the peak power densities about the same in all regions. Although this goal was not achieved in all cases, it was the basis on which the comparison was made. Results of the calculations are presented in Table 2.

For the two- and twelve-region cores the fuel annulus was divided into equally thick regions. In the five-region annulus, four of the regions were grouped in a 4-cm-thick region next to the island, leaving a fifth region 8 cm thick. The seventeen-region annulus was essentially equally divided. The maximum power density in the one-region annulus was at the inner surface of the annulus. For the two-region annulus the maximum power densities were at the inner and outer surfaces of the composite fuel annulus, the two values being so nearly equal to each other that for this type of comparison the values listed in Table 2 for the two-region annulus were considered "exact." As shown in Fig. 13, the individual region maximum power densities for the five-region annulus were not all the same, although the maximum of all the values occurred essentially at the inner surface. The same sort of "inexactness" was also obtained for the twelve- and seventeen-region annuli, although not to the same degree.

PREFACE TABLE FOR FIG. 12

Code calculation, Wanda
Cross-section set, No. 2 (GNU averaged two-group)
Thermal temperature, 80°C

Active core length, 45.72 cm
Axial buckling, 0.002591 cm^{-2}
k_{eff}, 1.20

Region No.	Outer Radius (cm)	Composition	$N^{25} \times 10^5$ (atom/barn-cm)
1	7	H_2O	
2	19	U-235 + H_2O + Al, M/W = 1	25
3	49	Be + 5% H_2O + Exp	

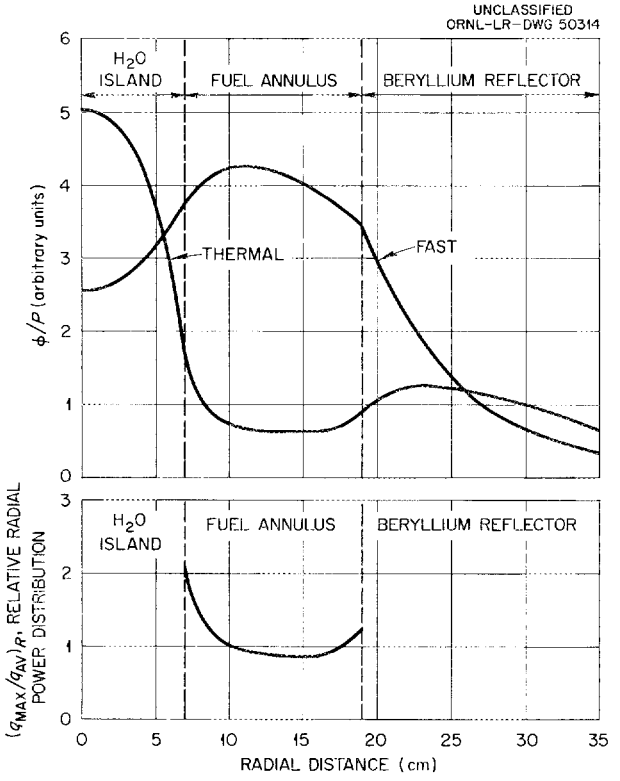

Fig. 12. Typical Neutron Flux and Power Distribution in the HFIR.

This explains, in part, why some of the values in Table 2 do not appear to be consistent; for example, ϕ/P for the five- twelve- and seventeen-region annuli should be less than for the two-region annuli (assuming each fuel annulus to be divided into equal-thickness fuel regions.) (However, the value of ϕ/P for the particular five-region core calculated would not be as small as would be expected with all regions being of equal thickness.) A more meaningful comparison of the results was obtained by plotting the data in Table 2 against the number of discrete fuel regions. Assuming that the variables must be smooth functions of this parameter (with each fuel annulus divided into equal-width regions) and further assuming that values for the one- and two-region annuli were "exact," the curves in Fig. 14 were obtained. (By more precise proportioning of the fuel among the various regions, the ratio of maximum-to-average power density could be reduced in the annuli whose points do not fall on the curves.

Table 2. Reactor Characteristics as a Function of Radial Power Distribution

	Number of Fuel Regions				
	1	2	5	12	17
$(q_{max}/q_{av})_R$	2.080	1.450	1.42	1.17	1.11
k_{eff}	1.205	1.205	1.205	1.205	1.205
ϕ/P (relative values)	4.735	4.50	4.65	4.55	4.50
$\phi/(P/V)_m$ (relative values)	0.6279	0.8512	0.90	1.08	1.15

The per cent reduction in ϕ/P would be small in comparison with the per cent decrease in (q_{max}/q_{av}), while the per cent increase in $\phi/(P/V)_m$ would be nearly equal to the decrease in (q_{max}/q_{av}).) These results indicate that a 90% increase in $\phi/(P/V)_m$ can be obtained by changing from one region to an infinite number, while losing only about 8% in ϕ/P.

There are, of course, a few practical considerations associated with obtaining a prescribed, continuously varying fuel concentration across a fuel plate. By comparison, the use of just two discrete regions in two separate annuli or possibly three regions in three separate annuli (in which case a single fuel-bearing plate would contain a uniform fuel concentration) would require essentially no development of fabrication techniques. However, because of the very strong dependence of transplutonium isotope production on neutron flux, it was tentatively concluded that the 25 to 50% effective loss of $\phi/(P/V)_m$ could not be tolerated, provided that there were alternatives. The next big step from the standpoint of plate fabrication was to incorporate two or more discrete fuel regions in a single plate. Assuming a three-region plate and two separate fuel annuli to be a practical limit, thus providing six regions of fuel, the effective loss in $\phi/(P/V)_m$ would be about 15%.

There is another advantage associated with the use of continuously-varying-concentration plates. At present it is visualized that the plates will be positioned radially; thus, as shown in Fig. 13, the radial power-density gradients in plates containing several discrete fuel regions would be quite steep. Since there is little conduction of heat in the plate parallel to the surface of the plate, the radial temperature distribution in the plate will be essentially the same as the power distribution. Thus the thermal stresses, which in this case would tend to buckle the plates, could limit reactor power. This problem will also exist to some extent with continuously varying fuel concentration because of nonuniform fuel burnup and control-plate movement. However, burnable poison can be used within limitations to reduce the required reactivity worth of the control plates and therefore the temperature gradients in the vicinity of the control region. Burnable poison can also be used to some extent to control nonuniform fuel burnup.

The preceding comparison was made on the basis of equal-width fuel regions and equal maximum power densities in each region; there are many other combinations one might study. However, the results in Table 2 and Fig. 14 indicate that the neutrons born deep in the fuel annulus contribute significantly to the flux in the water island; thus it appears that the curves in Fig. 14 would not change significantly.

In contrast to reducing $(q_{max}/q_{av})_R$ to improve the reactor performance, a case was considered in which $(q_{max}/q_{av})_R$ was made comparatively large by using uniform fuel distribution throughout the fuel annulus and by removing the side reflector. The objective was to obtain a large increase in ϕ/P at the expense of a comparatively small decrease in $\phi/(P/V)_m$. Results from the study indicate that a reflected core

PREFACE TABLE FOR FIGS. 13 AND 14

Code calculation, Wanda
Cross-section set, No. 2 (GNU averaged two-group)
Thermal temperature, 80°C

Active core length, 45.72 cm
Axial buckling, 0.002591 cm^{-2}
k_{eff}, 1.205

Region No.	Outer Radius (cm)	Composition	$N^{25} \times 10^5$ (atom/barn-cm)
		One Fuel Region	
1	7	H_2O	
2	19	U-235 + Al + H_2O, M/W = 1	25
3	49	Be + 5% H_2O + Exp	
		Two Fuel Regions	
1	7	H_2O	
2	13	U-235 + Al + H_2O, M/W = 1	15
3	19	Same as above	35
4	49	Be + 5% H_2O + Exp	
		Five Fuel Regions	
1	7	H_2O	
2	8	U-235 + Al + H_2O, M/W = 1	~15
3	9	↓	~23.8
4	10	↓	~31.3
5	11	↓	~36.0
6	19	↓	~25.3
7	49	Be + 5% H_2O + Exp	
		Twelve Fuel Regions	
1	7	H_2O	
2	8	U-235 + Al + H_2O, M/W = 1	
3 to 13	9 to 19 (1-cm increments)	Same as above	N^{25} not determined specifically for k_{eff} = 1.205; ranges from about 12 x 10^{-5} to 38 x 10^{-5}
14	49	Be + 5% H_2O + Exp	
		Seventeen Fuel Regions	
1	7	H_2O	
2 to 7	7.5 to 10 (1/2-cm increments)	U-235 + Al + H_2O, M/W = 1	See remarks above
8 to 14	11 to 17 (1-cm increments)	↓	
15	17.5	↓	
16	18	↓	
17	18.5	↓	
18	19	↓	
19	49	Be + 5% H_2O + Exp	

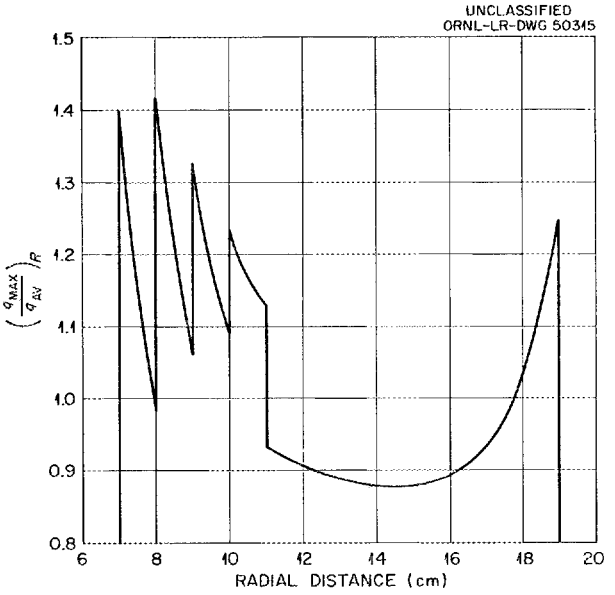

Fig. 13. Radial Power Distribution in a Fuel Annulus Containing Five Discrete Fuel Regions.

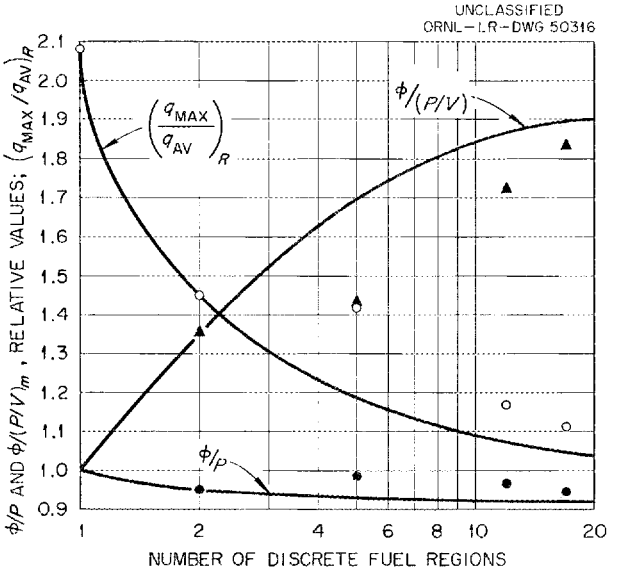

Fig. 14. Maximum Thermal Flux in Island per Unit Maximum Power Density and per Unit Power, and Ratio of Maximum-to-Average Power Density in the Radial Direction vs Number of Discrete Fuel Regions in the Fuel Annulus.

with essentially uniform power distribution produces a more favorable combination of ϕ/P and $\phi/(P/V)_m$ than the unreflected cores. Details of this study are given in Appendix 1.

All the comparisons above were made with $k_{eff} = 1.2$ and with no control surfaces present. The introduction of control poison in a 2-cm-thick annular region between the fuel annulus and the beryllium side reflector (the control-region location specified for the HFIR) increases $(q_{max}/q_{av})_R$ in all cores that initially have maximum power densities at the island-fuel interface, and during the fuel cycle, nonuniform burnup of the fuel and variations in control poison also change $(q_{max}/q_{av})_R$. Therefore in a practical sense it is not possible to maintain uniform radial power distribution over a core lifetime. However, with proper initial distribution of fuel and burnable poison it is possible to maintain $(q_{max}/q_{av})_R$ at or below about 1.2; in comparison to a core with uniform fuel distribution and with an equivalent control system the gain in $\phi/(P/V)_m$ is still about 90%.

Axial Power Distribution

Within limitations, peaking of the power at the horizontal midplane of the core increases ϕ_m/P significantly without appreciably decreasing $\phi_m/(P/V)_m$. With uniform fuel distribution in the longitudinal direction, power peaking of this type generally occurs. However, the presence of a light-water end reflector above and below the fuel annulus tends to result in even greater peaking of the thermal flux (and thus power density) at the longitudinal extremeties of the fuel zone, resulting in a significant decrease in $\phi_m/(P/V)_m$. Results from two-dimensional calculations predicted a relative power density of about 1.7 at the ends, as compared to a maximum of 1.2 at the horizontal midplane, assuming an essentially uniform radial power distribution at the horizontal midplane. Although at this time there are no intentions of deliberately

increasing power peaking at the horizontal midplane, it is desirable to reduce the peaking at the ends to a value equal to or less than that at the center.

Further investigations of end peaking were made using a one-dimensional, slab-geometry core with a light-water end reflector. One proposed method for controlling the end peaking was to extend the aluminum portion of the fuel plate beyond the fuel zone so as to increase the effective neutron age in the region adjacent to the fuel. If necessary, a small amount of poison could be added to the extension to reduce the flux further. Results of the calculations are presented in Fig. 15. It is observed

PREFACE TABLE FOR FIG. 15

Code calculation, Wanda
Cross-section set, No. 2 (GNU averaged, two-group)
Thermal temperature, 80°C

Geometry, finite slab
Extrapolated height and width, 48 cm
Transverse buckling $(\pi^2/a^2 + \pi^2/b^2)$, 0.008567 cm^{-2}

Region No.	Outer Boundary Dimension from Midplane (cm)	Composition
1	24	U-235 + Al + H_2O, M/W = 1, N^{25} = 25 x 10^{-5} atom/barn-cm
2	30	(A) H_2O; (B) Al + H_2O, M/W = 1; (C) Al + H_2O + $\Sigma^P_{a_{th}}$ = 0.01, M/W = 1
3	60	H_2O

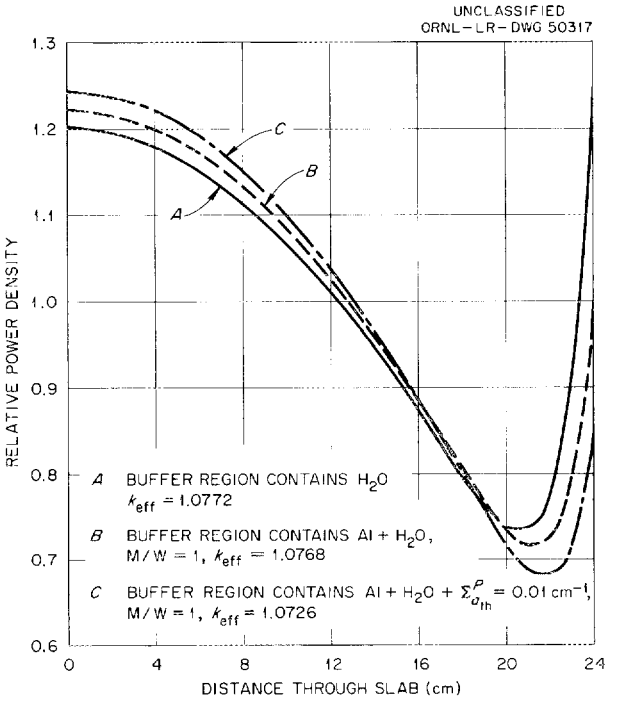

Fig. 15. Power Distribution in a Water-Reflected Slab, Using a Buffer Region Between Fuel and Reflector.

that for the slab core with no plate extension the power-density peak at the end is only about 3% higher than the value at the center of the slab. The lower peaking value obtained from this calculation, as compared to that obtained with the two-dimensional calculation, is attributed partly to the difference in fuel concentration for the two calculations. (The fuel concentration in the one-dimensional slab calculation was about one-half that in the earlier two-dimensional calculation since later calculations indicated that the smaller value was more representative of the concentration for the typical HFIR.) Even so, it was assumed that the power density at the ends would have to be reduced by about 20%. As indicated in Fig. 15, a 6-cm extension of the aluminum plates reduced the peak by about 20% while increasing the power density at the center by only 2% and decreasing k_{eff} by only 0.04%. The use of a neutron poison in the extension did not appear to be required.

The use of the unpoisoned 6-cm extension was investigated further, using a two-dimensional calculation and the latest typical HFIR core design. Since these calculations were made in conjunction with the fuel-cycle studies, the detailed results are discussed under that topic heading. It suffices to say here that the two-dimensional calculations indicate that the power density at the ends of the core will not exceed 80% of the maximum power density in the core at any time during the fuel cycle. Thus the length of the extension could probably be reduced some; however, an extension is required for establishing hydrodynamic stability of the coolant and since manufacturing tolerances on the length of the fuel zone will permit some fuel to extend into the high flux regions at the ends, the 6-cm extension was tentatively specified for the HFIR core.

Control-Surface Effects

As mentioned in the introduction, most of the calculations performed in the general parameter study were based on a core having $k_{eff} = 1.20$ with no reactivity controls present. Introduction of the control surfaces will of course perturb the fluxes throughout the core and will result in redistribution of the power in the fuel annulus. Since the "optimum" core design was selected on the basis of calculations made without reactivity control in the core, it is of interest to compare the results obtained for the supercritical and critical reactors.

In the solution of the steady-state reactor equations for a "noncritical" core, the particular calculational methods used in the HFIR studies employed a multiplier, λ, on the neutron fission source in order to balance the equations, or, in a sense, to make the noncritical reactor critical. Thus, if one considers λ to be a multiplier on only the fuel concentration, the "noncritical" reactor can be interpreted as a critical reactor with fuel concentration equal to λN^{25} (where N^{25} is the original U-235 concentration) and with sufficient nonfuel poison in the fuel region to make the macroscopic absorption cross sections equal to the original values. (Except for having no fission cross section, this poison has all the pertinent nuclear characteristics of the fuel.) It is apparent then that a comparison of the supercritical ($k_{eff} = 1.20 = 1/\lambda$) reactor with the critical reactor containing reactivity control surfaces is really a comparison of a critical reactor having $N^{25} = \lambda N^{25}$ (ORIGINAL) and $\Sigma_a = \Sigma_a$ (ORIGINAL), with a reactor having $N^{25} = N^{25}$ (ORIGINAL), $\Sigma_a = \Sigma_a$ (ORIGINAL), and containing control surfaces. A comparison of this type was made using a fixed value of N^{25} (ORIGINAL) and with varying amounts of poison in an annular control region located between the fuel annulus and outer beryllium reflector. Using one-dimensional, multigroup, diffusion theory, it was found that increasing the control-region poison concentration increased ϕ_m/P and $(q_{max}/q_{av})_R$ and decreased $\phi_m/(P/V)_m$. The increase in ϕ_m/P is attributed to the increase in $(q_{max}/q_{av})_R$ and to a hardening of the neutron energy spectrum, both of which increase neutron leakage from the fuel region since the absorption cross sections are the same in all cases. As shown in Fig. 16, an increase in $(q_{max}/q_{av})_R$ of about 35% by means of control-poison addition is accompanied by a 15% increase in ϕ_m/P, while

according to Fig. 14 a 35% increase in $(q_{max}/q_{av})_R$ by means of radial fuel distribution results in only a 4 to 5% increase in ϕ_m/P. Thus it appears that spectrum hardening associated with the increase in control-region poison accounts for about a 10% increase in ϕ_m/P. (The change in spectrum as determined from the multigroup calculations is shown in Figs. 17, 18, and 19. Although the spectrum is hardened much more near the control region when the control poison is inserted, hardening does take place throughout the annulus.)

The above results tend to imply that increasing the fuel concentration and compensating for the additional reactivity by means of increasing the poison concentration in the annular control region will result in an increase in ϕ_m/P. It must be remembered, however, that in these particular calculations a nonfuel absorber was removed from the fuel region as the fuel concentration was effectively increased. As will be discussed later under the subject heading "Fuel Concentration," an increase in fuel concentration in the normal sense will decrease ϕ_m/P.

In view of the results obtained from the above comparison calculations, it was concluded that the "optimum" core design that was selected on the basis of $k_{eff} = 1.20$ would be essentially unchanged had the calculations considered a core with a control poison, the same fuel loading, and $k_{eff} = 1.0$.

Fuel Concentration

As will be demonstrated later, increasing the fuel concentration in a particular core decreases the thermal-neutron flux in the island. Thus, increasing the fuel-cycle lifetime by increasing the loading results in a lower time-integrated flux for the actual operating time, but less down time per unit operating time. Therefore, from the standpoint of isotope production there would be some optimum loading and associated fuel-cycle time. However, based somewhat on the desired unperturbed flux level for the clean core, and on early evidence that the core life might be limited by corrosion, a fuel-cycle time of ten days was tentatively selected for the HFIR. Assuming about 5% $\Delta k/k$ for xenon and samarium, 4% for other fission-product poisoning, and 7.5×10^{-5} U-235 atom/barn-cm for ten days' burnup, the required k_{eff} was estimated from Fig. 20 to be about 1.18 (with no reactivity compensation by the control system). The calculations were for a reactor which contained a 100-g plutonium target in the island and experiments in the outer beryllium reflector amounting to about 2% in reactivity.

As shown in Fig. 21, the addition of fuel to the fuel region (in a uniform manner) decreases ϕ_m/P even though $(q_{max}/q_{av})_R$ is increased and the neutron energy spectrum is hardened some. This particular type of comparison, however, may not be realistic since in actuality the addition of fuel requires the addition of more control, and it has already been determined that the addition of control between the fuel and outer reflector hardens the spectrum sufficiently to increase ϕ/P. Thus, if the cores having different fuel loadings are compared on the basis of having the same k_{eff} and similar control schemes, a different relationship than indicated by Fig. 21 is obtained.

To investigate this problem, two-group calculations were performed on two cores having different fuel concentrations. Both cores were geometrically identical, being made up of 17 fuel regions with the fuel so distributed as to produce reasonably flat power distributions consistent with nonuniform fuel burnup during a fuel cycle. Both cores contained a uniformly distributed burnable poison in the fuel region so that k_{eff} without any poison in the control region between the fuel annulus and the outer reflector would be approximately the same for the two cores. As a result the poison concentrations in the control region were about the same for k_{eff} equal to unity. This was also a practical consideration having to do with the amount of poison that

PREFACE TABLE FOR FIGS. 16, 17, 18, AND 19

Code calculation, GNU
Cross-section set, GNU 34 groups (ORNL revised set)
Thermal temperature, 80°C

Active core length, 45.72 cm
Axial buckling, 0.002591 cm^{-2}
k_{eff}, 0.992 for Figs. 17, 18, and 19

Core same as that associated with Fig. 1 except that for Fig. 16 the boron concentration in the control region is a variable and for Figs. 17, 18, and 19 the control region contained either 200 x 10^{-5} atom/barn-cm of natural boron or contained no boron.

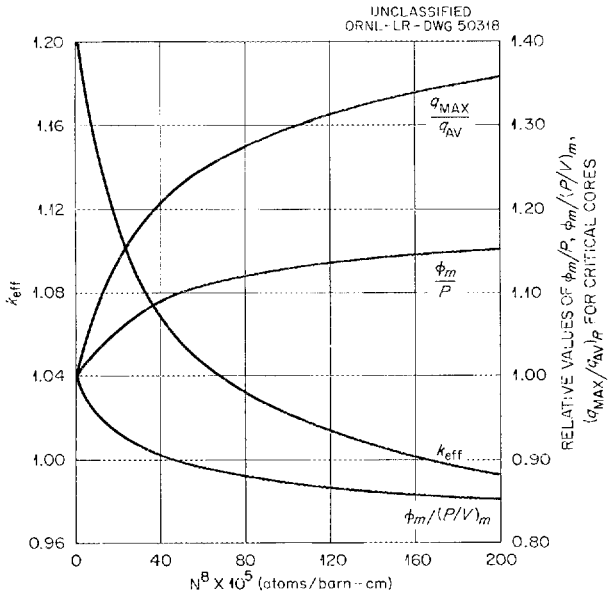

Fig. 16. Maximum Thermal Flux per Unit Maximum Power Density and per Unit Power, Ratio of Maximum-to-Average Power Density in the Radial Direction, and Reactivity vs Poison Concentration in Control Region Between Fuel and Outer Reflector.

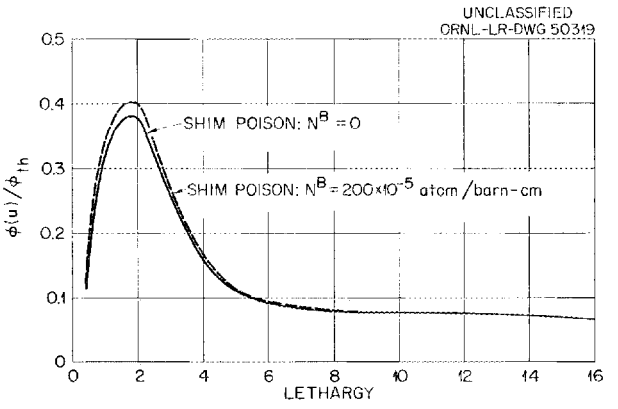

Fig. 17. Flux Energy Spectrum at Inside Surface of Fuel Annulus. (Normalized to thermal flux at same space point.)

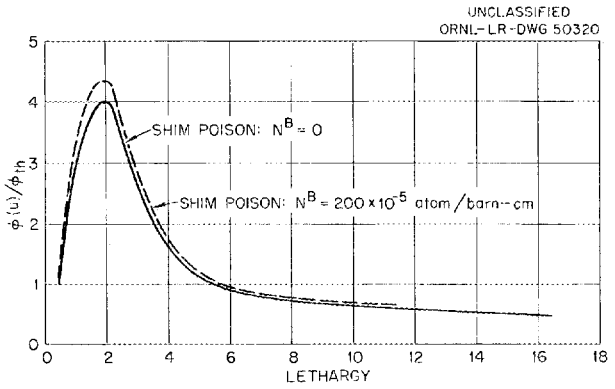

Fig. 18. Flux Energy Spectrum at the Midpoint of the Fuel Annulus. (Normalized to thermal flux at same space point.)

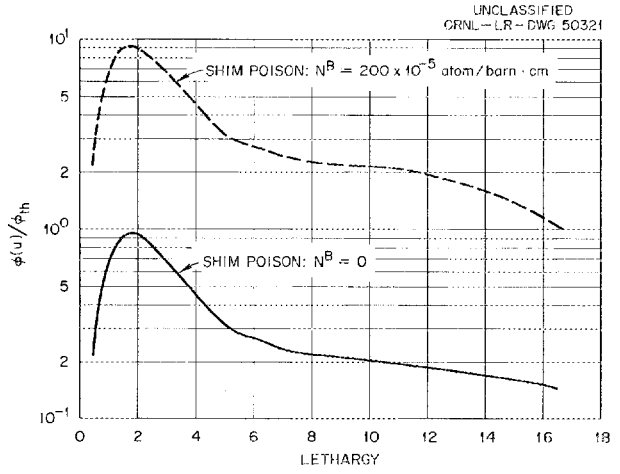

Fig. 19. Flux Energy Spectrum at the Outside Surface of Fuel Annulus. (Normalized to thermal flux at same space point.)

PREFACE TABLE FOR FIG. 20

Code calculation, Wanda
Cross-section set, No. 2 (GNU averaged two-group)
Thermal temperature, 80°C

Active core length, 45.72 cm
Axial buckling, 0.002591 cm^{-2}

Region No.	Outer Radius (cm)	Composition
1	2	100 g Pu-242 + Al + H_2O, M/W = 1
2	7	H_2O
3	19	U-235 + Al + H_2O, M/W = 1
4	49	Be + 5% H_2O + Exp

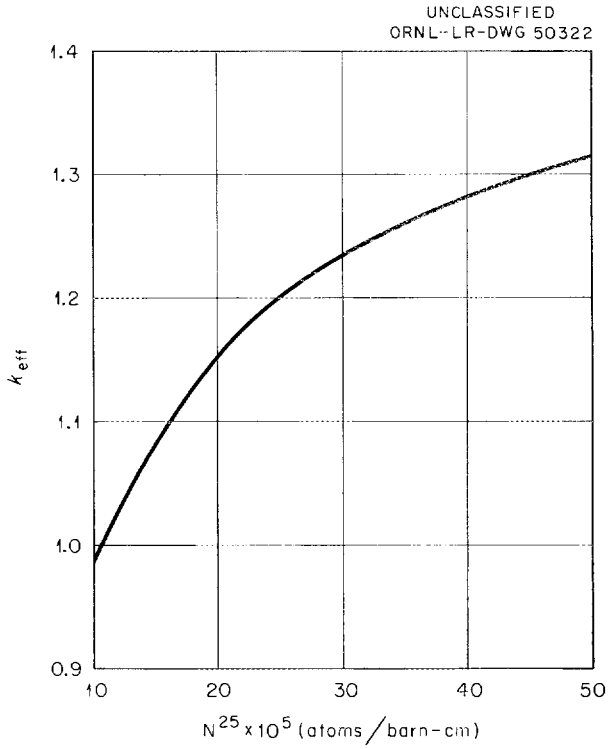

Fig. 20. Reactivity vs U^{235} Concentration for Typical HFIR Core.

can be added to such a control region without resulting in excessive distortion of the power distribution during the fuel cycle. However, for further comparison, this practical aspect of the core design was disregarded, and the cores were also calculated with no burnable poison but with sufficient poison in the control region to give the same value of k_{eff}.

The results of the above calculations are presented in Table 3. A comparison of columns 2 and 3, the two cores having burnable poison in the fuel, shows that the core with the greater fuel loading has lower values of ϕ/P and $\phi/(P/V)_m$. Even if it is assumed that the ratio of maximum-to-average power density in the more heavily loaded core can be reduced to the same lower value in the less heavily loaded core without appreciably reducing ϕ/P, the value of $\phi/(P/V)_m$ in column 3 will still be

PREFACE TABLE FOR FIG. 21

Code calculation, GNU
Cross-section set, GNU 34 group (ORNL revised set)
Thermal temperature, 80°C
Active core length, 45.72 cm
Axial buckling, 0.002591 cm^{-2}

Other dimensions and region compositions are the same as indicated for the 12-region fuel annulus associated with Figs. 13 and 14.

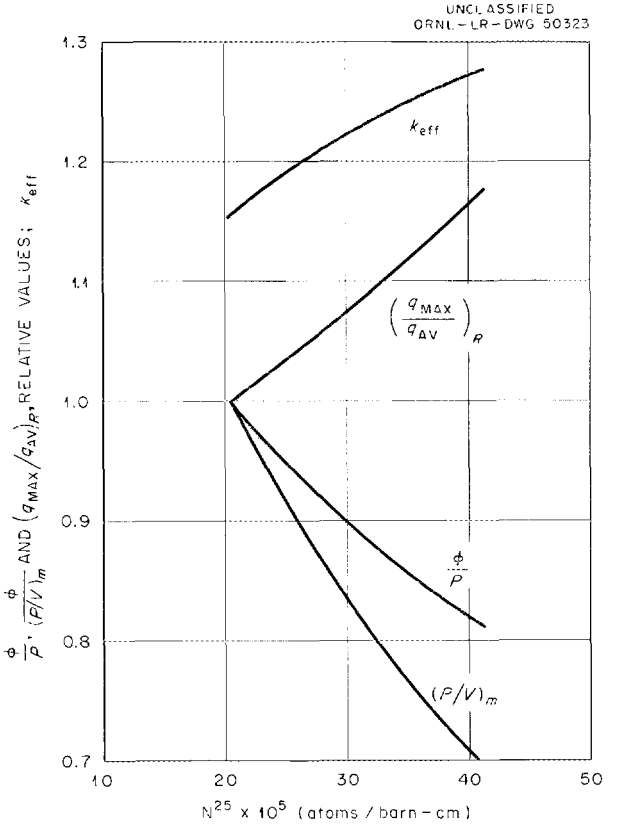

Fig. 21. Maximum Thermal Flux per Unit Maximum Power Density and per Unit Power, Ratio of Maximum-to-Average Power Density in the Radial Direction, and Reactivity vs Average Fuel Concentration for a 12-Region Fuel Annulus.

less. This is also true of a comparison between columns 1 and 4. A comparison of columns 1 and 4 with 2 and 3 indicates that the addition of the burnable poison in the fuel region decreases ϕ/P and $\phi/(P/V)_m$. Thus, in general, an increase in fuel concentration decreases the performance of the reactor at the beginning of the fuel cycle. As will be discussed later under the subject heading Fuel-Cycle Analysis, ϕ/P and $\phi/(P/V)_m$ remain essentially constant during the fuel cycle of the proposed HFIR; therefore it is concluded that an increase in fuel concentration will also decrease the time-integrated thermal-neutron flux in the island of the HFIR, where time is interpreted as actual operating time.

Table 3. Effect of Fuel Loading on ϕ/P and $\phi/(P/V)_m$

$N^{25} \times 10^5$, atom/barn-cm	23.47	23.47	45.26	45.26
Burnable poison	No	Yes	Yes	No
Σ_p(control region), cm^{-1}	0.321	0.137	0.289	3.00
k_{eff} ($\Sigma_p = 0$)	1.1798	1.1277	1.1217	1.1287
k_{eff} ($\Sigma_p \neq 0$)	1.000	1.000	1.000	1.000
$(\phi/P) \times 10^{-13}$, nv/Mw	5.973	5.601	5.120	5.565
$(q_{max}/q_{av})_R$	1.348	1.184	1.313	1.589
$\left[\phi/(P/V)_m\right] \times 10^{-15}$, nv/Mw/liter	1.223	1.306	1.076	0.967

Burnable-Poison Effects

The use of a burnable poison in the HFIR has been considered for power-distribution control and for reducing the reactivity requirements of the control system. From a nuclear aspect, however, there is in a sense a limit to how much should be added. As indicated by a comparison of columns 1 and 4 with 2 and 3 in Table 3, the addition of burnable poison to the fuel region can decrease ϕ/P at the beginning of the cycle. To investigate this effect further, varying amounts of burnable poison were added to the core described in column 1 of Table 3, and the poison in the control region was regulated to make k_{eff} equal to unity in each case. The burnable poison was added uniformly in density to only the inner half of the fuel annulus for the purpose of flattening the power in the radial direction. Figure 22 shows the relative radial power distribution in the core with and without the burnable poison.

When burnable poison is added to a core, control poison must be removed from the control region to maintain the same reactivity. This will have some effect on the neutron energy spectrum and thus on neutron leakage. Furthermore, moving the poison from the control region to the fuel region tends to erect a neutron barrier between the island and source. The net effects on ϕ/P and $\phi/(P/V)_m$ for a core with a fixed fuel distribution and loading are shown in Fig. 23. The addition of burnable poison to the fuel decreases ϕ/P; the increase in $\phi/(P/V)_m$ results from the reduction of $(q_{max}/q_{av})_R$. Further addition of poison to the core in Fig. 23 without fuel redistribution would eventually cause $(q_{max}/q_{av})_R$ to increase, in which case it is expected that both ϕ/P and $\phi/(P/V)_m$ would decrease. Suppose, however, that for each poison addition to the fuel the fuel distribution is changed to maintain a specified power distribution. Since reducing $(q_{max}/q_{av})_R$ tends to decrease ϕ/P, thus partially accounting for the decrease of ϕ/P in Fig. 23, it is expected that maintaining a specified power distribution would result in a smaller decrease in ϕ/P as poison is added to the fuel. Of course $\phi/(P/V)_m$ would then decrease the same as ϕ/P. An analysis of the HFIR fuel cycle (see Fuel-Cycle Analysis) indicates that the initial adverse

PREFACE TABLE FOR FIGS. 22 AND 23

Code calculation, Wanda
Cross-section set, No. 2 (GNU averaged two-group)
Thermal temperature, 80°C

Active core length, 45.72 cm
Axial buckling, 0.002591 cm^{-2}
k_{eff}, 1.00

Region No.	Outer Radius (cm)	Composition	$N^{25} \times 10^5$ (atom/barn-cm)	$N^{B-10} \times 10^5$ (atom/barn-cm)
1	7	H_2O		
2	7.5	U-235 + Al + H_2O	10	Same in regions
3	8	+ B-10, M/W = 1	11.52	2 through 10
4	8.5		13.18	
5	9		14.93	
6	9.5		16.77	
7	10		18.64	
8	11		20.74	
9	12		23.99	
10	13		26.86	
11	14		28.90	0
12	15		30.03	
13	16		29.03	
14	17		27.08	
15	17.5		25.79	
16	18		24.32	
17	18.5		22.73	
18	19		21.04	
19	21	Be + 5% H_2O + Exp + Control Poison		
20	51	Same as above		

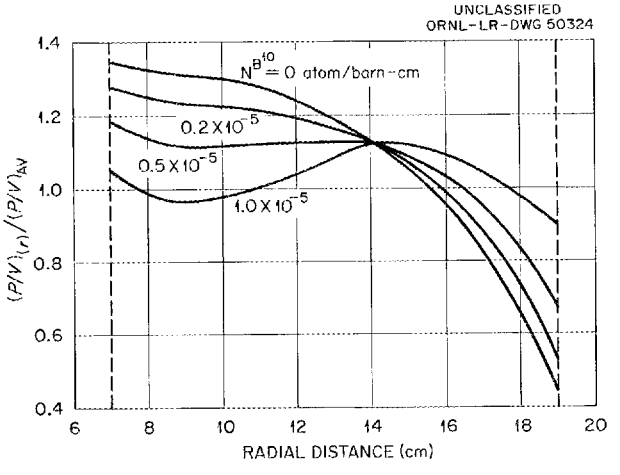

Fig. 22. Radial Power Distribution for Different Amounts of B^{10} Poison in Inner Regions of Fuel Annulus.

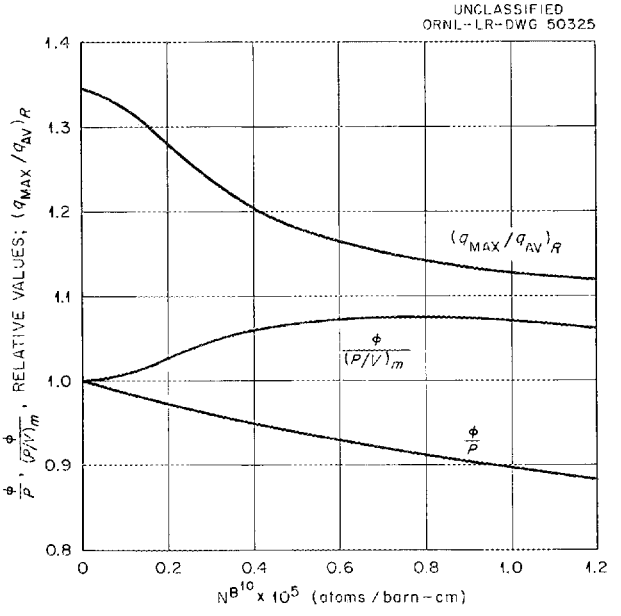

Fig. 23. Maximum Thermal Flux per Unit Maximum Power Density and per Unit Power, and Ratio of Maximum-to-Average Power Density in the Radial Direction vs B^{10} Concentration in Inner Regions of Fuel Annulus.

effect of a small amount of burnable poison in the fuel region is more than offset by the time-integrated gains in $\phi/(P/V)_m$ achieved through the use of the poison for power-density control. Thus the use of a burnable poison in the HFIR appears desirable.

Metal-to-Water Ratio

The metal-to-water ratio in the fuel annulus has an effect on the flux in the island, since fast leakage from the annulus is dependent on the ratio of fuel-to-moderator atom density. Increasing the metal-to-water ratio increases the effective age in aluminum-water mixtures and therefore increases the probability of neutron leakage into the island. There must, of course, be an increase in fuel concentration to compensate for the increased leakage from the fuel annulus. Results of calculations made to determine the magnitude of the effect show that increasing the metal-to-water ratio from 0.8 to 1.0 increases ϕ/P by about 3%. (Both cores used in the calculation had essentially uniform power distribution as a result of using 17 discrete fuel regions. For a single-fuel-region core $(q_{max}/q_{av})_R$ would be a little greater for the core with the larger metal-to-water ratio. Under such circumstances the increase in ϕ/P would be expected to be a little larger than the 3%.)

Because of heat removal requirements the largest metal-to-water ratio considered for the HFIR was 1.0. Even though the thermal-neutron flux in the island is higher for the larger metal-to-water ratios, it may be necessary, after considering the practical aspects of fuel-element fabrication and their effects on the hot-spot and hot-channel factors, to use a metal-to-water ratio less than unity.

A method considered for decreasing the effective metal-to-water ratio, and thus the fuel concentration, without decreasing reactor performance provided a water annulus between two annuli of fuel, each fuel annulus having a metal-to-water ratio of 1. As the thickness of the water annulus was increased, the thickness of the outer fuel annulus was held constant so that the fuel volume increased. Thus, if the addition of the water annulus had no effect other than to increase the fuel-region volume, it would be expected that ϕ/P would decrease and $\phi/(P/V)_m$ would increase with increasing fuel-region volume as shown in Fig. 11. The results presented in Fig. 24 show that there is an optimum water-annulus thickness from the standpoint of minimum fuel concentration and that both ϕ/P and $\phi/(P/V)_m$ decrease with increasing water-annulus thickness. The initial 2% increase in $\phi/(P/V)_m$ results from the lower value of $(q_{max}/q_{av})_R$ associated with the introduction of the water annulus; however, a comparison of cores on a uniform power rather than uniform fuel-distribution basis would not result in the 2% advantage. Thus the presence of a discrete water annulus in the fuel region will, in effect, reduce neutron leakage from the fuel into the water island.

Practical Core-Design Considerations

One of the fuel-element designs proposed for the HFIR consists essentially of an annulus (the fuel annulus) containing nearly radial plates (involute plates). Preliminary calculations indicate that in order for the plates to be sufficiently rigid the width of the plates or thickness of the annulus must be no greater than about 5 cm. Since the proposed HFIR core had a 12-cm-thick fuel annulus, it was decided to investigate cores having a fuel region that was divided into three fuel annuli, each separated by a 1-cm-thick annulus containing aluminum and water but no fuel.

In order to generate the same number of neutrons per unit of core length in the fuel regions of the three concentric annuli without exceeding the maximum permissible power density, it was necessary to increase the over-all fuel-annulus thickness. The greater neutron path length to the island meant less leakage into the island. In an

PREFACE TABLE FOR FIG. 24

Code calculation, Wanda
Cross-sections set, No. 2 (GNU averaged two-group)
Thermal temperature, 80°C

Active core length, 45.72 cm
Axial buckling, 0.002591 cm^{-2}
k_{eff}, 1.205

Region No.	Outer Radius (cm)	Composition
1	7	H_2O
2	13	U-235 + Al + H_2O, M/W = 1
3		H_2O
4	r_3 + 6	U-235 + Al + H_2O, M/W = 1
5	r_4 + 30	Be + 5% H_2O + Exp

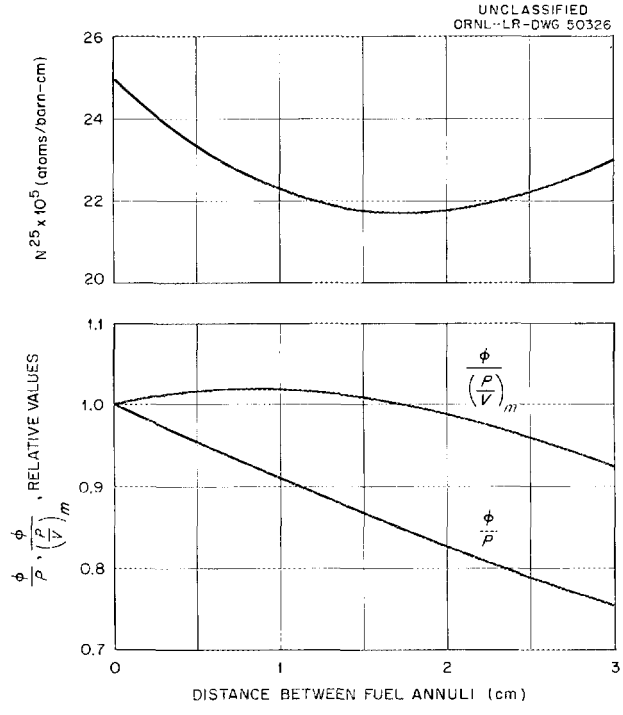

Fig. 24. Thermal Flux per Unit Maximum Power Density and per Unit Power, and U^{235} Concentration vs Thickness of Water Annulus Separating the Two Fuel annuli.

effort to compensate for the greater path length, the metal-to-water ratio in the central fuel annulus was reduced so as to reduce the fuel loading and thereby increase the leakage probability through the two outer fuel annuli. Two difficulties arise: For a fixed minimum plate thickness, decreasing the metal-to-water ratio while retaining plates of the same thickness decreases the heat transfer surface area so that the maximum permissible power density in the central annulus must be reduced proportionately, thus requiring a further increase in fuel-annulus thickness in order to produce the same number of neutrons. The reduced metal-to-water ratio, along with the added coolant water dividing the central annulus from the other two, reduces nonthermal neutron leakage. These effects, however, tend to be compensated by the lower

fuel concentration in the central region, which maintains the proper distribution of power in the three annuli. The net results and a brief description of the core are shown in Table 4. As indicated, decreasing the metal-to-water ratio in the central fuel annulus has essentially no effect on ϕ/P. However, since the region with the lower metal-to-water ratio must operate at a proportionately lower power density than the other fuel regions, the ratio of maximum-to-average power density increases with decreasing metal-to-water ratio, thus resulting in a lower value of $\phi/(P/V)_m$. Therefore, it appeared desirable to design the HFIR core with the same metal-to-water ratio in each of the fuel annuli.

Table 4. Comparison of Cores Which Contain Three Separate Fuel Annuli and Six Discrete Fuel Regions, on the Basis of Different Metal-to-Water Ratios in the Central Fuel Annulus

Region No.	Outer Radius (cm)	Composition			
1	7	H_2O			
2	8	$U^{235} + H_2O + Al$, (M/W = 1)			
3	9				
4	10				
5	11				
6	12	$H_2O + Al$, (M/W = 1)			
7	17	$U^{235} + H_2O + Al$, (M/W = variable)			
8	18	$H_2O + Al$, (M/W = 1)			
9	21	$U^{235} + H_2O + Al$, (M/W = 1)			
10	51	Be + 5% H_2O			
M/W (region 7)			1	0.7	0.5
k_{eff}			1.20	1.20	1.20
ϕ/P, relative			1	0.99	1.01
$\phi/(P/V)_m$, relative			1	0.89	0.69

A comparison of this latter type core with cores containing only one fuel annulus was made on the basis of equal-length cores, equal fuel-region volumes, and essentially uniform radial power distribution, the latter requirement being accomplished through the use of 12 to 17 discrete fuel regions across the entire fuel annulus. Thus for a given power level the average and maximum power densities were the same, making it necessary to compare only values of ϕ_m/P.

Since the two water annuli in the "practical" core design stand as a barrier to nonthermal neutron leakage into the island, it appeared that there would be some advantage in moving the water annuli as far to the outer edge of the entire fuel annulus as the rigidity of the involute fuel plates would permit. Therefore, in addition to making calculations for equal-thickness fuel annuli, calculations were also made for a case in which the outermost fuel annulus was considerably thinner than the other two equal-thickness fuel annuli. Further descriptive information concerning the cores calculated is presented in Table 5a.

The results of the above studies are presented in Table 5. Since the particular cores calculated did not have exactly the same volumes, the appropriate curves in Fig. 11 were used to make the necessary extrapolations. The results indicate that the presence of the two 1-cm-thick aluminum-water annuli in the fuel region decreases ϕ_m/P by about 9%. Moving the radial position of the two aluminum-water annuli, within the limits indicated in Table 5a, had no significant effect on ϕ_m/P.

Table 5. Comparison of Cores with One and Three Fuel Annuli

	Core Identification*			
	A*	B*	C*	D*
Fuel region M/W:	1.0	1.0	0.8	0.8
Number of fuel annuli:	1	3	3	3
Core volumes (fuel regions):				
For calculation, liters	44.8	48.3	48.3	41.5
Extrapolated to	44.8	44.8	44.8	44.8
$(q_{max}/q_{av})_R$	1.100	1.155	1.125	1.132
ϕ_m/P, relative	1.0	0.91	0.88	0.88

*See Table 5a for detailed description of cores.

Table 5a. Reactor Characteristics for Cores with One and Three Fuel Annuli

Code calculation, WANDA
Cross-section set, No. 2 (GNU-averaged, two-group)
Thermal temperature, 80°C

Active core length, 45.72 cm
Axial buckling, 0.002591 cm^{-2}
k_{eff}, 1.20

Region No.	Outer Radius (cm)	Composition	N^{25}
A. One Fuel Annulus (M/W = 1)			
1	7	H_2O	
2 to 7	7.5 to 10 (1/2-cm increments)	U-235 + Al + H_2O, M/W = 1	Distribution not determined specifically for k_{eff} = 1.20
8 to 14	11 to 17 (1-cm increments)		
15	17.5		
16	18		
17	18.5		
18	19		
19	49	Be + 5% H_2O + Exp	
B. Three Equally Thick Fuel Annuli (M/W = 1)			
1	7	H_2O	
2	8	U-235 + Al + H_2O, M/W = 1	Distribution not determined specifically for k_{eff} = 1.20
3	9		
4	10		
5	11		
6	12	Al + H_2O, M/W = 1	
7	13	U-235 + Al + H_2O, M/W = 1	
8	14		
9	15		
10	16		
11	17	Al + H_2O, M/W = 1	
12	18	U-235 + Al + H_2O, M/W = 1	
13	19		
14	20		
15	21		
16	51	Be + 5% H_2O + Exp	

C. Three Equally Thick Fuel Annuli (M/W = 0.8).
Same as above except the metal-to-water ratio in the fuel regions was 0.8 instead of 1.0.

D. Two Equally Thick Fuel Annuli, the Third One Thinner (M/W = 0.8)			
1	7	H_2O	
2 to 10	7.5 to 11.5 (1/2-cm increments)	U-235 + Al + H_2O, M/W = 0.8	Distribution not determined specifically for k_{eff} = 1.20
11	13	Al + H_2O, M/W = 1.0	
12 to 16	14 to 18 (1-cm increments)	U-235 + Al + H_2O, M/W = 0.8	
17	19	Al + H_2O, M/W = 1.0	
18	19.5	U-235 + Al + H_2O, M/W = 0.8	
19	20	Same as above	
20	50	Be + 5% H_2O + Exp	

Beryllium Side-Reflector Thickness

The thickness of the light-water-cooled beryllium side reflector selected for the HFIR was based on reactivity requirements and availability of space for experiments requiring unperturbed thermal-neutron fluxes in the range of about 2×10^{14} to 1×10^{15} neutrons/cm^2-sec. Calculations for determining the reflector thickness were made assuming that the beryllium contained 5% by volume of light water and sufficient thermal poison to represent experiments worth 2% in reactivity. In all cases the beryllium was surrounded on its outer periphery by an essentially infinite secondary reflector of water. The results of the calculations are presented in Fig. 25. As indicated, a 20- to 25-cm-thick beryllium reflector results in a neutron multiplication factor about 0.1% less than was obtained with an infinite thickness of beryllium. However, a portion of the beryllium reflector volume is to be occupied by beam and rabbit tubes, so a greater thickness was considered desirable. Figure 25 also shows that the maximum thermal flux in the side reflector was obtained with only light water in the reflector region. For beryllium thicknesses greater than about 10 cm the maximum flux in the reflector was essentially constant and about 50% less than for the all-water reflector. Actually, the variation in flux shown in Fig. 25 is

PREFACE TABLE FOR FIG. 25

Code calculation, Wanda
Cross-section set, No. 1
Thermal temperature, 80°C

Active core length, 30.5 cm
Axial buckling, 0.004568

Region No.	Outer Radius (cm)	Composition
1	2	100 g Pu-242 + Al + H_2O, M/W = 1, (g Al)/(g Pu) = 5
2	7	H_2O
3	18	U-235 + Al + H_2O, M/W = 1, N^{25} = 40×10^{-5} atom/barn-cm
4		H_2O or Be + 5% H_2O + Exp
5	68	H_2O

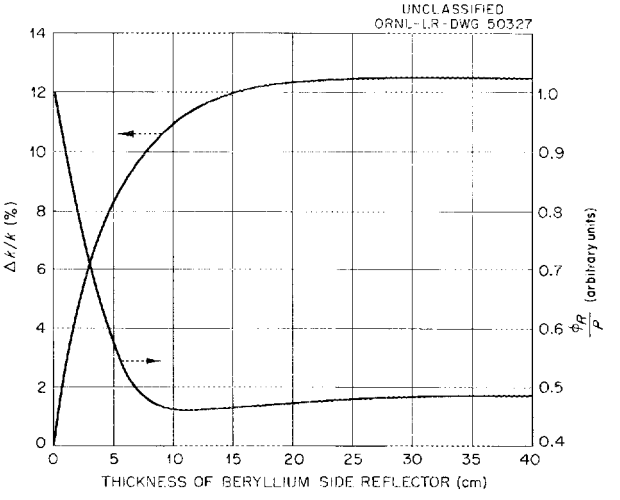

Fig. 25. Per Cent Change in Reactivity and Maximum Thermal Flux in Beryllium-Water Side Reflector per Unit of Power vs Thickness of Beryllium in Reflector.

somewhat exaggerated since the fuel concentrations were the same in all calculations; as indicated previously, increasing the fuel concentration, as would be necessary for the cores having thinner beryllium reflectors, decreases neutron leakage from the fuel region and therefore decreases the thermal flux in the reflectors. Furthermore, a comparison of thermal fluxes integrated over a volume extending 50 cm radially beyond the fuel region indicates that the volume-averaged thermal fluxes are approximately the same regardless of the beryllium thickness. Thus a 30-cm-thick beryllium side reflector was tentatively specified for the HFIR.

Target Size, Weight, and Heat Removal Considerations

The maximum amount of Cf-252 is produced in a given period of time when the volume-integrated product of neutron flux and density of Pu-242 in the target is a maximum. Increasing the weight of plutonium in the target will reduce the average thermal flux in the target; thus there is an optimum weight of Pu-242 associated with a given size target. For a given weight of Pu-242 and a given length target, there is also an optimum diameter for the target since concentrating the plutonium at the center depresses the thermal flux severely, while dilution of the given weight of feed material by increasing the target diameter eventually extends the outer portions of the target into the comparatively low thermal-flux regions of the island near the fuel annulus.

In order to provide adequate heat transfer surface area for the target, the plutonium oxide feed material was homogenized with aluminum. Thus the homogenized target used in the calculations contained water as coolant and moderator, aluminum, and plutonium oxide, the volume ratio of aluminum to plutonium oxide being maintained at 19.

Before determining the optimum weight of Pu-242 for a particular core, it was necessary to calculate the optimum target diameters for several weights of Pu-242. Figure 26 shows the results obtained for a reactor having an active core length and a target length of 45.72 cm, a fuel-annulus thickness of 12 cm, and an island radius of 7 cm. For this particular case the optimum target radius ranged from 3.3 cm for 50 g of Pu-242 to 5.3 cm for 300 g. (Optimum target diameters were also determined for several other combinations of plutonium weight, core diameters, and core lengths, as indicated previously under the topic heading "Fuel-Annulus Thickness and Length;" the results were then used in the calculations that led to the curves in Fig. 11). Knowing the average thermal flux associated with a particular weight and size target, it was then possible to estimate Cf-252 production as a function of Pu-242 weight; Fig. 27 shows the total production of Cf-252 for one-year exposures at flux levels determined from Fig. 26 assuming a power level of 100 Mw.

When making the above calculations, it was assumed that the plutonium plus the subsequent transplutonium isotopes had an average microscopic cross section of 60 barns and an effective atomic mass of 242 amu. Actually, the thermal cross section of the target changes with time and is a function of the thermal-flux level. Therefore, when optimizing the weight of the plutonium feed material and the dimensions of the target on the basis of maximum total production of Cf-252 in a given period of time, it is desirable to use a time-averaged cross section in the calculations. The curve in Fig. 30, which neglects nonthermal irradiation effects, implies that the production of Cf-252 from Pu-242 is dependent on the product of neutron flux and time rather than on just the flux. If it is assumed that the optimum irradiation period is also dependent on ϕt, then the average cross section of the target should be based on the particular value of ϕt rather than on time alone. Figure 28 gives effective instantaneous, time-averaged, and flux-time-averaged thermal cross sections for the plutonium feed material (neglecting nonthermal irradiation) as a function of time and

PREFACE TABLE FOR FIG. 26

Code calculation, Wanda
Cross-section set, No. 2 (GNU averaged two-group)
Thermal temperature, 80°C

Active core length, 45.72 cm
Axial buckling, 0.002591 cm^{-2}
k_{eff}, ~1.20

Region No.	Outer Radius (cm)	Composition
1		Pu-242 + Al + H_2O, (g Al)/(g Pu) = 5
2	7	H_2O
3	19	U-235 + Al + H_2O, M/W = 1, $N^{25} \cong 25 \times 10^{-5}$ atom/barn-cm
4	49	Be + 5% H_2O + Exp

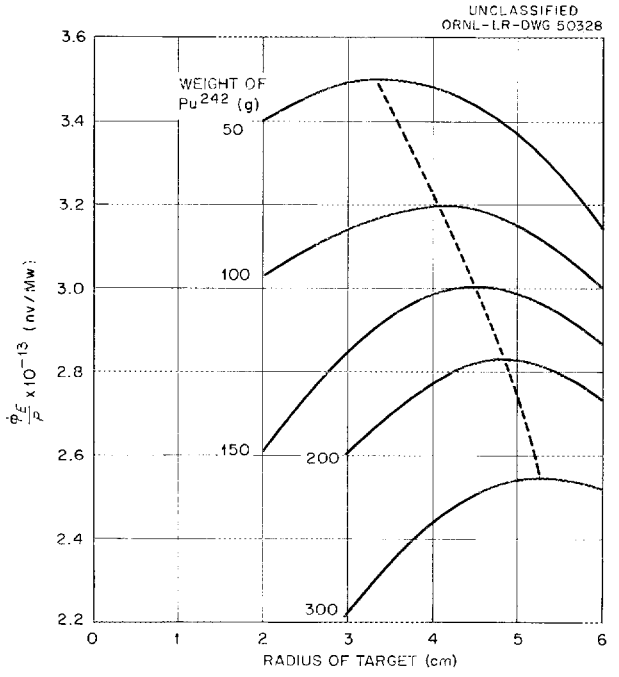

Fig. 26. Average Thermal Flux in the Central Target vs Weight of Pu^{242} Feed Material and Radius of Target.

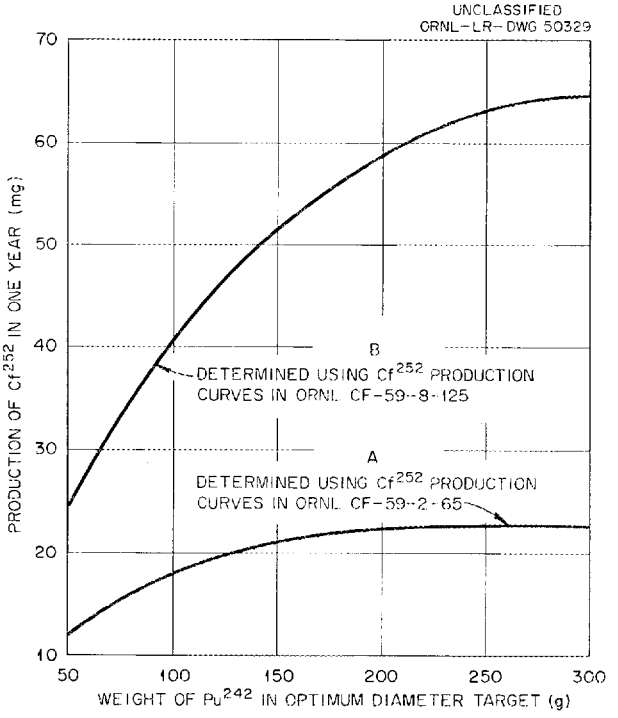

Fig. 27. Production of Cf^{252} from Pu^{242} for a One-Year Period vs Weight of Pu^{242} Feed Material.

flux level. Assuming a target exposure of about 3×10^{15} nv-yr, the time-averaged cross section appears to be about 56 barns for flux levels ranging from 1.5×10^{15} to 5×10^{15} nv. Therefore the optimum target size shown in Fig. 26 should be nearly independent of the flux level.

The method of determining the optimum weight of the Pu-242 feed material is somewhat ambiguous because in general it requires detailed and accurate information concerning the time- and space-averaged neutron fluxes and the production rates of Cf-252 from Pu-242, both of which are interrelated and uncertain. In order to obtain an estimate of the optimum weight, it was assumed that only the thermal flux contributed significantly to californium production, and that the appropriate average fluxes were those given in Fig. 26 for the optimum target diameters. The production of Cf-252

from Pu-242 feed material can then be estimated from Figs. 29 and 30. Using Fig. 30 in preference to Fig. 29,* the optimum weight of Pu-242 was estimated to be about 300 g, as indicated by curve B in Fig. 27. If the shape of the curve in Fig. 30 is reasonably correct, and since it is nearly a straight line in the region of interest, the optimum weight would be insensitive to variations in the thermal-flux level, thus alleviating to some extent the need for an accurate determination of the effective average flux during target exposure.

In the above analysis only thermal irradiation of the plutonium feed material was considered. Recently, a report[10] has been issued which discusses the contribution of nonthermal neutron irradiation to transplutonium isotope production. Under certain conditions the contribution is definitely significant. Therefore further studies might possibly indicate a different optimum weight, depending on the ratio of thermal to nonthermal flux in the target.

The above values of optimum diameter and weight of the target were based on an island radius of 7 cm (that proposed for the HFIR). It is possible that a larger island would result in greater californium production, since increasing the island diameter tends to maintain adequate neutron moderation as the weight and therefore volume of the target is increased. Of course this would result in a decrease in the

*The results in Fig. 29 represent an early estimate of californium production and are now considered less accurate than those in Fig. 30. Since the latter results were not available until after the parameter studies were made, an effective optimum weight of 200 g, as determined from curve A in Fig. 27, was used in the parameter studies and target heat transfer studies. Curve B, however, indicates a significant increase in production if a 300-g target is used.

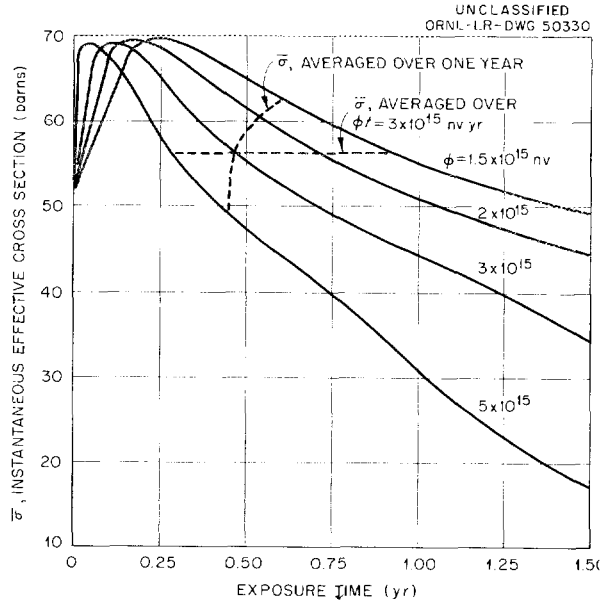

Fig. 28. Instantaneous Effective Microscopic Thermal Cross Section of Target When Starting with Pu^{242} vs Thermal-Neutron Exposure Time and Thermal-Flux Level. (Extracted from supplementary data to ORNL CF-59-8-125.)

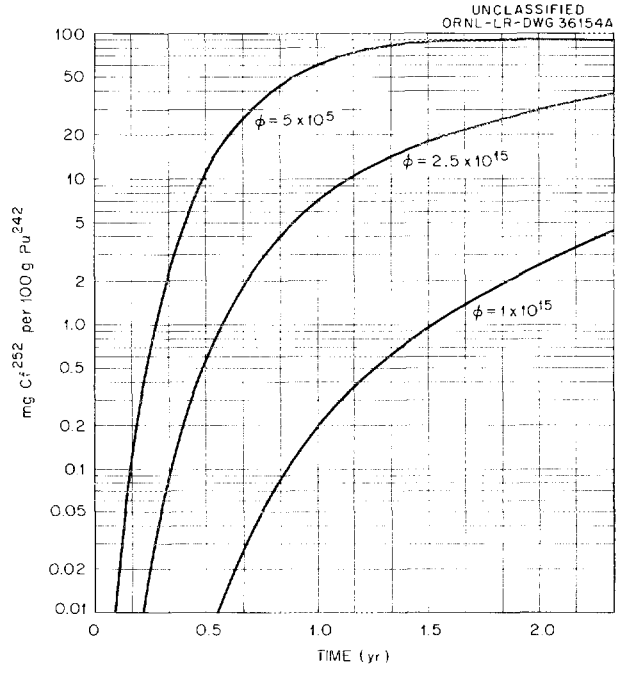

Fig. 29. Production of Cf^{252} from Pu^{242} (an Early Estimate).

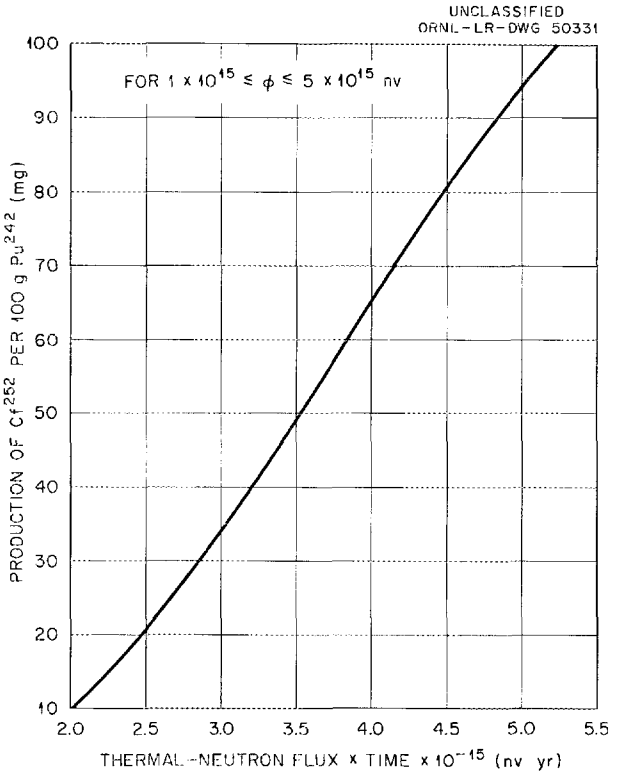

Fig. 30. Production of Cf^{252} from Pu^{242} vs Product of Thermal Flux and Time. (Extracted from supplementary data to ORNL CF-59-8-125.)

unperturbed thermal flux in the island, and therefore it is not planned at present to increase the island radius.

When selecting the weight of plutonium to be irradiated, it is also necessary to consider the problem of heat removal. Several of the isotopes in the chain connecting Pu-242 and Cf-252 are fissionable, requiring that provisions be made for removing appreciable amounts of heat from the target material. The estimated heat generation rate in the feed material as a function of time and average thermal-flux level is shown in Figs. 31 and 32. With the reactor operating at 100 Mw, the target containing 200 g of Pu-242 feed material, and assuming that the maximum thermal flux (Fig. 26) and the maximum heat generation rate (Fig. 32) occur simultaneously, the volume-averaged maximum heat generation rate in the feed material, during the one-year irradiation cycle, was about 460 kw. The validity of the assumption in connection with the time-wise occurrence of the maximum flux and target power can be substantiated by superimposing the cross-section curves in Fig. 28 on the heat generation curves in Fig. 31, and observing that for each flux level the instantaneous cross section that occurs simultaneously with the maximum heat generation rate is about 60 barns. Since the curves in Fig. 26 are based on a 60-barn cross section, the method of arriving at the 460-kw heat generation rate should be reasonably accurate. However, this value is based on the assumption that the target is exposed to a constant flux level at least up to the time the maximum heat generation rate is reached. Since the reactor will probably be operated at constant power, and since for a given cross section in the feed material the flux in the target does not change appreciably with time, the flux in the actual target will change with time in accordance with the change in feed-material cross section.

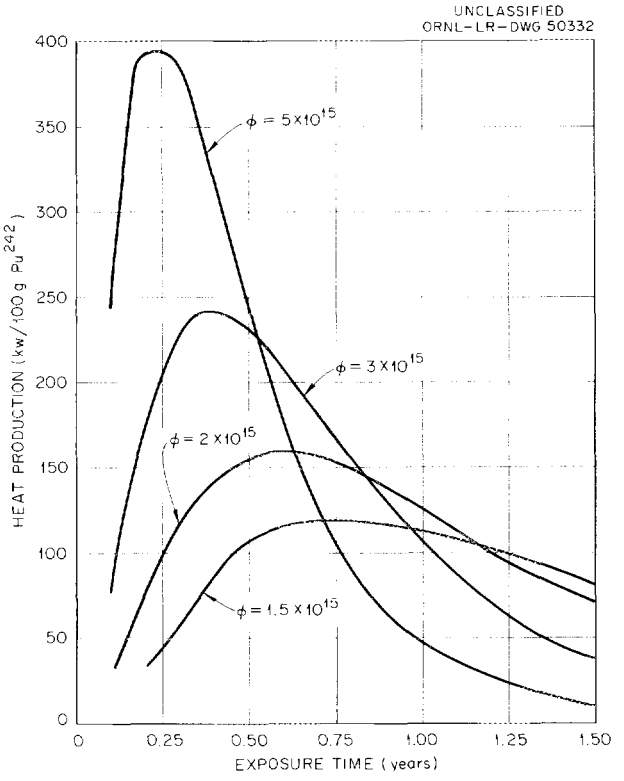

Fig. 31. Power Generation in Target, When Starting with Pu^{242} Feed Material and Considering Only Thermal-Neutron Irradiation vs Exposure Time and Thermal-Flux Level. (Extracted from supplementary data to ORNL CF-59-8-126.)

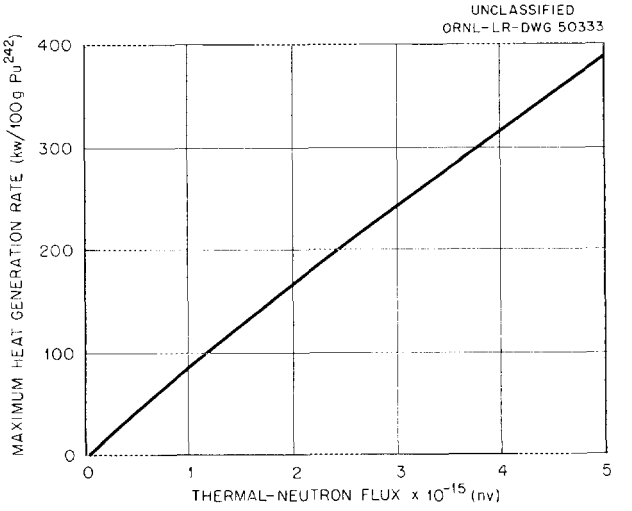

Fig. 32. Maximum Heat Generation Rate in Target, When Starting with Pu^{242} Feed Material and Considering Only Thermal-Neutron Irradiation vs Thermal-Flux Level.

The effect this has on heat generation and production has not yet been studied in detail. However, it is interesting to note that dividing the maximum heat generation rate for each flux level by the corresponding flux level gives essentially the same effective macroscopic fission cross section. As indicated by Fig. 28, the maximum total cross sections are also about the same. This tends to indicate that small variations in flux with time will not significantly affect the maximum heat generation rate as determined from Figs. 31 and 32.

The 460-kw heat generation rate obtained from the above analysis was somewhat greater than estimated at the time the volume ratio of aluminum to plutonium oxide was selected as 19. In order to reduce the maximum heat flux to a tentatively acceptable value of 1×10^6 Btu/hr-ft^2, the volume ratio of aluminum to plutonium oxide was increased from 19 to about 26. The resultant increased displacement of water from the target in the island will harden the neutron energy spectrum and thus decrease the heat generation slightly. The net effect on Cf-252 production, considering the nonthermal contribution, has not yet been determined.

In estimating the target heat generation rates, the neutron flux values (Fig. 26) were determined by a two-group diffusion calculation; these fluxes are about 20% lower than those predicted by a more sophisticated multigroup calculation. Assuming the latter calculation to be more accurate, the heat generation rate in a 200-g target would be about 540 kw. For the 300-g target the corresponding heat generation rate would be about 740 kw.

The high power densities associated with the optimum-size targets introduces a problem in connection with the selection of the target cladding and matrix materials. The optimum diameter of the experiment is such that with 200 g of feed material and an aluminum-to-plutonium-oxide volume ratio of 26 the metal-to-water ratio is only about 0.3. Therefore, nuclearwise there is not much difference between the use of aluminum, beryllium, and zirconium for the target matrix and cladding material. However, the thermal conductivity of aluminum is about three times that of beryllium and twenty-three times that of zirconium. Using a solid 3/8-in.-diameter aluminum matrix rod, the maximum temperature drop in the rod would be about 43°F as compared to 124°F for a beryllium rod and 1000°F for a zirconium rod.

CONTROL STUDIES

The maximum achievable neutron flux in the HFIR is limited by the maximum permissible heat flux; and, generally speaking, the closer the core-averaged heat flux to the maximum heat flux, the higher the island neutron flux will be. Thus a prime requirement for the HFIR was that the control system should not increase the ratio of maximum-to-average power density above a certain specified value during full-power operation of the reactor. Actually, a maximum value of (q_{max}/q_{av}) was not initially specified; instead, several control schemes were studied in order to determine practical limits for power-distribution control. In these studies the effects of nonuniform fuel burnup, time-wise distortion of power distribution resulting from possible xenon instability, and flux variations due to experiments were considered in addition to the characteristics of the particular control system.

Two basic types of control systems were considered for the HFIR: (1) a soluble-poison system and (2) the more conventional mechanical control system. The soluble-poison system had the advantage of being able to maintain uniform distribution of poison in a particular region, but had the immediate disadvantage of not having an extensive backlog of practical application in reactor control. Various mechanical control systems are also capable of maintaining symmetry to some extent; however, the more conventional systems cause very significant variations in power distribution. Therefore it was necessary to investigate advanced control-scheme concepts for the HFIR, and the decision was made to study both the soluble-poison and mechanical systems.

As the studies of the soluble-poison and mechanical systems progressed simultaneously, it became apparent that a reasonably conventional mechanical system could be designed for the HFIR that would provide adequate control of reactivity and power distribution. It also became apparent that the soluble-poison system not only introduced difficult problems such as gas formation in the solution and radiation effects on solubility, for which little experience exists, but that it was also sufficiently slow acting to require a supplementary mechanical control system for emergency shutdown and possibly for fine control. Thus the control studies indicated that an all-mechanical system should be used in the HFIR. Although the following discussion on controls includes only the particular system presently proposed for the HFIR, a discussion of other control systems that were studied in some detail is included in Appendix 3.

Results from the various control-scheme studies indicated that the proper location for the control region was a narrow annular space between the fuel annulus and the beryllium side reflector. After completing preliminary nonuniform-fuel-burnup calculations for a core having soluble poison in this annulus, it became apparent that it would be necessary, even with a soluble poison system, to tolerate a significant depression in power density close to the control region at the beginning of the fuel cycle. Thus, during the early part of a fuel cycle, a limited amount of circumferential and/or axial power distortion in that vicinity, resulting from the use of plate or closely-spaced rod-type control elements as opposed to the soluble poison, could be tolerated without exceeding the maximum permissible power density.

As the end of the fuel cycle is approached, the power density near the control region increases toward, and perhaps beyond, the average. Therefore disturbances caused by the control elements would have to diminish sufficiently by the end of the fuel cycle to maintain the power density within allowable limits. It appeared that

it would be possible to achieve this goal through the use of a control plate that would completely surround the fuel-region outer circumference, and that would extend the full length of the fuel region with the core clean and critical. The conventional method of withdrawing the controls from only one end of the core results in an axial maximum-to-average power density ratio that is of the order of two or three to one. If, however, the cylindrical control plate is split at the horizontal midplane and each half withdrawn from its respective end of the core, the variation in power distribution is much less. A further improvement is made by extending each half shell over the full length of the core so that at the beginning of the fuel cycle the control region consists of two thin, concentric cylinders, each extending the core length or a little more when criticality is reached. After about half of the reactivity has been burned up, the control plates are end to end, forming a complete and uniformly thick cylinder around the core. To eliminate the off-set vacancies that would fill with water and cause power-density peaking, core-length extensions of beryllium or zirconium would be added to the appropriate end of each cylinder. At the other end of each cylinder an emergency shutdown ("black") section would be attached. Thus each of the two control plates would be about three core lengths long and would consist of three equal-length vertical sections: black, gray, and white. A schematic representation of this control scheme is shown in Fig. 33.

At the beginning and, of course, at the end of a fuel cycle the above control scheme would satisfy the requirement of minimum axial and circumferential power-distribution disturbances. However, as the rods are withdrawn to compensate for fuel burnup, a step appears in the total thickness of the gray plates and remains until the ends of the gray plates meet. Beyond this point another step appears, leaving a neutron window at the center of the core. Thus a further improvement in power-distribution control could be achieved by gradually varying the poison concentration in each plate from one end to the other, the length of the poison taper being sufficient to maintain power-density peaking within tolerable limits. The necessary length of the plates would depend to a large extent on how much reactivity must be controlled; thus the use of a burnable poison in the fuel region would reduce the length of, and possibly alleviate the need for, the tapered design.

As a first step in the detailed investigation of the plate-type control system, two-dimensional fuel-cycle-time calculations (which included nonuniform burnup of the fuel) were made for a typical HFIR core equipped with the untapered plates (as shown in Fig. 33). The results of these calculations are discussed in detail under the topic heading "Fuel-Cycle Analysis." In summary, the results show that for a ten-day core

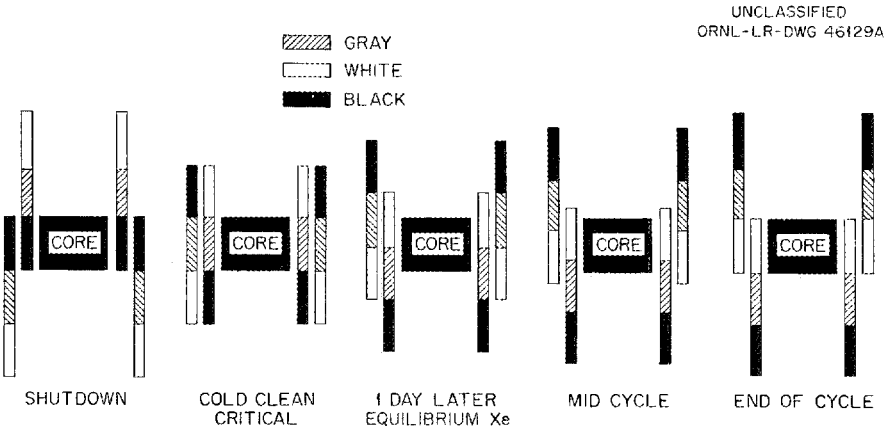

Fig. 33. HFIR Control-Scheme Schematic Diagram.

initially having about 13% reactivity (with burnable poisons present) the maximum power density at no time exceeds the permissible value. Therefore it appeared that tapering of the poison was unnecessary.

Further control-system studies were concerned with the reactivity worth of the gray and black regions of the control plates and the selection of materials for the neutron absorbers. Fuel-cycle-time calculations indicated that for 1/4-in.-thick control plates a thermal absorption cross section of about 0.3 cm^{-1} would be required for the gray sections. Comparatively-low-cross-section materials such as titanium, nickel, and possibly a stainless steel alloyed with manganese appear satisfactory for this application. Small amounts of high-cross-section materials should not be used in the gray plates because they will burn out too rapidly. (Assuming only one significant poison isotope for each element and no successive production of significant poison isotopes that would prolong the poison life, the fraction of poison atoms remaining at the end of one year at a thermal flux of 5×10^{14} neutrons/cm^2-sec is determined from N [one year] /N [initial] = $e^{-\sigma_a \times 0.015/\text{barn}}$.) The maximum significant isotopic cross section of the above-mentioned materials is 13 barns (Mn^{55}). Its concentration is reduced by about 20% in one year when exposed to a thermal flux of 5×10^{14} neutrons/cm^2-sec. From a practical point of view it would appear that a reasonable limit on cross section would be about 20 barns. For a 100-barn cross section only 20% of the poison would be left after a one-year exposure at 5×10^{14} flux.

The desired reactivity worth of the black sections of the control plates depends upon the type of reactivity accidents that might occur, how fast the plates can be inserted, and upon what fraction of the control surface area can always be inserted. In this particular study only the statics of the HFIR control system were considered.

In the event of an emergency shutdown of the HFIR only the upper control cylinder, which is accelerated by both gravity and coolant flow, will be actuated rapidly. To further improve the reliability of the emergency system, the upper cylinder will be divided into four segments since it is more likely that three out of four plates will drop during an emergency shutdown than one out of one. During the control-system studies it was assumed that the lower control cylinder was also divided into four segments, and that the lower and upper segments overlapped each other in the circumferential direction by 45 degrees. (At the time the calculations were being performed, this scheme was in keeping with practical design considerations.)

Usually during a scram only small amounts of reactivity are involved, so that very little insertion of the control plates is required to compensate for the reactivity addition. However, incidents could occur which involve larger reactivity additions. For the purpose of estimating the required reactivity worth of the black plates, two specific accidents were considered: (1) inadvertent exclusion of burnable poison from a new core, and (2) at the beginning of a cycle one of the four lower sectors falls, leaving a white sector in the core as shown in Fig. 34. In the case of the first accident, it was assumed that both black cylinders would be fully inserted at the time the fuel was placed in the core. Under these circumstances the reactivity worth of the control region in a typical HFIR core can be estimated from Fig. 35, which gives k_{eff} as a function of boron or cadmium concentration in a 2-cm-thick annular control region. (Figures 36 and 37 are supplementary curves that will be discussed in greater detail in Appendix 3.) For boron, these results indicate that in order to maintain the reactor subcritical under the conditions of no burnable poison in the core, the minimum required thermal cross section for two 1/4-in.-thick plates would be approximately 3 cm^{-1}.

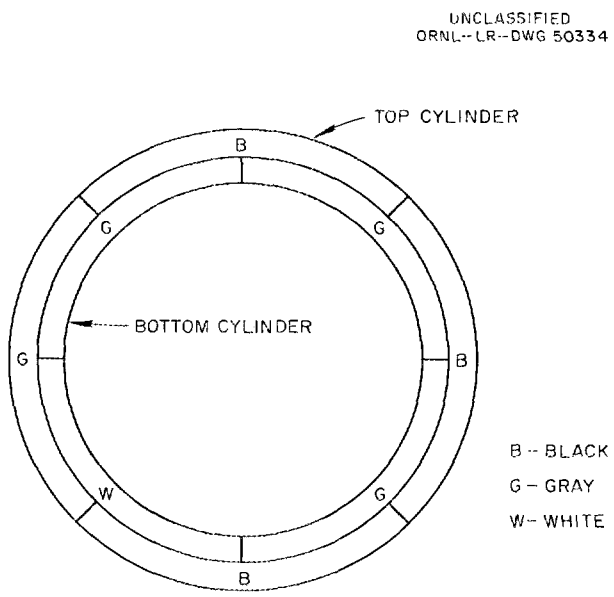

Fig. 34. Circumferential Position of Control-Plate Sectors When One of the Four Bottom Sectors Falls Out and Only Three of the Four Top Black Sectors Insert.

To investigate the second anticipated accident, a two-dimensional calculation in r, θ geometry was made using an absorption cross section of about 3 cm^{-1} in the 1/4-in.-thick black regions and 0.4 cm^{-1} in the gray regions. A burnable poison was added uniformly to the fuel region to reduce k_{eff} from 1.22 to 1.15. Without the burnable poison in the fuel, all the black plates inserted reduced k_{eff} from 1.22 to 0 98; with the burnable poison in, k_{eff} was reduced to 0.92. For the particular situation described by accident (2), k_{eff} was reduced from 1.15 to 0.96. Thus it appears that the control plates described above will have adequate reactivity worth for the HFIR.

An absorption cross section of 3 cm^{-1} in the black control plates does not, however, leave much allowance for poison burnup. To compensate for boron burnup during a one-year exposure at an average thermal flux of 10^{13} neutrons/cm^2-sec, the initial absorption cross section would have to be increased to approximately 10 cm^{-1}. About the only practical method of obtaining this high a cross section in a structural material is by incorporating, by some means, a small amount of a comparatively-high-cross-section element in the structural material. The conventional absorbers, boron and cadmium, have certain disadvantages that make their use in the HFIR questionable. The required concentration of boron-10 in a boron-Zircaloy alloy would be about 0.7 wt %, thus probably requiring the use of enriched boron, since alloying is limited to about 2 wt %.[13] During normal operation of the HFIR, the thermal nvt accumulated in one year by the end of the black rod is approximately 3×10^{20}. This results in about 70% burnup of the B^{10} atoms or 7 at. % (0.5 wt %) of the alloy. For boron-titanium and boron-stainless steel alloy the weight per cents and atom per cent burnups are somewhat greater. According to Dunning,[13] these boron alloys are limited to about 2 at. % burnup, and, furthermore, the corrosion resistance of irradiated boron alloys in zirconium or Zircaloy-2 is such that exposure of the meat alloy to high-temperature water would cause a catastrophic failure.

PREFACE TABLE FOR FIGS. 35, 36, AND 37

Code calculation, GNU
Cross-section set, GNU 34 groups (ORNL revised set)
Thermal temperature, 80°C
Active core length, 45.72 cm
Axial buckling, 0.002591 cm^{-2}

Other dimensions and compositions are the same as on preface table for Fig. 12 except that region 18, for Figs. 35, 36, and 37 contained varying amounts of either natural boron or cadmium.

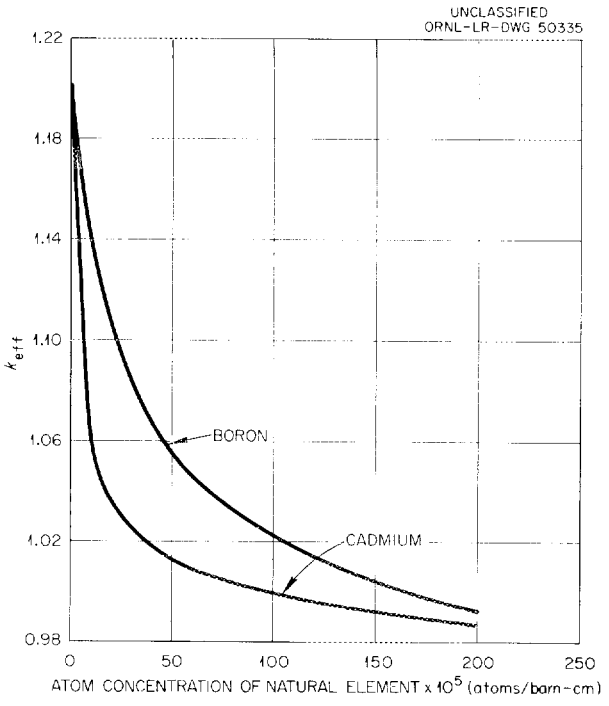

Fig. 35. Reactivity Worth of Natural Boron and Cadmium in the Annular Control Region of the HFIR.

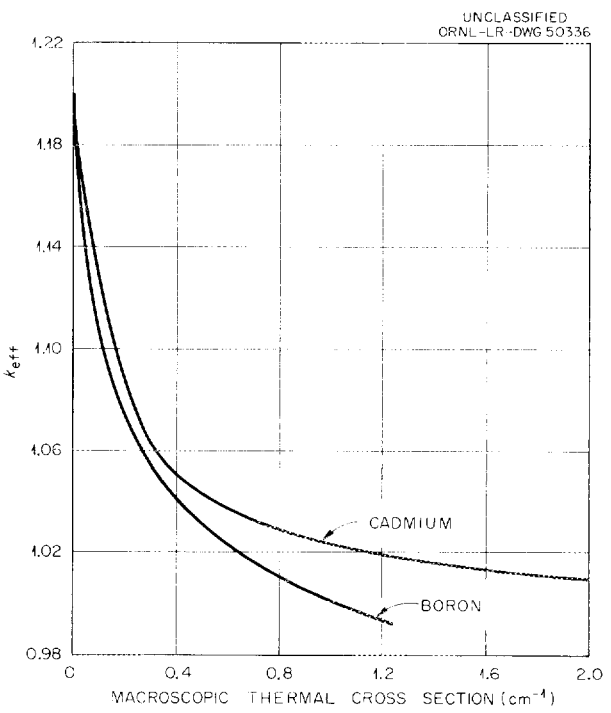

Fig. 36. Reactivity vs Macroscopic Thermal Cross Section of Annular Control Region for Natural Boron and Cadmium Poisons.

The use of boron carbide has been considered for reactor control applications because of its ability to retain a significant portion of helium in the B_4C lattice structure. Barney[14] reports 50% B^{10} burnup for 2.43 wt % B_4C dispersed in zirconium without dimensional instability. Similar results were reported for B_4C in Al_2O_3. However, it was generally concluded that it would be necessary to provide a venting system for the helium that is not retained in the B_4C or matrix; this could lead to undesirable design complications and reduced reliability.

The use of a solid cadmium plate clad with Zircaloy or stainless steel was considered as a possibility for the HFIR; however, in addition to having poor resonance capture, cadmium has a comparatively high isotopic absorption cross section that could result in excessively fast burnup. (A thermal nvt of 3×10^{20} results in about 98% burnup of the absorbing atoms.)

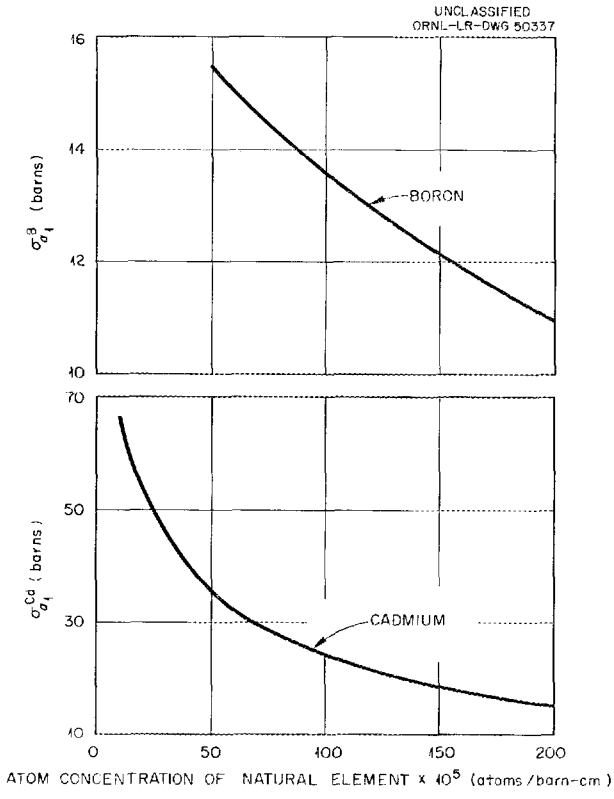

Fig. 37. Fast-Group (5.5 KT to 10^7 ev) Microscopic Cross Sections of Natural Boron and Cadmium vs Their Concentration in the Annular Control Region.

One poison material that looks promising for the black region is Eu_2O_3. Europium has a good resonance structure and has a successive capture scheme that prolongs its life beyond that of both boron and cadmium. The reaction paths of importance for capture, when starting with elemental europium, are shown in Fig. 38. Considering only the thermal cross sections and a time-averaged thermal-neutron flux of 1×10^{13} at the black-gray intersection of the control rod, solution of the necessary time-dependent isotope equations reveals that the macroscopic absorption cross section would be reduced by about 69% by the end of one year. The variation of the cross section with time up to one year is shown in Fig. 39. To compensate for burnup of the europium chain to the extent of providing an acceptable cross section after an accumulation of 3×10^{20} nvt, it would be necessary to start with approximately three times the amount required to provide the above minimum acceptable cross section. If cadmium were used, fifty times the minimum amount would be required initially.

Of course, the life of a poison region can be extended by making the region thicker and thus by taking advantage of self-shielding. One important limitation on this scheme is heat removal from the control plates. Since the plates are very close to the fuel annulus, the neutron and gamma heating will be very high.

A possible alternative or supplementary method for retaining sufficient poison cross section in the black regions would be to provide a separate neutron shield above and below the core to reduce the thermal flux in the black region when the core is at power. A preliminary analysis not reported herein indicates that even without the

UNCLASSIFIED
ORNL-LR-DWG 50338

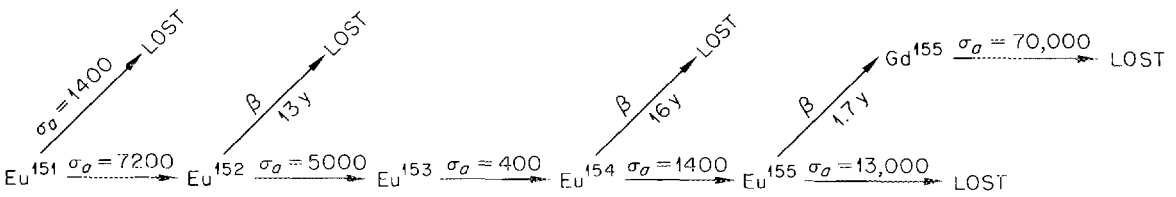

Fig. 38. Reaction Paths for Europium.

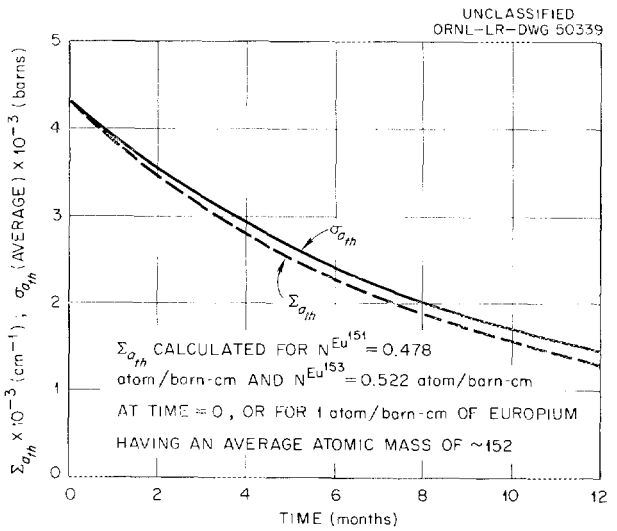

Fig. 39. Variation of Europium Thermal Cross Section with Time at $\phi_{th} = 1 \times 10^{13}$ nv.

shield the necessary amount of Eu_2O_3 can be incorporated in a 1/4-in.-thick plate of conventional reactor structural material such as a zirconium alloy.

On the bases of the calculations and results described herein, it is tentatively concluded that the plate-type control system as described will be satisfactory for the HFIR. If one assumes that adequate protection against accidental excessive reactivity addition can be achieved through the use of traverse stops or similar devices, then the composite plate system could be used for regulation as well as shim and safety control. This is presently being proposed for the HFIR.

FUEL-CYCLE ANALYSIS

From the viewpoint of isotope production the HFIR core life should be that which produces a product such as californium at the lowest possible cost, consistent with the time allowed for the production of a desired quantity of the product. Optimization of the fuel cycle on this basis requires detailed and accurate information on production and processing schemes for the particular isotopes and information on refueling down time. Increasing the length of the cycle will decrease the total down time per year; however, the associated increase in fuel loading would result in a lower thermal flux in the island target and an increase in reactivity control requirements. Increasing the amount of control poison to compensate for the additional reactivity would also contribute to a flux reduction, as a result of an associated increase in the ratio of maximum-to-average power density if the poison is added to the annular control region, or as a result of a decrease in neutron leakage from the fuel region to the island if the poison is added to the fuel region as a burnable poison. Thus, independent of other considerations there exists a fuel-cycle time for maximum total isotope production over a specified period of time and another fuel-cycle time for minimum isotope unit production cost.

Another important consideration affecting the core life is fuel-plate corrosion. Information available to date[15,16,17] indicates that under the proposed HFIR operating conditions a 10-day cycle may approach the practical duration for aluminum plates. From an operational point of view, a 14-day cycle appears preferable, and perhaps later studies will reveal conditions that will permit the longer cycle. However, on the basis of present corrosion data and on the premise that the optimum fuel-cycle times associated with isotope production are greater than 10 days, it was concluded that the first HFIR core should be designed for a 10-day cycle. Such a design will result in a satisfactory unperturbed thermal-flux level (about 5×10^{15} nv) in the island and in the production of reasonable quantities of Cf-252.

During the early stages of the reactor calculations it was estimated, using two-group results, that a core initially having 18% reactivity (with all control poisons removed) would have a 10-day fuel cycle and would produce an unperturbed thermal flux in the island of about 5×10^{15} at 100 Mw. Therefore, nearly all the clean-core calculations performed in the parameter studies were based on $k_{eff} = 1.20$ with no controls present. After a core design had been selected on the basis of the parameter studies, fuel-cycle-time calculations were made using a two-group, one-dimensional model. The core that was selected had a fuel annulus that was divided into 17 fuel regions, the purpose being to simulate a continuous radial fuel distribution. The large number of regions also facilitated consideration of nonuniform fuel burnup in the radial direction. Reactivity was controlled by a uniform poison region between the fuel annulus and the outer reflector, the poison concentration being adjusted at each time step to maintain $k_{eff} = 1$. The power level was maintained at 100 Mw.

For the first fuel-cycle-time calculation, the radial fuel distribution was such as to provide a uniform radial power distribution in a clean core with no controls. The results of these calculations are shown in Figs. 40, 41, and 42. In Fig. 40 the value of k_{eff} represents the potential reactivity; the thermal poison cross section represents the value required to maintain $k_{eff} = 1$. With an initial $k_{eff} = 1.184$ the fuel-cycle time was approximately 10 days. The results in Fig. 41 show that the ratio of maximum-to-average power density in the radial direction decreased from 1.36 at

PREFACE TABLE FOR FIGS. 40, 41, AND 42

Code calculation, Candle
Cross-section set, No. 3 (GNU averaged, two-group)
Thermal temperature, 80°C

Active core length, 45.72 cm
Axial buckling, 0.002591 cm^{-2}

Region No.	Outer Radius (cm)	Composition	$N^{25} \times 10^5$, (atom/barn-cm)
1	7	H_2O	
2	7.5	U-235 + Al + H_2O, M/W = 1	10
3	8		11.5
4	8.5		13.2
5	9		14.9
6	9.5		16.8
7	10		18.6
8	11		20.7
9	12		24.0
10	13		26.9
11	14		28.9
12	15		30.0
13	16		28.8
14	17		26.5
15	17.5		24.9
16	18		23.1
17	18.5		21.3
18	19		19.3
19	21	Be + 5% H_2O + Exp + Control Poison	
20	51	Be + 5% H_2O + Exp	

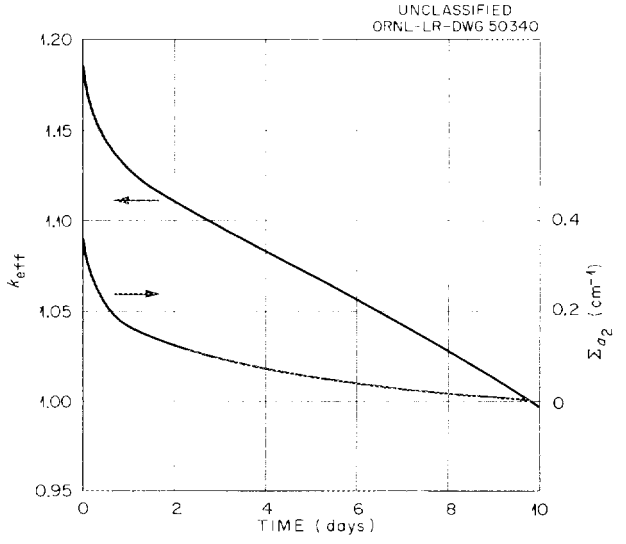

Fig. 40. Available Reactivity and Control-Poison Thermal Cross Section vs Time of Reactor Operation for a Core with No Burnable Poison.

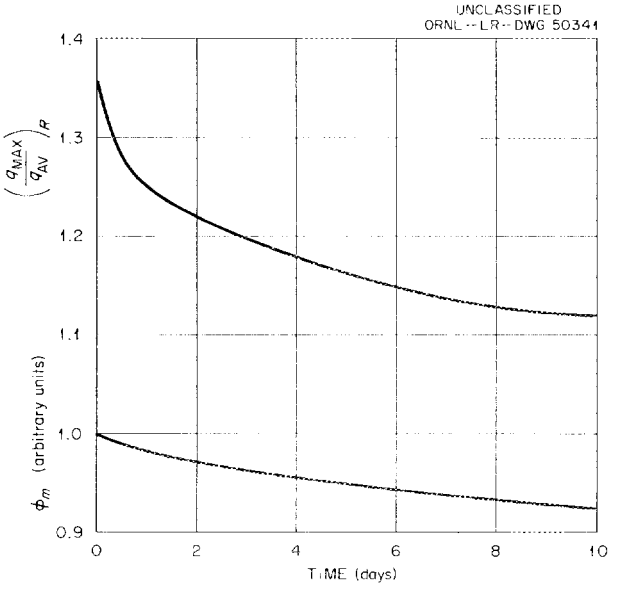

Fig. 41. Maximum Thermal Flux in the Island, and Ratio of Maximum-to-Average Power Density in the Radial Direction vs Time of Reactor Operation for a Core Containing No Burnable Poison.

time zero to 1.12 after 10 days. During the first day of operation, the location of the maximum power density moved from the innermost surface of the fuel annulus to a point nearer the center of the annulus, as shown in Fig. 42. At the inner surface the relative radial power density decreased from 1.36 to 0.53 over the 10-day period; however, as shown in Fig. 41, the maximum thermal flux in the island decreased only 7% during the cycle. The comparatively small decrease in flux is attributed in part to an increase in the point-wise leakage probability (resulting from the decrease in fuel concentration accompanying fuel burnup), which partially compensates for the greater decrease in neutron leakage to the island that results from the shift in power distribution.

Since the maximum relative radial power density at the beginning of the cycle exceeded the tentative maximum design value of 1.2, the reactor would actually have to begin operation at about 88 Mw instead of 100 Mw. If provisions were made to program the power level so as to maintain the limiting power density throughout the cycle, a power level of 100 Mw would be reached by the end of about three days, and by the end of the cycle the power level would be about 107 Mw. Under these circumstances the maximum variation of the island thermal flux during the cycle would be about 12%; however, this sort of operating procedure would produce the maximum time-integrated neutron flux for the particular core.

The reactor power could, by practical means, be programmed as described above. However, it seems reasonable to expect that there are advantages in simultaneously maintaining constant power, constant maximum power density, and constant experimental neutron flux in the island. In an effort to accomplish this feat, the use of burnable poison was considered specifically for maintaining the ratio of maximum-to-average power density constant. This, in turn, would allow constant power operation and thus would tend to maintain a constant flux in the island. (As mentioned previously, the

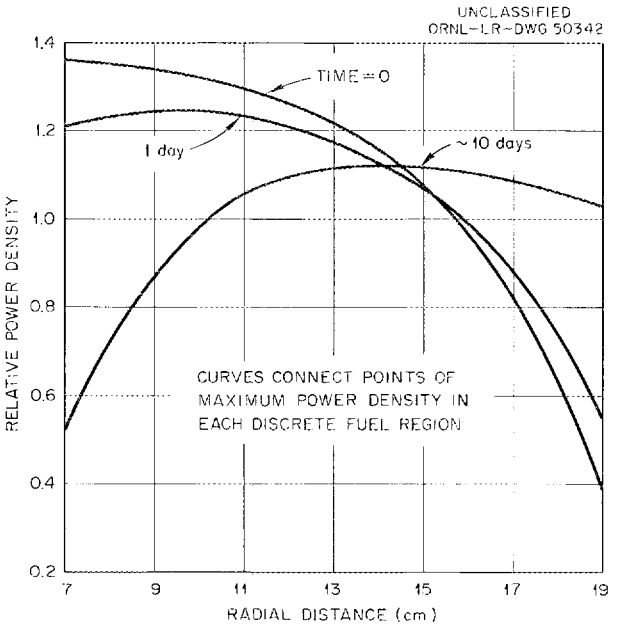

Fig. 42. Radial Power Distribution in Fuel Annulus at the Beginning and End of the Fuel Cycle for a Core with No Burnable Poison.

burnable poison also provides the important advantage of reducing the excess reactivity at the beginning of the cycle and thus the required worth of the control surfaces.)

Proper distribution of the burnable poison and fuel in the fuel region must be determined by trial and error, although a good first approximation can be obtained from an examination of the power distribution vs time curves for a core not containing the poison. The results in Fig. 41 indicate that the addition of a burnable poison near the inside surface of the fuel annulus would reduce the maximum power density at the beginning of the cycle and would tend to result in an increase in the relatively low power density in that location near the end of the cycle. Reduction of the fuel concentration in this same location would also reduce the maximum power density at the beginning of the cycle, but would reduce the already low power density in this location at the end of the cycle. Further examination of Fig. 41 indicates that fuel rather than burnable poison should be added to the outer regions of the fuel annulus so as to increase the power density in that location both at the beginning and end of the cycle. Thus the effective absorption of the poison should be greatest at the inner surface and diminish toward the outer surface. Since the fuel concentration was the least and the thermal flux the greatest at the inner surface and, respectively, greatest and least near the center of the fuel annulus, a reasonable distribution of burnable poison in the radial direction appeared to be a uniform distribution across the inner half of the annulus with no poison in the outer half.

Figures 43, 44, and 45 show the results of fuel-cycle-time calculations for a core having the above burnable-poison distribution and using boron-10 as the poison; except for the boron inclusion and a gradual increase in fuel concentration from the center of the fuel annulus to the outer surface, the core was the same as that associated with Figs. 40, 41, and 42. Sufficient boron-10 was added to reduce the maximum relative radial power density to about 1.2. (As shown in Fig. 22, this required a B^{10} concentration of 5×10^{8} atoms/cm^3.) To the outer regions of the fuel annulus, sufficient fuel was added to increase the end-of-cycle power density in those regions to the maximum permissible power density.

A comparison of Figs. 40 and 43 shows that the addition of the burnable poison initially reduces the potential reactivity by about 5%, but does not siguificantly change the core lifetimes, thus indicating that the poison is effectively burned out by the end of the cycle. Figures 44 and 45 show that the relative radial maximum power density did not exceed 1.2, and with the exception of the first day of operation the maximum power density remained essentially constant. As shown in Fig. 45, the thermal flux at the center of the island had a maximum variation of only 2% from the beginning to the end of the cycle; however, the time-integrated flux (1000-MwD reactor operation) in the island was about 2% less than for the core with no burnable poison. Thus, based on these studies, it appears that with a small sacrifice in time-integrated thermal flux in the island it is possible through the use of a burnable poison and a continuous radial fuel distribution to simultaneously maintain constant 100-Mw operation and essentially constant island thermal flux without exceeding the maximum permissible power density.

For the purpose of studying the power distribution in the axial as well as the radial direction, two-group, two-dimensional calculations were made. The first core calculated was that shown in Fig. 46. The fuel and boron concentrations and distribution were the same as used in the second fuel-cycle-time calculation. A 6-cm-long extension of the aluminum fuel plates was added to each end of the fuel annulus to reduce the power-density peaking at the extremities. The control region, as in the one-dimensional fuel-cycle-time calculations, was assumed to be a uniform gray region surrounding the fuel annulus. Calculational results indicate that at the beginning of the cycle the two-dimensional thermal-flux distribution for such a core is that

PREFACE TABLE FOR FIGS. 43, 44, AND 45

Code calculation, Candle
Cross-section set, No. 3 (GNU averaged, two-group)
Thermal temperature, 80°C

Active core length, 45.72 cm
Axial buckling, 0.002591 cm^{-2}

Region No.	Outer Radius (cm)	Composition	$N^{B-10} \times 10^5$ (atom/barn-cm)	$N^{25} \times 10^5$ (atom/barn-cm)
1	7	H_2O		
2	7.5	U-235 + Al + H_2O + B, M/W = 1	0.5	10
3	8			11.5
4	8.5			13.2
5	9			14.9
6	9.5			16.8
7	10			18.6
8	11			20.7
9	12			24.0
10	13			26.9
11	14		0	28.9
12	15			30.0
13	16			29.0
14	17			27.1
15	17.5			25.8
16	18			24.3
17	18.5			22.7
18	19			21.0
19	21	Be + 5% H_2O + Exp + Control Poison		
20	51	Be + 5% H_2O + Exp		

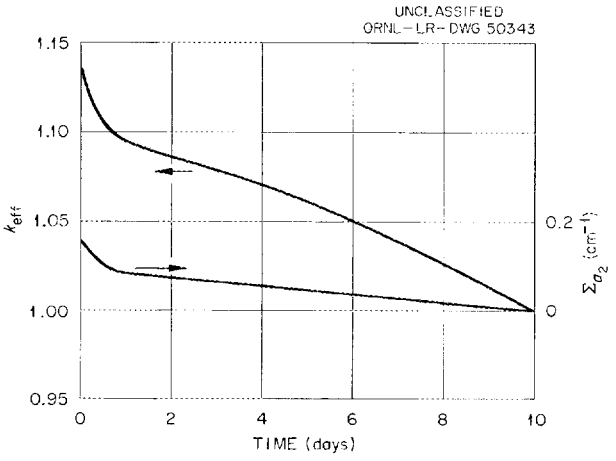

Fig. 43. Available Reactivity and Control-Poison Thermal Cross Section vs Time of Reactor Operation for a Core Containing Burnable Poison.

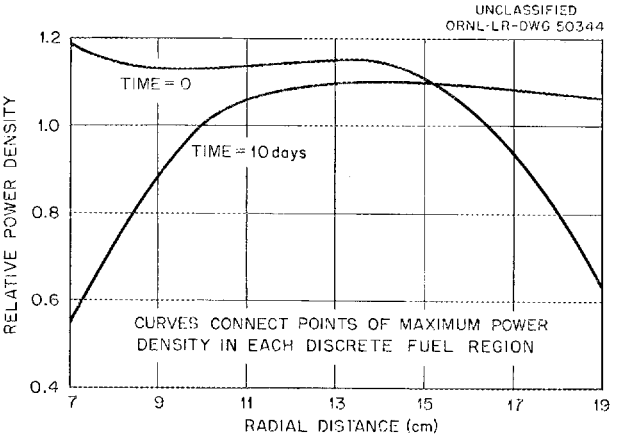

Fig. 44. Radial Power Distribution in Fuel Annulus at the Beginning and End of the Fuel Cycle for a Core Containing Burnable Poison.

shown in Fig. 47, and that the relative power distribution in the fuel annulus is that shown in Fig. 48. As indicated by Fig. 48, the power density in the outside corners is quite low at the beginning of the cycle, a condition that results from the presence of the control poison and from the comparatively large neutron leakage at the fuel-region corners. Such a power distribution suggested that near the corners of the fuel annulus the control region could become more transparent to neutrons without increasing the maximum power density beyond the permissible value. Thus it was assumed that the

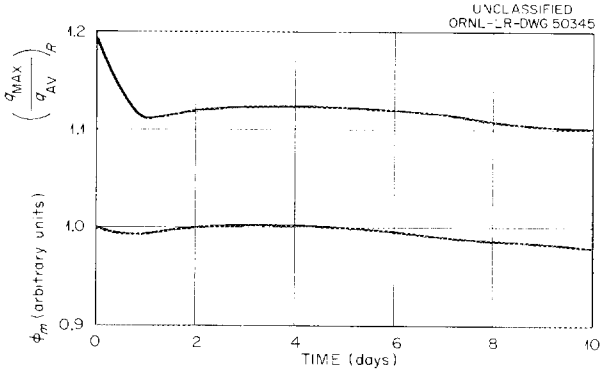

Fig. 45. Maximum Thermal Flux in the Island, and Ratio of Maximum-to-Average Power Density in the Radial Direction vs Time of Reactor Operation for a Core Containing Burnable Poison.

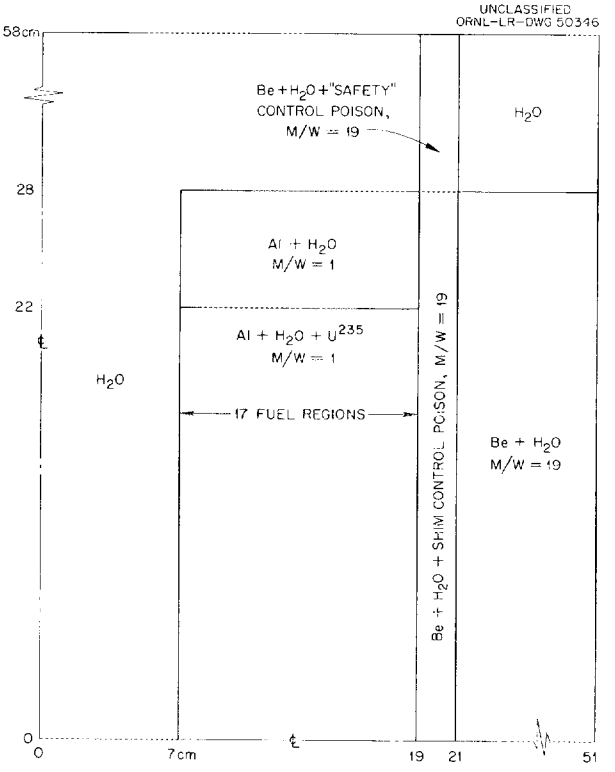

Fig. 46. Core Geometry Used for Two-Dimensional Study of the HFIR with Uniform Shim Poison in the Control Region.

PREFACE TABLE FOR FIG. 47

Core calculation, PDQ
Cross-section set, No. 2 (GNU averaged two-group)

Thermal temperature, 80°C
k_{eff}, 0.981

Region No.	Outer Radius at Horizontal Midplane, cm	Composition	$N^{25} \times 10^5$ (atom/barn-cm)	$N^{B-10} \times 10^5$ (atom/barn-cm)
1	7	H_2O		
2	7.5	U-235 + Al + H_2O + B-10, M/W = 1	10	0.5
3	8		11.52	
4	8.5		13.18	
5	9		14.93	
6	9.5		16.77	
7	10		18.64	
8	11		20.74	
9	12		23.99	
10	13		26.86	
11	14		28.90	0
12	15		30.03	
13	16		29.03	
14	17		27.08	
15	17.5		25.79	
16	18		24.32	
17	18.5		22.73	
18	19		21.04	
19	21	Be + 5% H_2O + Σ_a(gray); Σ_{a1} = 0.00937, Σ_{a2} = 0.1585		
20	49	Be + 5% H_2O + Exp		
19a	21	Be + 5% H_2O + Σ_a(black); Σ_{a1} = 0.120, Σ_{a2} = 2.000		

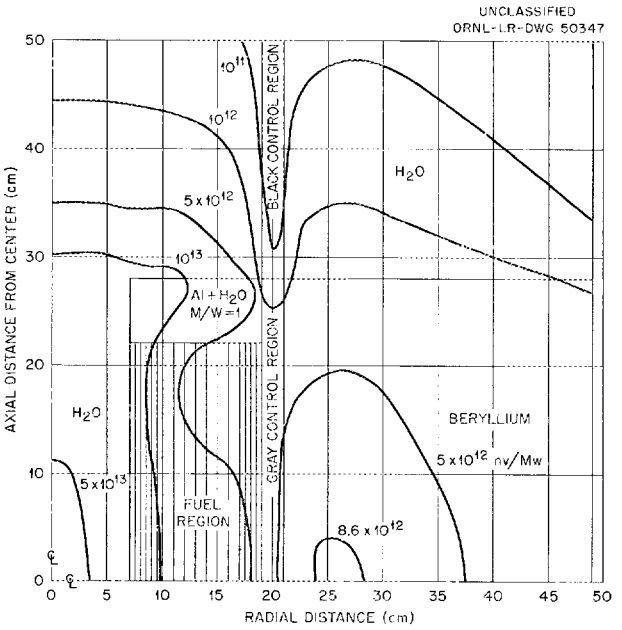

Fig. 47. Two-Dimensional Plot of Thermal-Neutron Flux in a Clean HFIR Core.

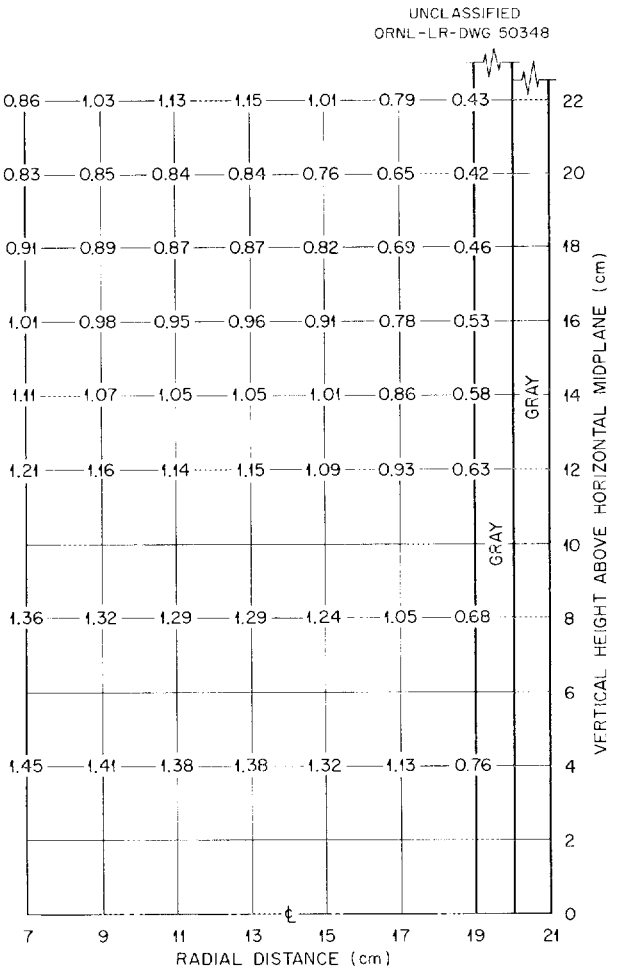

Fig. 48. Relative Power Distribution in the HFIR Core at Time Zero with Uniform Shim.

control region consisted of two thin (about 1-cm-thick) concentric cylinders separating the fuel annulus from the beryllium reflector. The two cylinders would be moved axially and in opposite directions, maintaining symmetry about the longitudinal axis and the horizontal midplane. Each cylinder was divided into a black, gray, and white (beryllium) vertical region, each region being one core-length long and arranged in that order; the poison concentration in the gray regions was adjusted to make $k_{eff} = 1$ at the beginning of the cycle with both gray regions fully inserted. The arrangement is shown schematically in Fig. 49. As the control plates are withdrawn, the core will be more heavily poisoned near the center than at the ends, thus tending to cause power-density peaking in the outside corners where the power density is comparatively low at the start. When the ends of the gray plates meet at the longitudinal center of the core, the shim poison will again be essentially uniform. (Up to this point it was anticipated that the power density would not exceed the maximum design value.) Further withdrawal of the control plates creates a neutron window at the horizontal midplane, resulting in power-density peaking in the vicinity of the window. The degree of peaking, of course, depends upon several factors, including the size of the window, the time at which the window appears, and the reactivity worth of the gray portion of the control plates. Using the results from the one-dimensional fuel-cycle-time calculations (and

thus neglecting nonuniform burnup in the axial direction) associated with Figs. 43, 44, and 45, shim-plate positions for $k_{eff} = 1$ were determined for one day, three days, and six days of operation. By the end of the first day, xenon had reached its maximum value, and therefore about 4% in reactivity had to be compensated for by the shim plates. As shown in Fig. 50, this required that the ends of the gray plates be positioned approximately at the longitudinal center. By the end of the sixth day, the plates had been withdrawn another one-quarter core length, allowing a half-core-length window at the longitudinal center. The relative power distributions for the zero, one-day, three-day, and six-day cores are shown in Figs. 48, 51, 52, and 53. (Figure 52 actually represents a case in which there was some overlapping of the gray and white plates; however, as mentioned in a later paragraph, the effect was not large.) As indicated, the window did not result in an excessively high power density. Since nonuniform axial fuel burnup will result in axial flattening of the power, the above values should be somewhat conservative.

Anticipating that the window effect might result in adverse peaking, consideration was given to overlapping or tapering of the gray and essentially white control plates. Comparison of Figs. 53 and 54 shows the difference in relative power distribution for a six-day core with and without the tapered plates. For these calculations the tapered section was represented by a 12-cm-long, equal-thickness overlap of the gray and white regions of the control plates. This system was also used in the three-day core of Fig. 52. Although the power density next to the control region was about 4% less for the overlapped plates, the maximum value in the core was the same.

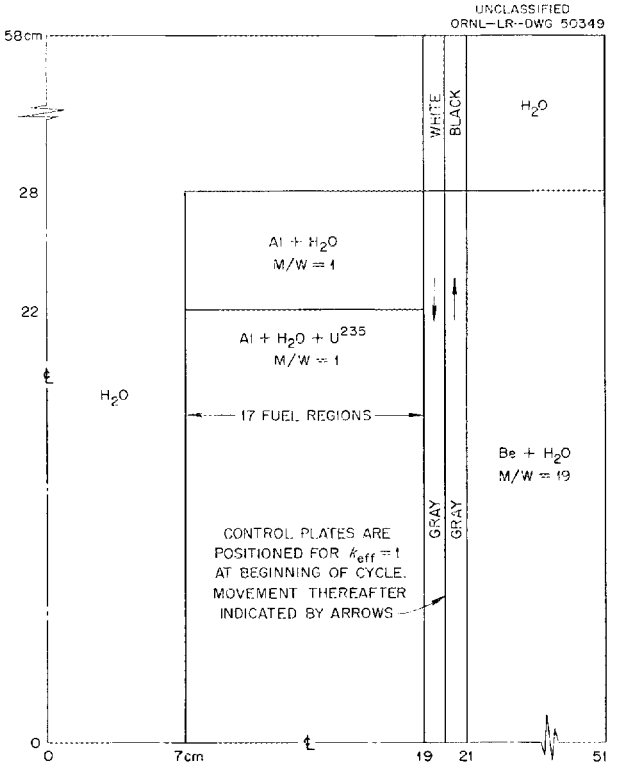

Fig. 49. Core Geometry Used for Two-Dimensional Study of the HFIR with the Three-Region Control Plates.

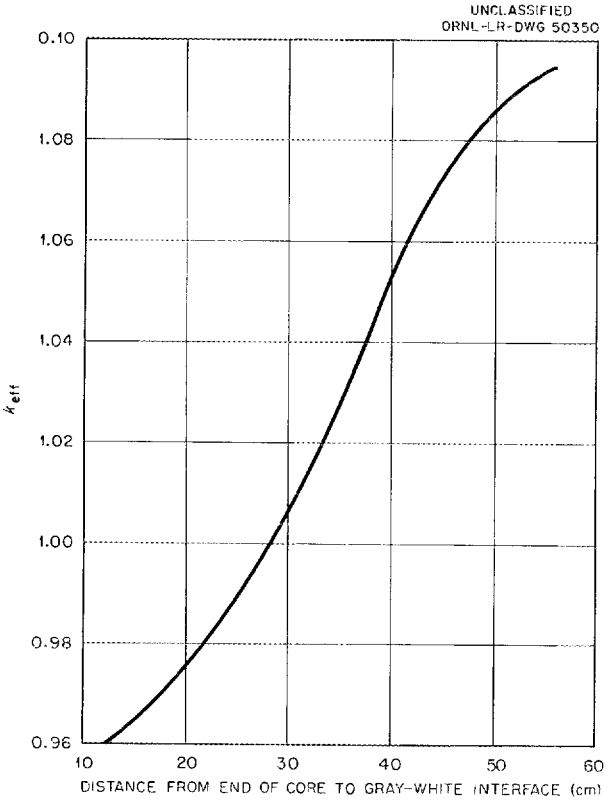

Fig. 50. Reactivity vs Vertical Distance Between Extended End of Fuel Annulus and Gray-White Interface of Control Plates for a One-Day-Old Core (100 Mwd).

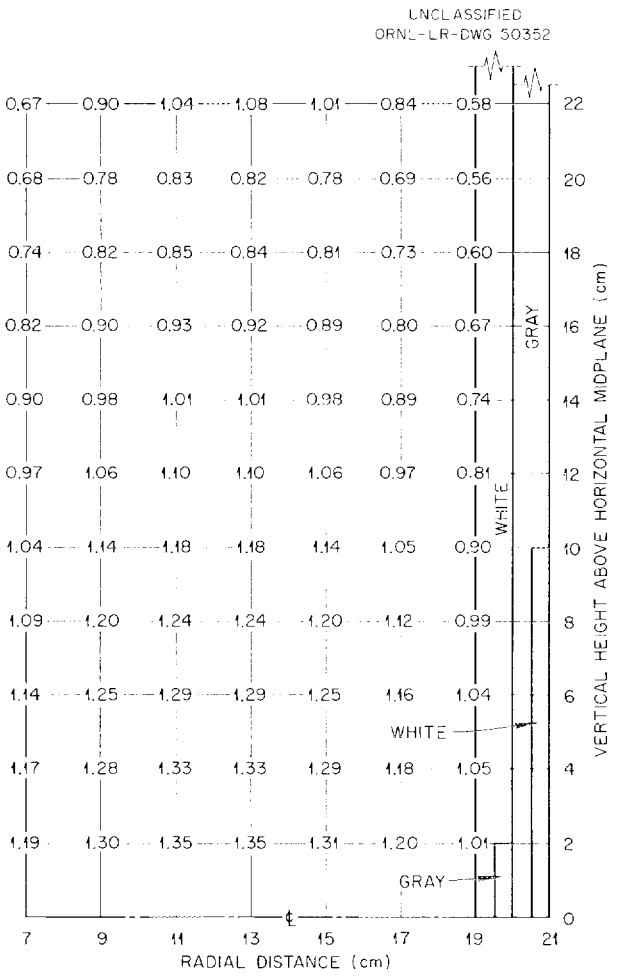

Fig. 51. Relative Power Distribution in the HFIR Core at the End of One Day at 100 Mw.

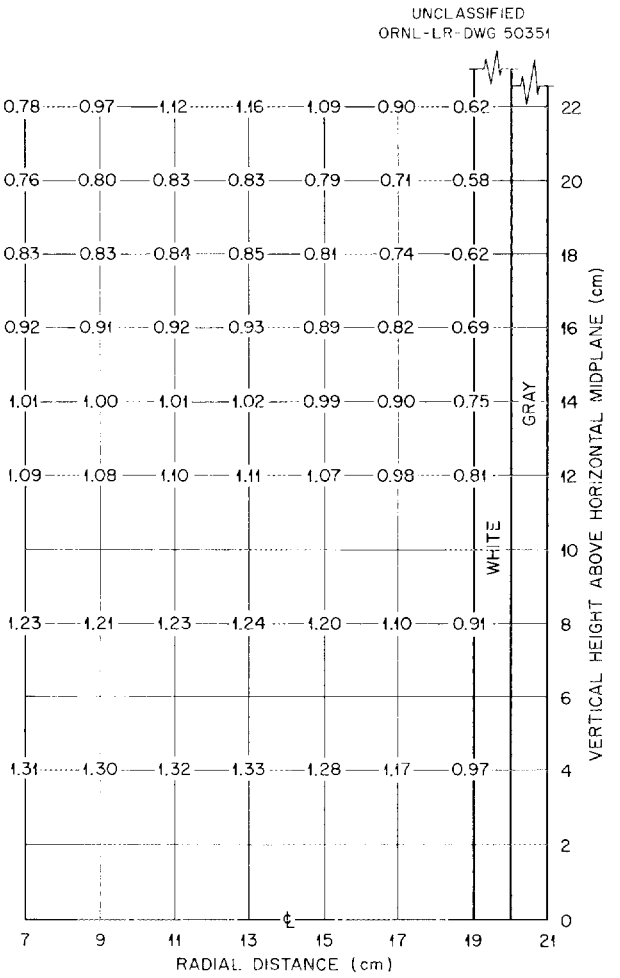

Fig. 52. Relative Power Distribution in the HFIR Core at the End of Three Days at 100 Mw, Using Overlapped Gray-White Regions.

The amount of peaking in the window region depends to some extent on the poison concentration in the gray shim plates. More peaking would be expected in the core with no burnable poison since the shim poison would have to be increased considerably. For the particular core calculated, the burnable poison takes care of about 5% in reactivity, leaving only about 13% for the shim plates. Under these conditions 1/4-in.-thick plates of a material such as titanium would be sufficient. For the black regions, of course, more highly absorbing plates would be required.

Window peaking will also increase with increasing volume fraction of coolant water in and adjacent to the control plates. Calculations thus far included only 5% by volume of H_2O in the homogenized control-plate area. A practical control-system design will probably include about 25% by volume of H_2O in the control-plate region, in which case the coolant would be introduced in channels separating the plates from each other, and the adjacent components. Such a case has yet to be investigated.

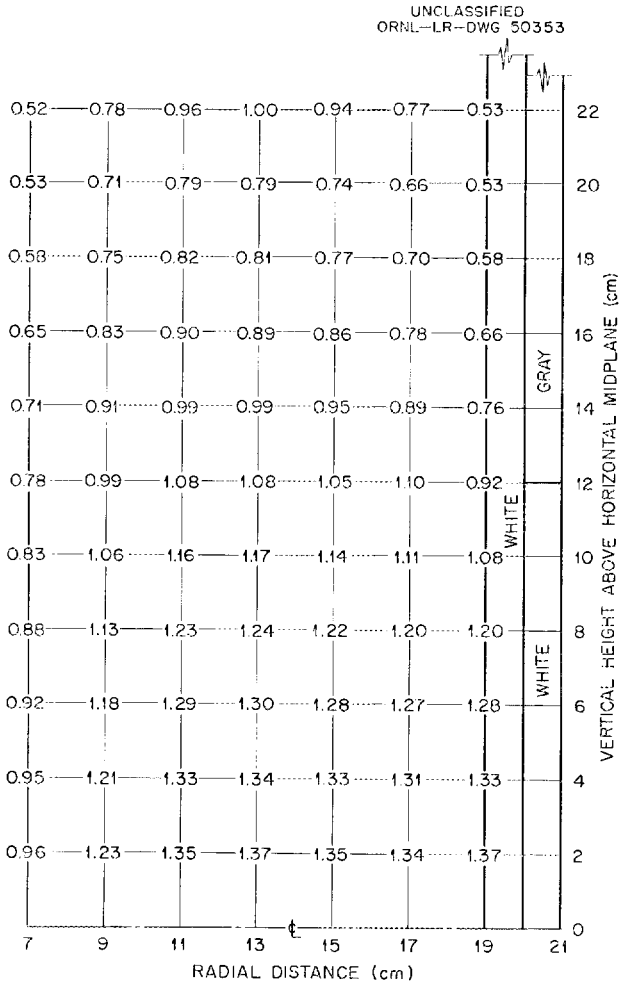

Fig. 53. Relative Power Distribution in the HFIR Core at the End of Six Days at 100 Mw.

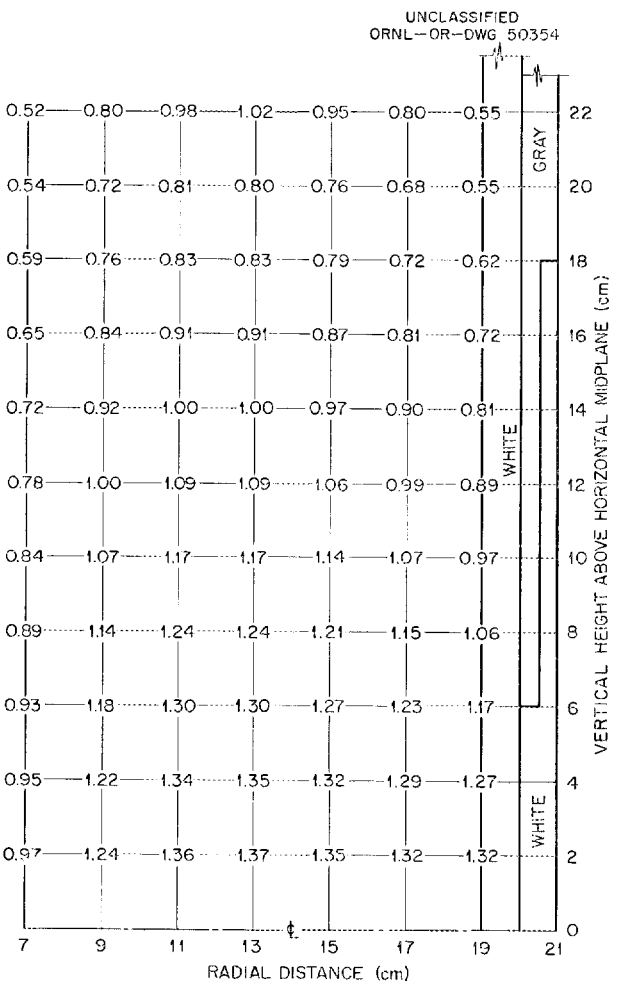

Fig. 54. Relative Power Distribution in the HFIR Core at the End of Six Days at 100 Mw, Using Overlapped Gray-White Regions.

KINETICS CONSTANTS

In preparation for HFIR time-behavior studies, calculations were made to obtain estimates of the temperature coefficient of reactivity, the void coefficients of reactivity, and the prompt-neutron lifetime. Following is a discussion of the methods of calculation used and the results obtained.

Temperature Coefficients of Reactivity

Since the various regions of the HFIR core will not necessarily be at the same temperature or experience the same changes in temperature, it was necessary to calculate separate coefficients for individual regions as well as for the over-all core. The coefficients have been calculated several times for the HFIR, using several different sets of nuclear constants. In all cases the coefficients were determined by adjusting the nuclear constants for changes in water density and thermal-neutron energy associated with changes in average bulk water temperatures. (The effects of dimensional changes on reactivity were found to be negligible.) Available reactor codes were then used to calculate the corresponding values of k_{eff}. The results of the calculations indicated that increasing only the island temperature over a wide range of temperatures (70 to ~300°F) increased k_{eff} while increasing only the fuel-region average coolant temperature decreased k_{eff} for all temperatures of interest. The explanation for the island coefficient being positive appears to be that the island in a sense is over-moderated, so that a reduction in water density reduces the absorption cross section without significantly increasing leakage until very large changes in density are achieved. The fuel region, on the other hand, is under-moderated, and in addition the thermal absorption cross section is largely due to the fuel and cladding; therefore the fuel-region coefficient is negative.

The over-all core temperature coefficient depends on the relative magnitudes of the island and fuel-region coefficients. Results of the various coefficient calculations referred to above did not agree on the magnitude or sign of the over-all coefficient, the indication being that in the temperature range of about 70 to 120°F the magnitudes of the separate coefficients are so strongly dependent on the microscopic cross sections that at least three significant figures in the cross-section values are required to avoid meaningless scatter of calculated data points for the over-all k_{eff}-temperature curves. This also implies, of course, that the absolute values of the nuclear constants must be quite accurate. Thus the most recent calculations* were performed using what were believed to be the best available cross sections.[18,19] Detailed results of these calculations are presented in Table 6 and Fig. 55 for the beginning and end of a typical HFIR 10-day fuel cycle.

---

*These calculations were made by M. L. Tobias (ORNL) and D. R. Vondy (ORNL) in connection with the HFIR studies. Since their constants and therefore results are considered to be the most accurate to date, the ensuing discussion is based primarily on their results.

Table 6. Temperature Coefficients of Reactivity for the HFIR

Region	Reactor Temp. (°F)	dk/dt (°F^{-1}) Beginning of Cycle	dk/dt (°F^{-1}) End of Cycle
Fuel	70	$\sim -0.8 \times 10^{-4}$	
Island	70	$+1.0 \times 10^{-4}$	
Reflector	70	$<+0.1 \times 10^{-4}$	
Control region	70	$\sim +0.3 \times 10^{-4}$	
Over-all	70	$\sim +0.8 \times 10^{-4}$	
Fuel	150	-2.0×10^{-4}	
Island	150	$+1.1 \times 10^{-4}$	$\sim +1.1 \times 10^{-4}$
Reflector	150	$<+0.1 \times 10^{-4}$	
Control region	150	$+0.3 \times 10^{-4}$	
Over-all	150	-1.0×10^{-4}	-0.2×10^{-4}

As shown, the calculations indicated that in the temperature range of 70 to about 110°F the over-all coefficient (with all regions at the same temperature) might be positive, but that above 110°F the over-all coefficient appeared to be negative. At the end of the fuel cycle the fuel-region coefficient and the over-all coefficient are still negative above 110°F but less in magnitude than at the beginning of the cycle. This results from the withdrawal of the control plates and the subsequent increase in the changes of a wayward neutron being returned to the fuel by the outer reflector.

The strong dependence of the over-all calculated temperature coefficient on the relative values of certain nuclear constants is illustrated in Fig. 56, which shows the variation of $(\nu\Sigma_f/\Sigma_a)_{thermal}$ and k_{eff} with changes in the average core temperature, assuming all regions to be at the same temperature. It is observed that at the lower temperatures (70 to 100°F) the irregularities in the cross-section ratio are definitely reflected in the calculated multiplication constant (the irregularities are associated with the scatter in cross-section data). Above 100°F there is still a resemblance; however, it appears that neutron leakage is predominant, resulting in an over-all negative temperature coefficient. These results focus attention on the accuracy with which cross sections or cross-section ratios are known. As indicated by Fig. 56, a change in the fourth significant figure of the ratio $(\nu\Sigma_f/\Sigma_a)$ will result in significant irregularities in k. Certainly it is reasonable to expect that the ratio is not known that accurately; however, the results of the calculations do indicate what effects small variations in the nuclear constants can make. If for example a constant value of the above ratio is arbitrarily used in the calculations, the k_{eff} curve becomes monotonic with a negative slope. It is interesting to note, however, that the results from HFIR critical experiments and ASTR calibration experiments[20]* indicate an over-all positive temperature coefficient in the vicinity of 70°F. Thus, in view of the calculated and experimental results obtained thus far, it must be concluded that the over-all temperature coefficient below about 100°F is positive. The maximum positive change in k_{eff} with increasing temperature from 70°F appears to be about 0.002.

As mentioned previously, the over-all temperature coefficient was calculated assuming all regions of the core to have the same average temperature and, more important, the same change in average temperature. In the event the core receives a

*At the particular time the temperature coefficients were measured, the Al-H_2O ASTR core had sizable water volumes within the core created by three control-rod ports.

PREFACE TABLE FOR FIG. 55

Code calculation, Wanda
Cross-section set, GNU averaged two-group (with all regions at same temperature)

Thermal temperature, variable
Active core length, 45.72 cm
Axial buckling, 0.002718 cm^{-2}

Core same as for Fig. 56.

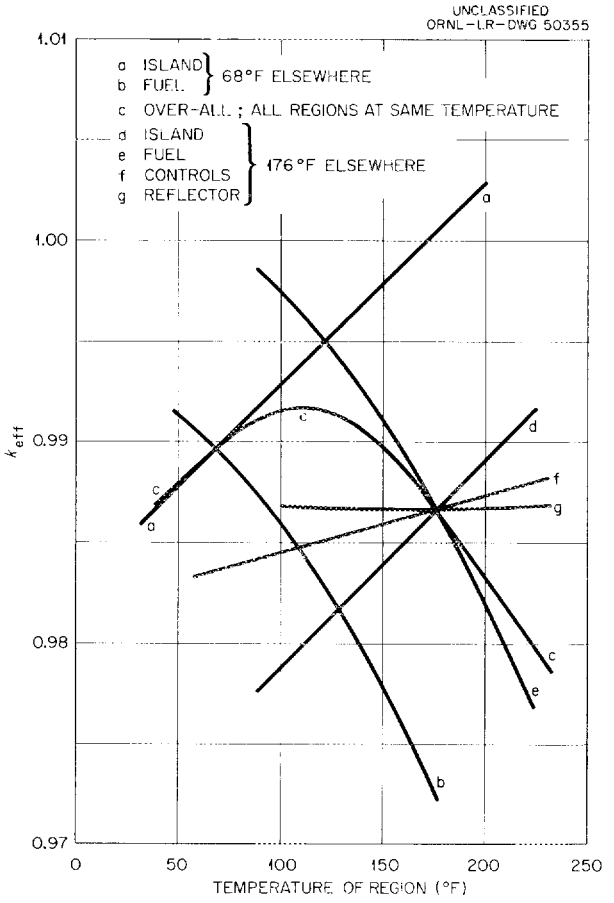

Fig. 55. Multiplication Constant vs Average Temperature of Various Regions in a Clean HFIR Core.

uniformly distributed hot slug of coolant, this coefficient should be used to predict the corresponding change in k_{eff}. However, once the reactor is on a positive period, the relative changes in the island and fuel-region temperatures and thus the actual value of the over-all coefficient depend on the relative amount of heat generated in and transferred to the island, the relative coolant flow rate in the island, and of course the initial average temperatures of the core. If it is assumed in the case of the HFIR that the temperature coefficient of reactivity for an individual region is independent of the temperatures of all other regions (according to Fig. 55 this appears to be a reasonably valid assumption for the island and fuel regions) and that the over-all coefficient is equal to the sum of the island and fuel-region coefficients, then

PREFACE TABLE FOR FIG. 56

Code calculations, GNU
Cross-section set, GNU 34 groups (ORNL revised set)
Thermal temperature, variable; all regions the same

Active core length, 45.72 cm
Axial buckling, 0.002718 cm^{-2}

Region No.	Outer Radius (cm)	Composition
1	7	H_2O
2	19	U-235 + Al + H_2O + B, M/W = 1, N^{25} = 0.00025 atom/barn-cm, N^{B} = 0.000016 atom/barn-cm
3	20.27	Be + B, N^{B} = 0.00067 atom/barn-cm
4	50.27	Be + 5% H_2O + Exp
5	121.92	H_2O
6	138.16	Fe

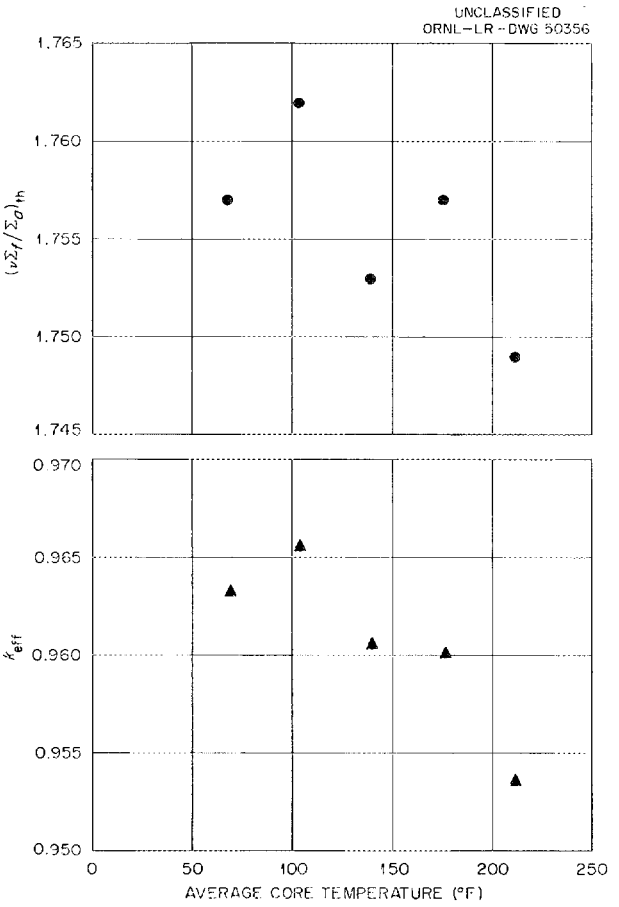

Fig. 56. Multiplication Constant and $(\nu\Sigma_f/\Sigma_a)_{thermal}$ vs Average Temperature of Core.

the multiplication constant may be represented by

$$k_{eff} = 1 + \int \left(\frac{dk}{dt}\right)_{is} dt + \int \left(\frac{dk}{dt}\right)_{f} dt, \qquad (1)$$

where the island and fuel-region coefficients are integrated over their respective temperature ranges corresponding to a change in reactor power. A typical accident for which Eq. (1) could be used entails jamming of the control rods immediately after the reactor is made critical at a core temperature below about 100°F. In such a case the power would rise, if the initial effective over-all temperature coefficient were positive, until k_{eff} was returned to unity as a result of the increase in core temperature and the change in sign of the effective coefficient. It is necessary then to determine how high the power level will rise. In order to examine this particular accident for the HFIR, it was assumed that the relative island heat removal rate was 1%, that the relative flow rate through the island was 10%, that the initial temperatures of all core regions was 40°F, and that the primary-coolant circuit time was such that the inlet core temperature remained at 40°F during the power transient. The island and fuel-region coefficients were approximated by the derivatives of equations fit to the curves in Fig. 55, in which case the fuel-region coefficient was taken as the difference between the over-all and island coefficients. Making the appropriate substitutions, Eq. (1) becomes

$$k_{eff} = 1 + \int_{40}^{40 + 0.1\,(\bar{T}_f - 40)} 1.0 \times 10^{-4}\, dt + \int_{40}^{\bar{T}_f} [-9.796 \times 10^{-5} \sin 0.2856\,(t - 110) - 1.0 \times 10^{-4}]\, dt,$$

where $\bar{T}_f$ is the average fuel-region temperature. To determine the temperature at which $k_{eff} = 1$, the integrals are set equal to zero. In this particular case the maximum average fuel-region temperature was 84°F, while the lower value, of course, was 40°F. Since the proposed HFIR core has a 70°F increase in the fuel-region coolant temperature for each 100 Mw, the maximum power level reached in the postulated startup accident was 124 Mw. Although this power level is not excessive for reasonable periods of operation, similar power increases could be avoided by preheating the coolant above 100°F, and/or by increasing the coolant flow rate through the island from 10% to about 20% of the fuel-region flow rate.

Void Coefficients of Reactivity

Void coefficients of reactivity were determined separately for the water island, the fuel annulus, the water-reflector region surrounding the outer beryllium reflector, and for the over-all core. Calculations were first made using a one-dimensional, 34-group model in order to obtain two-group constants for a two-group, two-dimensional calculation. Thus the one-dimensional calculations represent a case in which the voids extend over the full length of the core, including the end reflectors. In the two-dimensional calculations the voids were confined to the volume within the active core length.

In the island region (which contained only water) two types of voids were considered: (1) a central cylindrical void and (2) uniform voids (equivalent to a reduction in water density throughout the region). Results of the cylindrical-void calculations are presented in Fig. 57. As indicated, a void essentially unreflected on the ends results in a negative void coefficient, while the end-reflected cylindrical

PREFACE TABLE FOR FIG. 57

Code calculation, GNU; PDQ
Cross-section set, GNU 34 groups;
GNU averaged two-group
Thermal temperature, 80°C

Active core length, 45.72 cm
Axial buckling, 0.002591 cm^{-2} (GNU)
Length of water end-reflector, 15 cm (PDQ)

Region No.	Outer Radius (cm)	Composition
1	Variable	5% H_2O
2	7	H_2O
3	19	U-235 + Al + H_2O, M/W = 1, N^{25} = 45.31 x 10^{-2} atom/barn-cm
4	21	Be + 5% H_2O + Exp + B
5	51	Be + 5% H_2O + Exp

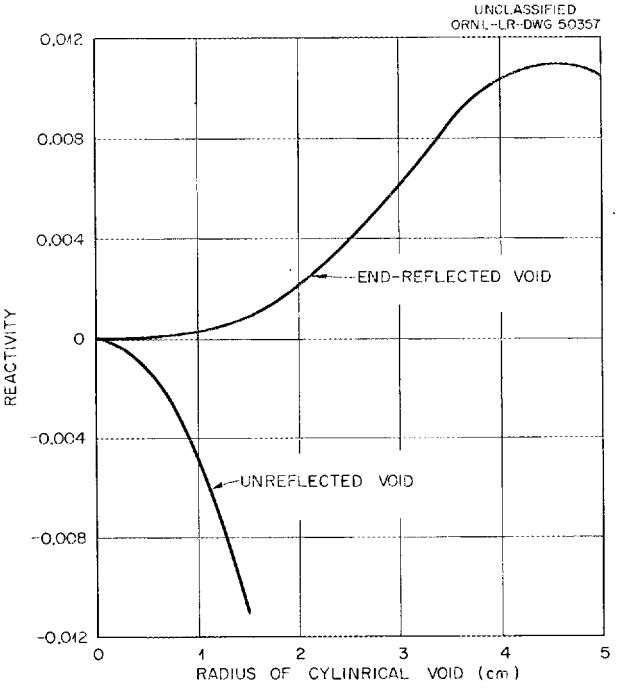

Fig. 57. Reactivity vs Radius of a Central Cylindrical Void in a 7-cm-Radius Water Island.

void in the 7-cm-radius island results in a maximum positive reactivity addition of about 1% at a void radius of about 4.5 cm. As in the case of the positive island temperature coefficient, the positive island void coefficient is explained by the over-moderation of the water island region and the reduction in absorption as the void is increased.

Results of the uniform-void calculations are presented in Fig. 58. With the voids in the island region only and confined within the active core length, a void fraction of 45% produces a maximum positive reactivity addition of about 2.5%. For the two cases of voids in the fuel region only and in all regions, the void coefficients are negative for all void fractions. The one-dimensional calculations also indicate negative coefficients for the fuel region and the over-all core. In the island region

PREFACE TABLE FOR FIGS. 58 AND 60

Code calculation, GNU; PDQ
Cross-section set, GNU 34 group; GNU averaged two-group
Thermal temperature, 80°C

Active core length, 45.72 cm
Axial buckling, 0.002591 cm^{-2} (GNU)
Height of water end-reflectors, 15 cm (PDQ)

Region No.	Outer Radius, cm	Composition
1	7	H_2O
2	19	U-235 + Al + H_2O, M/W = 1, N^{25} = 45.31 x 10^{-5} atom/barn-cm
3	21	Be + 25% H_2O + B
4	51	Be + 5% H_2O + Exp

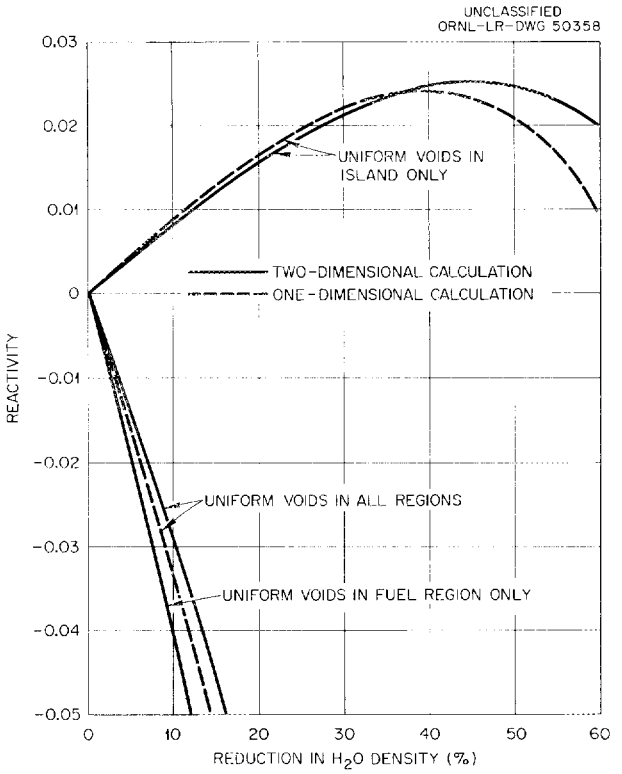

Fig. 58. Reactivity vs Uniform-Void Fraction in a Typical HFIR Core.

the one-dimensional calculation gives about the same maximum change in k but at 40% rather than 45% voids.

The outer water reflector, which is adjacent to and outside of the beryllium reflector, has very little effect on reactivity if the beryllium reflector is at least 30 cm thick. Calculational results shown in Fig. 59 for beryllium thicknesses of 10, 20, and 30 cm indicate that up to about 10% voids there is a small positive reactivity addition (<0.001), and that for void fractions greater than about 10% the void coefficient is negative.

If a void fraction greater than about 15% should, by some means, be obtained and retained in the all-water island for a few moments, it is likely that an increase in power would occur, even with the control system operable, that would damage the core. By placing permanent voids in the island such accidents can be avoided; however, as shown in Fig. 60, the introduction of 20% uniform voids in the island (about the minimum permanent void fraction that will permit adequate control by the control system) reduces ϕ_m/P by about 10%, and practical methods of permanent void simulation will reduce the flux even further. It is interesting to note, however, that the presently conceived island target (200 g of Pu in nineteen 0.95-cm-dia, 46-cm-long aluminum rods) occupies nearly 20% of the island volume, and since the target significantly reduces moderation and increases absorption in the island it simulates a permanent void with no additional flux perturbation associated with this secondary function. Therefore flux perturbations resulting from permanent void simulation will not necessarily affect heavy-isotope production unless targets smaller than presently designed are used.

PREFACE TABLE FOR FIG. 59

Code calculation, Wanda
Cross-section set, No. 1
(two-group, modified for voids)
Thermal temperature, 80°C

Active core length, 30.5 cm
Axial buckling, 0.004568 cm^{-2}

Region No.	Outer Radius, cm	Composition
1	2	100 g Pu-242 + Al + H_2O, M/W = 1
2	7	H_2O
3	18	U-235 + Al + H_2O, M/W = 1, N^{25} = 23.6 x 10^{-5} atom/barn-cm
4		Be + 5% H_2O + Exp
5	68	H_2O (variable density)

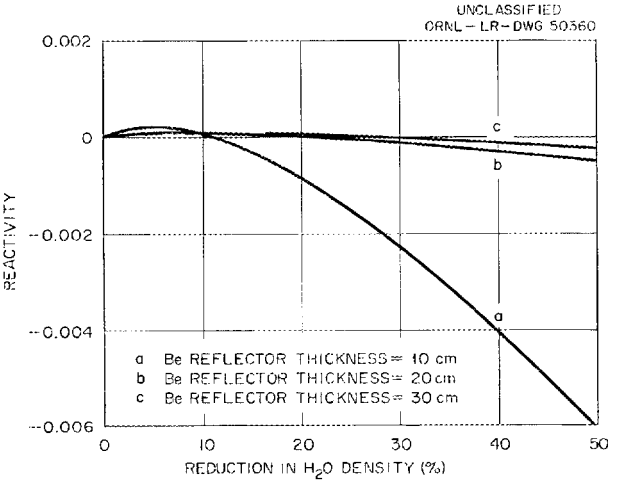

Fig. 59. Reactivity vs Void Fraction in Outer Water Reflector.

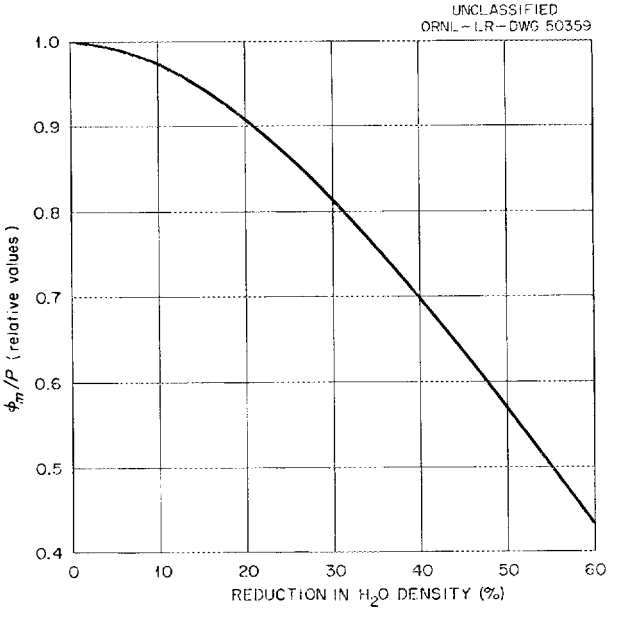

Fig. 60. Maximum Unperturbed Thermal Flux in Island per Unit Power vs Uniform-Void Fraction in Island. (Preface table same as for Fig. 58.)

Since it is expected that targets occupying much less than 20% of the island volume will eventually be used for various purposes in the island of the HFIR, provisions may have to be made for including permanent voids in the island. The use of beryllium as a void has been considered because in addition to being generally compatible with an aluminum-water reactor system it results in less island thermal-flux perturbation than other readily available materials. However, the good scattering properties and low absorption cross section of beryllium might require that more than 20% by volume of beryllium be added to the island or that some permanent absorber be added to smaller amounts of the beryllium. Studies of these possibilities have not yet been completed, but indications are that the use of beryllium as a permanent island void will result in about a 20% decrease in the otherwise maximum unperturbed island thermal flux. Actually, the best materials to use for void simulation appear to be those with comparatively large neutron slowing-down distances and with absorption cross sections close to that of water. This would make zirconium and aluminum possible contenders.

Prompt-Neutron Lifetime

Because of the comparatively high neutron leakage rate from the under-moderated HFIR fuel annulus, the neutron lifetime is rather strongly dependent on the return current from both the island and outer beryllium reflector. Since the neutron diffusion length in the two reflector regions, particularly the beryllium reflector region, is large in comparison with that of the fuel region, a clean core, having less leakage and less return current due to the presence of the circumferential control plates, will have the shortest prompt-neutron lifetime. Near the end of the fuel cycle, when the fuel concentration is low and the control plates are removed, the increased leakage into the beryllium about doubles the neutron lifetime.

Two methods of calculation were used to obtain the neutron lifetime. In the first method[21] the reactor was made supercritical, and the resultant period was determined. The prompt-neutron lifetime was then calculated from

$$\ell = \frac{k_{ex}}{w}, \qquad (2)$$

where k_{ex} is the step change in reactivity that put the reactor on the period $1/w$. The inverse period, w, was obtained by first assuming that

$$\phi(t) = \phi(0)e^{wt}$$

so that

$$\frac{\partial \phi}{\partial t} = w\phi(t).$$

This quantity was then substituted into the time-dependent diffusion equation and terms rearranged so that

$$D\nabla^2\phi - (\Sigma + \frac{w}{v})\phi + \text{source} = 0, \qquad (3)$$

where v is the neutron velocity corresponding to the particular energy group. Since Eq. (3) has the form of the critical equation, the quantity w/v can be interpreted as a poison that is sufficient to make the supercritical reactor just critical. Thus the change in poison cross section (w/v) associated with Δk is used to calculate the

reactor period. If k_{ex} is small, then the required addition of w/v to each region does not result in a significant change in the flux distribution.

The other method used for calculating the neutron lifetime employed first-order perturbation theory. The lifetime was calculated from the following expression:[22]

$$\ell = \frac{\int \sum_i \frac{\phi_i^*(r)\phi_i(r)dr}{v_i}}{\int \sum_i \sum_j \chi_j \phi_j^*(r)\ \nu\Sigma_{fi}\ \phi_i(r)\ dr}\ , \qquad (4)$$

where χ_j is the fraction of neutrons born in each group, and ϕ_i^* represents the adjoint flux for the i th group.

For the period method two-group, one-dimensional and two-group, two-dimensional diffusion-theory calculations were used. A two-group, one-dimensional calculation was used for the perturbation method.

Results of the calculations are presented in Table 7. The lifetimes obtained with the period and perturbation methods are in very good agreement, both methods giving a neutron lifetime of about 40 μsec for a clean core having control plates positioned for k_{eff} equal unity in a clean core. As shown in Table 7, a somewhat larger value was predicted by the two-dimensional calculation, and an even greater value was calculated for the end of the fuel cycle when the control plates are withdrawn.

When using the period method for calculating the lifetime, two values of k_{eff} were used in an effort to determine whether the smallest value was small enough to avoid significant flux variations. The results indicated essentially no difference in neutron lifetime for k_{eff} = 0.1% and 1.0%.

Table 7. Prompt-Neutron Lifetime

Method	k_{ex}	ℓ (μsec)
Period		
One-dimensional		
Clean core	0.0010	42.0
	0.0101	42.1
Burned core	0.00172	71.6
	0.00852	71.0
Two-dimensional		
Clean core	0.0067	56
Perturbation		
One-dimensional		
Clean core	-	38.9

XENON-INSTABILITY STUDIES

If the thermal flux in all or a portion of the fuel region is suddenly increased as a result of increased power or withdrawal of the control plates to compensate for a poison addition, the xenon concentration in the vicinity of the increased flux will be decreased, resulting in a further increase in flux. For an initial average thermal flux of 5×10^{14} nv the above occurrence would result in a 50-sec reactor period,[23] provided the control plates were not moved. (For higher flux levels the period would be shorter.) Movement of the control plates following the initial change tends to cause oscillatory variations in the xenon, neutron flux, and power distribution, a problem that is more acute in high-flux reactors.[24] It is possible that such variations could cause momentary localized excessive peaking of the power density, if provisions were not made for detecting the power shift and for controlling it within permissible limits. Such variations in power distribution, sometimes referred to as xenon flux instability, were studied in connection with the HFIR and were determined to be insignificant, requiring no special provisions in the control system. Following is a brief discussion of the calculational methods and results of the studies.

Both digital and analog computer techniques were used in the xenon-instability studies. In the former case a one-dimensional fuel-burnup calculation was used. The core was first "burned" for two days at 100 Mw to reach equilibrium xenon, criticality being maintained by means of a variable poison in the control region. Sufficient poison was then added to all regions to cause a 1% decrease in reactivity and the control-region poison concentration was changed to maintain criticality (operation was continued at 100 Mw). The resultant xenon concentrations and flux distributions were then calculated. Close to the control region the xenon concentration oscillated with a period of about one day and assumed an equilibrium value by about the end of the first day after the perturbation. The maximum variation in xenon concentration was about 5%, not enough to have a significant effect on the power distribution.

The analog computer calculations were made by Stone.[25] Results using a three-dimensional model indicated that for step changes in reactivity up to 100% there was no significant oscillations in the power distribution. Results using a one-dimensional model (longitudinal direction) indicated that for step changes in reactivity less than 1 or 2% there were no significant oscillations.

HEAT REMOVAL CONSIDERATIONS

The heat transfer characteristics for the HFIR aluminum plate-type element were estimated using the experimental results obtained by Gambill[26] for friction factors, film coefficients, and burnout heat fluxes for the unusually thin coolant channels (~0.050 in.), and the results obtained by Griess[17,27] in connection with the heat flow resistance of the aluminum oxide film. Using the correlations proposed by Gambill for the water film coefficient and the burnout heat flux, Hilvety[28] made a study of the hot-spot and hot-channel factors for a typical HFIR core. Following is a brief summary of the HFIR heat transfer studies.

The correlation proposed by Gambill for the average water-film heat transfer coefficient is the Hausen equation multiplied by 0.94 and is given by

$$(Nu)_b = 0.109 \left[(Re)_b^{2/3} - 125 \right] (Pr)_b^{1/3} \left[1 + \left(\frac{De}{L} \right)^{2/3} \right] \left(\frac{u_b}{u_w} \right)^{0.14} . \qquad (5)$$

Of the 31 experimentally determined values of average h, only one was less than that predicted by Eq. (5). Thus, according to Gambill, this equation will predict the minimum value of h for the HFIR.

Forced-convection burnout-heat-flux data were obtained from seven tests that spanned the values of flow gap, heated length, velocity, and pressure proposed for the HFIR. The correlation proposed by Gambill is the Zenkevich-Subbatin equation divided by an uncertainty factor of 1.3 and is given by

$$(q_{bo}) = 305\ G^{0.5}\ (\Delta T_{sub})^{0.33} \left(\frac{\rho_\ell - \rho_v}{\rho_\ell} \right)^{1.8} . \qquad (6)$$

The uncertainty factor of 1.3 is applicable to the HFIR design, and therefore Eq. (6) will predict the minimum burnout heat flux for the HFIR.

As indicated by the experimental work done by Griess, the temperature drop across the oxide film on aluminum plates is appreciable and depends strongly on the pH of the coolant water. Tests presently being conducted in connection with HFIR development indicate that changing from a pH of 7 to 5 reduces the aluminum oxide film resistance obtained at the end of the 10-day fuel cycle by a factor of 4. Since this resulted in a very significant decrease in the plate temperature and maximum water temperature (assuming water to be entrained in the oxide), the lower pH was considered for the HFIR, and heat transfer calculations were made accordingly.

Using the above information plus the proposed HFIR design specifications in Table 8 and the "hot spot" data in Table 9, the heat transfer characteristics in Table 10 were obtained. As indicated by the heat-flux values in Table 10, the power level could be raised slowly from the design value of 100 Mw to about 200 Mw before burnout occurred, provided that the increase in fuel-plate temperature did not result in premature core failure. The results also show that for a pH of 5 and 0.050-in.-thick fuel plates a pump discharge pressure of about 350 psi (assuming 67 psi across the core) is required to prevent boiling in the aluminum oxide film. A pH of 7 results in a 140°F higher plate temperature and thus a system pressure of about 525 psi.

Table 8. HFIR Characteristics Used in Heat Transfer Calculations

Power	100 Mw (97.5 in core)
Active core volume	44.8 liters
Active core length, L	18 in.
Coolant-channel thickness, ϵ	0.050 in.
Fuel-plate thickness, w	0.050 or 0.040 in.
Coolant velocity	40 ft/sec
Inlet temperature	120°F
Ratio of maximum to average power density (nominal)*	1.45
Ratio of maximum to average power per channel (nominal)*	1.15
Pressure at core discharge	850 and 450 psia

*Calculated value based on two-dimensional calculations associated with Fig. 47. These values do not include "hot spot" effects.

Table 9. Design, Manufacturing, and Operating Tolerances Plus Resultant Hot-Spot Hot-Channel, and Burnout Reduction Factors*

Variable	Variation	Hot-Spot Factor, F_s**	Hot-Channel Factor, F_c**	Burnout Reduction Factor, F_b***
Plate thickness, w	+0.001 in.	1.0005	1.0002	0.9996
Coolant-channel thickness, ϵ	-0.005 in.	0.98	1.18	0.910
Uncertainty factors				
Fuel-element flow distribution	0.95	1.022	1.055	0.963
Local flow disturbances	1.00	-	-	-
Channel roughness	1.00	-	-	-
Channel mixing	0.00	-	-	-
Power-level measurement and regulation	1.02	1.020	1.020	-
Inlet temperature measurement and regulation	1.01	0.997	0.9992	0.9984
Operating-pressure measurement and regulation	0.90	-	-	0.9872
Heat-transfer-coefficient uncertainty	1.00	-	-	-
Burnout-heat-flux uncertainty	1.00	-	-	-
Local flux peaking	1.00	-	-	-
Calculated vs experimental power distribution	1.10	1.077	1.098	-
Time-wise power-density variation	1.00	-	-	-
Meat homogeneity	1.10	1.078	1.100	-
Deviation in plate fuel content	1.02	0.997	1.020	0.991
Over-all factors		1.180	1.563	0.856

*Information extracted from ref. 28.

**Maximum coolant film temperature = (coolant inlet temperature + variation) + (F_c x bulk coolant rise) + (F_s x coolant film drop).

***Minimum burnout heat flux = F_b x nominal burnout heat flux.

Table 10. HFIR Heat Transfer Characteristics

Power, Mw	100 (97.5 in plates and core coolant)	
Power density (av), Mw/liter	2.18	
Power density (max), Mw/liter	3.90	
Ratio of max-to-av power density	1.79	
Fuel-plate thickness, in.	0.050	0.040
Heat flux (av), Btu/hr-ft^2	8.77×10^5	7.89×10^5
Heat flux (max), Btu/hr-ft^2	1.57×10^6	1.41×10^6
Burnout heat flux (min), Btu/hr-ft^2		
Core outlet pressure = 850 psia	3.3×10^6	3.3×10^6
Core outlet pressure = 450 psia	3.0×10^6	3.0×10^6
Temperatures, °F		
Coolant inlet	120	120
Coolant outlet (av)	192	184
Bulk water (av)	156	152
Bulk water increase (max)	129	116
Drop across coolant film (max)	115	105
Drop across aluminum oxide film (max)		
Coolant pH = 7	192	172
Coolant pH = 5	52	47
Coolant film (max)	365	343
Oxide-aluminum interface (max)		
Coolant pH = 7	557	515
Coolant pH = 5	417	390
Metal temperature (max)		
Coolant pH = 7	570	524
Coolant pH = 5	430	399

TABLE OF NOMENCLATURE

D	Neutron diffusion coefficient
D_e	Hydraulic diameter, ft
G	Mass flow rate, lb/hr-ft^2
h	Heat transfer coefficient, Btu/hr-ft^2-°F
k_b	Thermal conductivity for average bulk water temperature, Btu/hr-ft-°F
k_{eff}	Effective neutron multiplication factor
ℓ	Prompt-neutron lifetime
L	Active length of core
N	Atomic density
$(Nu)_b$	Nusselt number for average bulk water temperature
P	Power
(P/V)	Power density in homogenized fuel annulus
$(Pr)_b$	Prandtl number for average bulk water temperature
(q_{max}/q_{av})	Ratio of maximum to average power density
R_I, R_V	Radius of island and cylindrical void, respectively
$(Re)_b$	Reynolds number for average bulk water temperature
ΔT_{sub}	Bulk water subcooling at burnout location and at burnout conditions, °F
v	Neutron velocity
V	Volume
w	Inverse reactor period
μ_b, μ_w	Viscosity of average bulk water and of local wall temperature, respectively, lb/hr-ft
ν	Neutrons produced per fission
ρ	Density, lb/ft^3
ρ_ℓ	Liquid density at saturation temperature for system pressure

ρ_v	Vapor density at saturation temperature for system pressure
Σ	Macroscopic neutron cross section
τ	Neutron Fermi age
ϕ	Neutron flux, (neutrons/cm^3)($\frac{cm}{sec}$)
ϕ^*	Neutron adjoint flux
ϕ_E	Volume-averaged thermal-neutron flux in island target
ϕ_M	Maximum unperturbed thermal-neutron flux in island
χ_j	Fraction of neutrons born in jth group

Appendix 1

UNREFLECTED CORE

At one time it was suggested that the thermal flux in the island would be essentially independent of all but a comparatively thin annular region of the fuel next to the water island. This perhaps would be the case if the island neutron flux were due primarily to thermal leakage from the fuel annulus. Then, according to Eq. (7),

$$\frac{\phi}{P} = \left[\frac{\phi}{(P/V)_m} \right] \frac{q_{max}/q_{av}}{V} , \qquad (7)$$

the term in brackets would be essentially constant regardless of variations in the ratio of maximum-to-average power density and the fuel-region volume. It appeared then that ϕ/P could be increased significantly with little reduction in $\phi/(P/V)_m$ by increasing the ratio $(q_{max}/q_{av})/V$. The results discussed in the body of the report under the topic heading "Radial Power Distribution" indicate that if (q_{max}/q_{av}) is increased in a fixed-size core by reducing the number of discrete fuel regions in the fuel annulus, assuming that each region had the same maximum power density, then the sought-after objective is not attainable. Two other approaches were considered: (1) for a single-fuel-concentration core the outer reflector was removed and the outer radius of the fuel annulus was extended to obtain the same k_{eff} with the same uniform fuel concentration, and (2) the fuel annulus of an unreflected core was divided into two discrete fuel regions, the inner region being 4 cm thick and containing a fuel concentration five times that of the outer region. Using two fixed fuel concentrations, the outer diameter of the core was increased to achieve the desired k_{eff}.

For approach (1) three cases in addition to the single-region-fuel-annulus reflected core were calculated. One had the same fuel concentration as the reflected core. The concentrations in the other two were reduced in order to increase the neutron diffusion length. The results in Table 11 indicate that in each case, including the two-fuel-region core, the necessary large increase in the core diameter

Table 11. Characteristics of Reflected and Unreflected Flux-Trap Cores

	HFIR	Unreflected Cores			
Number of fuel regions	1	1	1	1	2
$N^{25} \times 10^{-19}$ atoms/cm^3	25	25	20	15	50-10
Outer radius of fuel region, cm	19	36.8	39.8	42.9	11-51.5
Inner radius of fuel region, cm	7	7	7	7	7-11
Length of core, cm	45.72	45.72	45.72	45.72	45.72
$(q_{max}/q_{av})_R$	2.080	4.4	4.1	3.6	10.3
ϕ/P, relative	1	0.496	0.450	0.363	0.401
$\phi/(P/V)_m$, relative	1	1.00	1.14	1.34	0.67
P, relative for equal $(P/V)_m$	1	2.01	2.22	2.75	1.67

reduced ϕ/P by about 50%. $\phi/(P/V)_m$ did remain fairly constant, but the ratio $(q_{max}/q_{av})/V$ decreased significantly even though (q_{max}/q_{av}) was about doubled by the removal of the reflector. To avoid the large volume increase, a case was considered in which the fuel concentration was increased in the smallest core. The results indicated that criticality could not be obtained with reasonable fuel concentrations. There are, of course, many more combinations of fuel concentration and core size. However, an analysis of the results reported herein implies to the author that a reflected core with essentially uniform power distribution produces a more favorable combination of ϕ/P and $\phi/(P/V)_m$ than the unreflected cores.

Appendix 2

CYLINDRICAL CORE WITH NO WATER ISLAND

As mentioned in the introduction, the possibility of using a cylindrical core with no island for isotope production was considered. In such a core the thermal-flux region of interest would probably be the flux peaking region in the side reflector, where there is perhaps more space for feed material than in the island of the flux-trap geometry. In order to compare thermal-flux values and californium production rates in the island and side-reflector regions of the respective reactors, cylindrical cores without the island in the middle were calculated and compared to a flux-trap core of the same length. The curves in Fig. 61 show the variation of ϕ/P and $\phi/(P/V)_{av}$ with the radius of the solid-cylinder core. The cylindrical cores, represented by Fig. 61, and a typical HFIR core of the same length have been compared in Table 12 on the basis of equal power, equal volume, and therefore equal maximum power density, assuming that

Table 12. Comparison of Maximum Thermal Flux in Island of Typical HFIR with That in Beryllium Side-Reflector of Cylindrical Core with No Island

	HFIR	Cylindrical Core (No Island)
Power, Mw	100	100
$(P/V)_{av}$, Mw/liter	2.23	2.23
Core volume, liters	44.8	44.8
Core length, cm	45.72	45.72
Core radius, cm	-	17.64
ϕ_m, nv	6.88×10^{15}	2.35×10^{15}

the ratios of maximum-to-average power density are the same in the two cores. As indicated, the maximum thermal flux in the beryllium side-reflector of the cylindrical core is about one-third the maximum flux in the water island of the typical HFIR.

The use of a water side-reflector with the cylindrical core tends to increase the flux peaking. However, the much higher fuel concentration and/or larger core volume required to maintain criticality decrease the neutron leakage so that ϕ/P tends to be less with the water reflector.

For a further comparison of the two cores it is necessary to know how much more feed material, such as Pu^{242}, can be placed in the beryllium side-reflector of the cylindrical core than in the water island of the HFIR for the same amount of flux depression. Such calculations have not been made. However, assume for the present that about five times as much Pu^{242} could be used, and further assume that in both reactors the material would be irradiated for one year. Under such conditions indications are

PREFACE TABLE FOR FIG. 61

Code calculation, Wanda
Cross-section set, No. 2 (GNU averaged two-group)
Thermal temperature, 80°C

Active core length, 45.72 cm
Axial buckling, 0.002591 cm^{-2}
k_{eff}, 1.00

Region No.	Outer Radius, cm	Composition
1		U-235 + Al + H_2O, M/W = 1
2	r_1 + 30	Be + 5% H_2O + Exp (does not include Pu)

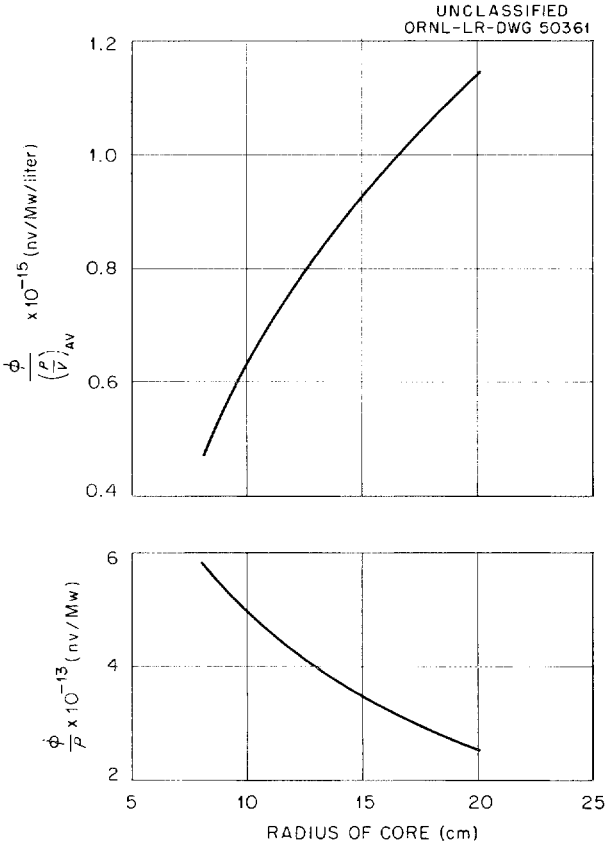

Fig. 61. Maximum Thermal Flux in the Beryllium Side Reflector of a Cylindrical Core per Unit Average Power Density and per Unit Power vs Radius of the Cylindrical Core.

that the HFIR would produce about 35 times as much Cf^{252} per unit of Pu^{242} feed material or seven times as much, total. If the material in the cylindrical core is irradiated until the same total amount of Cf^{252} is produced, it would take nearly twice as long as in the HFIR.

Appendix 3

ALTERNATIVE CONTROL SCHEMES

As mentioned under the topic heading "Control Studies," both soluble-poison and mechanical control schemes were considered for the HFIR, and several variations of each were studied in sufficient detail to permit the selection of one on its nuclear, mechanical, and operational merits. The particular system selected for the HFIR is described and discussed in detail in the body of the report. A brief discussion of the alternative systems is included herein in order to provide information that may be useful in the future.

Soluble-Poison Systems

Soluble-poison systems appeared at first to offer the most in the way of power-distribution control, since the control-region poison density could be essentially uniform over the length and around the circumference of the core. Thus considerable effort was expended in analytical analysis of the soluble-control systems. An additional report with the emphasis on the chemistry of the soluble-poison systems has been issued by McLain.[29]

Three possible methods of applying soluble poison to the HFIR were: (1) soluble poison in the coolant, (2) soluble poison in a D_2O reflector, or (3) soluble poison in an annular D_2O region between the fuel annulus and the outer reflector. The first method requires that a separate cooling system be provided for the island region since poisons in that area rob the island experiment of neutrons; another point to consider is that soluble poison in the fuel region contributes a positive effect to the temperature coefficient of reactivity. The second method requires the use of a D_2O reflector; this introduces mechanical design complications in providing for beam and rabbit type experiments in the reflector, and as is the case with the first method it would be very difficult to provide several control regions with separate poison-concentration regulation for taking care of power-distribution disturbances that might result from possible xenon instability.

The use of soluble poison in a separate region or regions located between the fuel and a beryllium reflector was preferred because the short residence time of the solution in the vicinity of the core region minimized temperature effects on reactivity, and because separate flow paths could be provided which would in principle allow for xenon instability control. Thus this system was selected for some additional study.

A basic requirement of a soluble-poison control system is that amounts of a specified poison material sufficient to take care of the reactivity requirements be soluble in the solvent. Therefore, assuming the annular control region to be uniform and homogeneous, calculations were performed to determine the reactivity worth vs concentration of two of the more promising poisons, boron and cadmium. (Multigroup calculations were used to compare the two poisons, since there is a rather strong dependence of worth on the nonthermal cross sections.) The results of the calculations are presented in Figs. 35 and 36. Figure 35, which compares boron and cadmium on the bases of their thermal macroscopic cross sections, indicates the effectiveness of the nonthermal cross section.

If all the reflected neutrons were stopped by the control region, as would be the case with the outer reflector removed, k_{eff} would be decreased from 1.20 to about 0.70. Although from a practical point of view all the neutrons could not be captured by the shim region, the results do suggest that the use of poisons with comparatively high resonance capture would provide significantly greater control-region worth. Calculations have not been made to determine the actual worth of the various resonance absorbers.

Most of the parameter-type studies were made with two-group calculations, using fast-group capture cross sections for boron and cadmium that were obtained from the multigroup results. The cross sections used are shown in Fig. 37. Making use of Figs. 35, 36, and 37 indicates that for k_{eff} equal to unity the fast cross sections of boron and cadmium were essentially the same, but the thermal cross section of cadmium was three times that of boron. This apparent disagreement emphasizes the inadequacy of a two-group analysis for determining gray-rod worths in a reactor where nonthermal neutron capture is significant.

The limitation on excess reactivity that is imposed by the eventual insensitivity of the control region (illustrated in Figs. 35 and 36) can be circumvented in part by the use of burnable poison and of course by simply decreasing the fuel loading. However, use of the latter method must be avoided in order to retain a desired fuel-cycle time. If a burnable poison is used, the curves in Figs. 35 and 36 will be shifted down. Since the presence of the additional poison in the fuel decreases neutron leakage from the fuel annulus, the worth of the control region will be decreased, resulting in a slight flattening of the curves. Just the opposite is true when the fuel loading is decreased. This is shown in Fig. 62.

The application of a soluble poison for a control system implies the use of an independent safety or emergency shutdown system and perhaps also an independent regulating system, both of which would more than likely be of the mechanical type. The location of these rods or plates will of course determine to an appreciable extent their reactivity worth. Outside of the very compact fuel annulus the regions of greatest worth are located between the water island and the fuel and between the side reflector and fuel. The former location requires space that could otherwise be used for experiments; and regulating rods in this area, though not requiring much in reactivity, would have a deleterious effect on target irradiation. Therefore it was assumed that the safety and regulating rods or plates would be located adjacent to the soluble-poison shim region. The worth of the safety plates, assuming that the plates form a complete curtain around the fuel annulus, is essentially that determined for the soluble-poison shim.

Generally, it appears desirable that the total worth of the regulating rods should be no more than one dollar. If at the beginning of the fuel cycle (when the shim has its highest concentration for a critical core) the worth of the regulating rods is just under a dollar, then at the end of the cycle (when the poison concentration in the shim is at its lowest) the worth of the regulating rods would be greater than one dollar. This effect was investigated with an annular regulating region located between the fuel annulus and the shim region. It was assumed that the problem could be adequately studied by changing the poison concentration of the regulating region uniformly, rather than by changing its vertical position. The worth of the regulating region as a function of its poison concentration was determined for three different poison concentrations in the shim region. As indicated by the slopes of the curves in Fig. 63, $\Delta k/\Delta N^B$ for $k_{eff} \cong 1.20$ (a case which approximately represents the core at the end of the cycle when the shim poison concentration is zero) is about ten times greater than at the beginning of the cycle. (The reduced fuel concentration and redistribution of power at the end of the cycle permit greater neutron leakage into the outer reflector, resulting

PREFACE TABLE FOR FIG. 62

Code calculation, Wanda
Cross-section set, No. 1 (two-group)
Thermal temperature, 80°C

Active core length, 30.5 cm
Axial buckling, 0.004568 cm^{-2}

Region No.	Outer Radius, cm	Composition	$N^{25} \times 10^5$ (atom/barn-cm) A	B	C
1	2	100 g Pu-242 + Al + H_2O, M/W = 1			
2	7	H_2O			
3	9.2	U-235 + Al + H_2O, M/W = 1	14	17	20
4	11.4	↓	26.1	31.7	37.3
5	13.6	↓	37.6	45.6	53.7
6	15.8	↓	40.5	49.2	57.8
7	18	↓	33.2	40.3	47.4
8	20.2	Be + 5% H_2O + Exp + B			
9	70.2	Be + 5% H_2O + Exp			

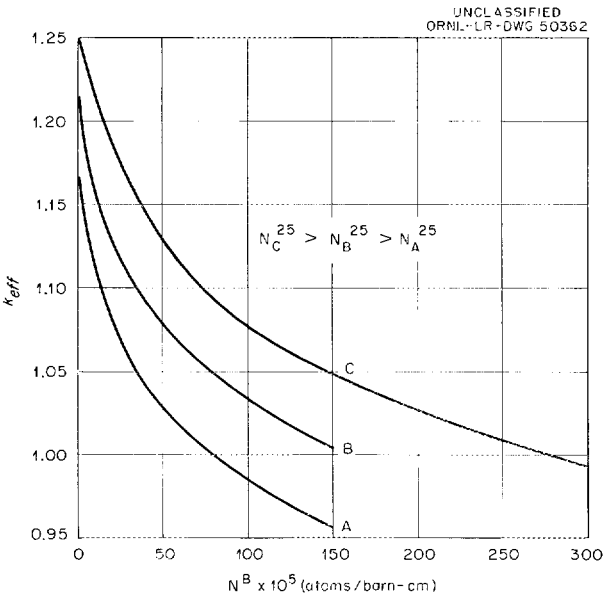

Fig. 62. Reactivity vs Boron Concentration in Control Region for Different Fuel Loadings.

in greater control worth. Therefore the factor of 10 is somewhat underestimated.) These results indicate that a mechanical regulating system with variable maximum stops would have to be used to limit the worth to one dollar. The position of the stops presumably would be programed with the poison concentration in the shim region.

In some instances the reflector region close to the core, where the spectrum is significantly harder than elsewhere in the reflector, is desirable for experimental space. Making this space available for such apparatus as rabbit tubes would require the shim region to be moved outward, leaving a portion of the reflector between the core and shim region. Thus for a particular poison concentration the worth of the shim region would be less. The variation of k_{eff} and thermal-flux distribution with shim position is shown in Figs. 64 and 65. In these calculations the shim poison concentration was constant, the assumption being made that a greater concentration was not

PREFACE TABLE FOR FIG. 63

Code calculation, Wanda
Cross-section set, No. 2 (GNU averaged two-group)
Thermal temperature, 80°C

Active core length, 45.72 cm
Axial buckling, 0.002591 cm^{-2}

Region No.	Outer Radius, cm	Composition
1	7	H_2O
2	19	U-235 + Al + H_2O, M/W = 1, N^{25} = 25 x 10^{-5} atom/barn-cm
3	20	Be + 5% H_2O + regulating boron
4	22	D_2O + shim boron
5	52	Be + 5% H_2O + Exp

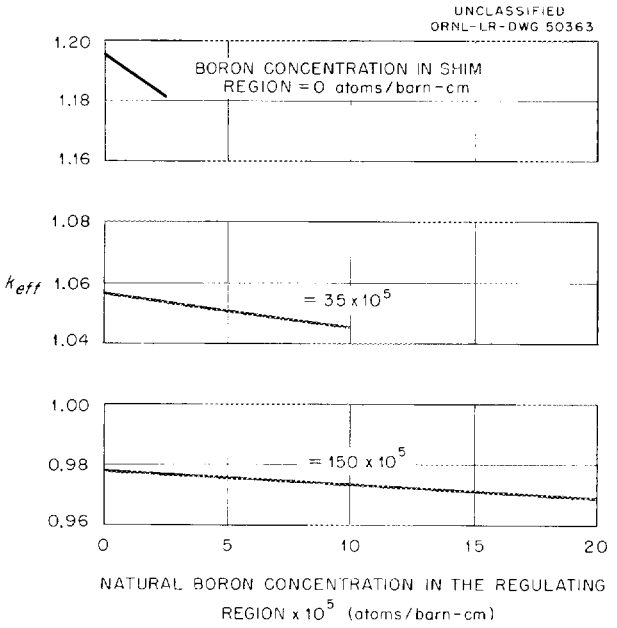

Fig. 63. Reactivity Worth of Regulating Region for Different Poison Concentrations in the Control Region.

attainable. If poison solubility is a problem in the shim region, burnable poison could be added within practical limits to the fuel region to make up the difference in control requirements as the shim is moved out. Since the inclusion of the burnable poison in the fuel region would have little effect on the flux distribution in the side reflector, the curves in Fig. 65 are reasonably representative of the case in which k_{eff} would be maintained at a particular value by means of the burnable poison.

Even though it did not appear feasible to add soluble poison to the coolant, island, and reflector regions, a few calculations were made to determine the worth of the poison in these regions and the effects it would have on ϕ/P. For comparison purposes two cases were considered: (1) poison added to the coolant in all regions, including the island region, and (2) poison added to the coolant in all regions except the island. The latter case would of course require a separate cooling system and vessel; however, such a vessel was not considered in the calculations. The results of the calculations are shown in Figs. 66 and 67. As would be expected, the core with

PREFACE TABLE FOR FIGS. 64 AND 65

Code calculation, Wanda
Cross-section set, No. 1 (two-group)
Thermal temperature, 80°C

Active core length, 30.5 cm
Axial buckling, 0.004568 cm^{-2}

Region No.	Outer Radius, cm	Composition	$N^{25} \times 10^{5}$ (atom/barn-cm)
1	2	100 g Pu-242 + Al + H_2O, M/W = 1	
2	7	H_2O	
3	9.2	U-235 + Al + H_2O, M/W = 1	17
4	11.4	↓	31.7
5	13.6	↓	45.6
6	15.8	↓	49.2
7	18	↓	40.3
8		Be + 5% H_2O + Exp	
9	r_8 + 2.2	Be + 5% H_2O + Exp + B, N^{B} = 100 x 10^{-5} atom/barn-cm	
10	~71	Be + 5% H_2O + Exp	

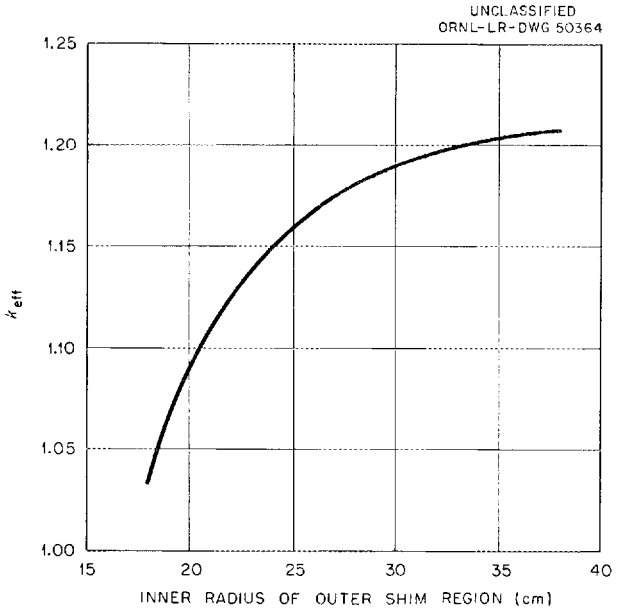

Fig. 64. Reactivity Worth of Control Region as a Function of Control-Region Position.

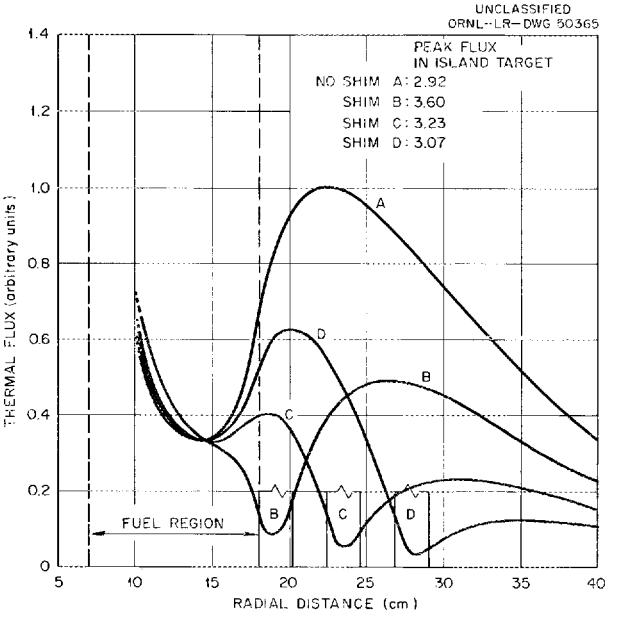

Fig. 65. Thermal-Flux Distribution in the Beryllium Side Reflector as a Function of Control-Region Position.

poison added to all regions requires a lower concentration of the poison in the coolant. However, for a 5% decrease in reactivity there is a 30% decrease in thermal flux in the island because of the presence of the control poison in the island. When the poison is not permitted in the island, a similar change in reactivity actually results in about a 0.2% increase in the island thermal flux.

An advantage in putting the soluble poison in the coolant, as compared with the narrow soluble-poison region between the fuel annulus and the beryllium reflector, is the lower poison concentration for a specified change in reactivity and the elimination of the D_2O required in the separate soluble-poison control region. A comparison of

PREFACE TABLE FOR FIGS. 66 AND 67

Code calculation, Wanda
Cross-section set, No. 1 (Two-group)
Thermal temperature, 80°C

Active core length, 30.5 cm
Axial buckling, 0.004568 cm^{-2}

Region No.	Outer Radius, cm	Composition*	$N^{25} \times 10^5$ (atom/barn-cm)
1	2	100 g Pu-242 + Al + H_2O, M/W = 1	
2	7	H_2O	
3	9.2	U-235 + Al + H_2O + B^{10}, M/W = 1,	
		N^{B-10}/N^{25} = 0.05	13.6
4	11.4	↓	29.4
5	13.6	↓	43.5
6	15.8	↓	52.7
7	18	↓	52.2
8	28	Be + 5% H_2O + Exp	
9	68	H_2O	

*For one curve in Figs. 66 and 67, regions 1 through 9 contained natural boron in the water. For the other curve, only regions 2 through 9 contained boron in the water. For each point on the curves, regions containing boron contained the same concentration (N^B/N^{H_2O}) of boron.

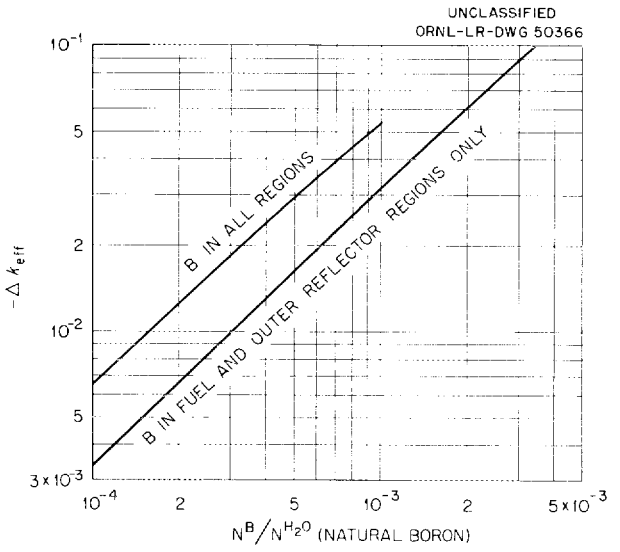

Fig. 66. Reactivity Worth of Natural Boron in Various Core Regions.

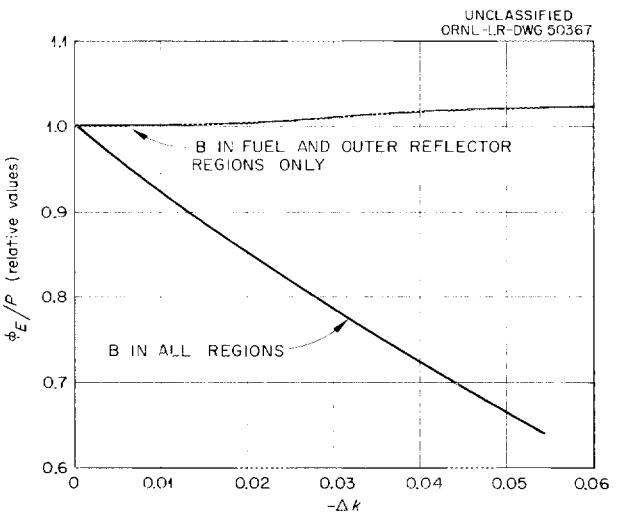

Fig. 67. Average Thermal Flux in the Central Experiment per Unit Power vs Change in Reactivity Caused by Boron Concentration Changes in the Coolant.

reactivity worths indicates that for a 10% change in reactivity a 2.2-cm-thick annular soluble-poison region between the fuel and outer reflector would require a boron concentration about three times greater than that necessary when the boron is added to the coolant in all regions except the central island.

Another method for reducing the soluble-poison concentration is to use two poison regions, one adjacent to each circumferential terminator of the fuel annulus. This would have the obvious disadvantage of inserting a sink for thermal neutrons between

the island and the source of neutrons. Nevertheless, it should be very effective control, since the fuel would be partially isolated from both the inner and outer moderating-reflector regions. The reactivity worth of the double shim system was compared to that of the single, outer shim system. The results in Fig. 68 indicate a very significant reduction in boron concentration when both the inner and outer shim regions

PREFACE TABLE FOR FIGS. 68 AND 69

Code calculation, Wanda
Cross-section set, No. 1 (two-group)
Thermal temperature, 80°C

Active core length, 30.5 cm
Axial buckling, 0.004568 cm^{-2}

Region No.	Outer Radius, cm	Composition	$N^{25} \times 10^{5}$ (atom/barn-cm)
1	2	100 g Pu-242 + Al + H_2O, M/W = 1	
2	4.8	H_2O	
3	7	H_2O or Be + 5% H_2O + Exp + B	
4	9.2	U-235 + Al + H_2O, M/W = 1	17
5	11.4	↓	31.7
6	13.6	↓	45.6
7	15.8	↓	49.2
8	18	↓	40.3
9	20.2	Be + 5% H_2O + Exp + B	
10	70.2	Be + 5% H_2O + Exp	

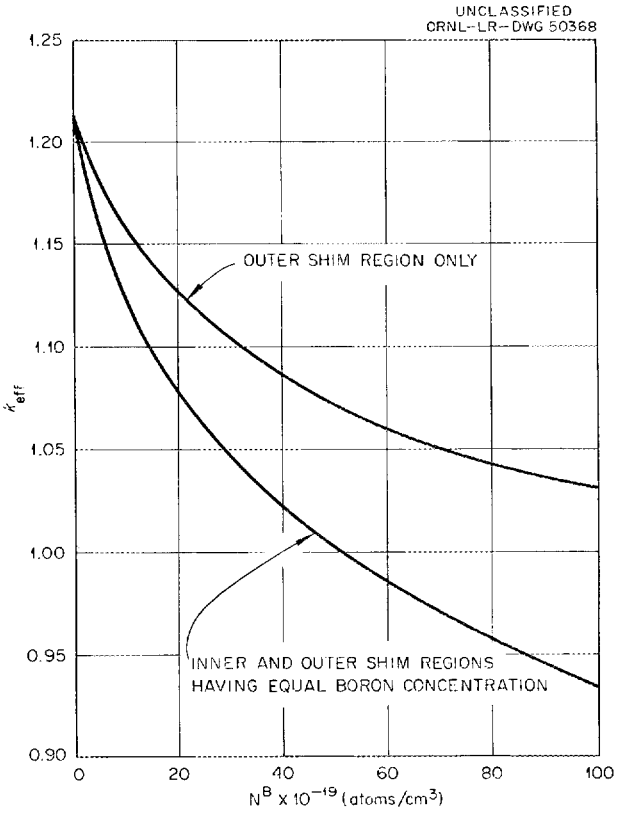

Fig. 68. Reactivity vs Boron Concentration in the Control Region for a Single Outer Control Region and an Inner and Outer Combined Control Region.

are used. For very high boron concentrations the inner shim region accounts for about 10% more in reactivity.

By comparison to the single, outer shim system the big disadvantage of the double shim system is the reduction in thermal-neutron flux in the island as the poison concentration is increased. According to the results presented in Fig. 69, reducing k_{eff} to unity ($\Delta k \cong 0.21$) reduces the thermal flux by 40%, as compared to a 20% increase for the single shim system. Actually, this comparison is not exactly fair because in the double shim core the addition of poison to the shim regions caused the maximum power density to shift away from the island region to the center of the fuel annulus, thus reducing neutron leakage to the island. For a particular initial shim poison concentration the fuel would be distributed in the annulus so as to maintain at the inner fuel-annulus surface as high a power density as possible during the entire fuel burnup cycle. Under such circumstances the results would not be quite as severe as indicated by Fig. 69.

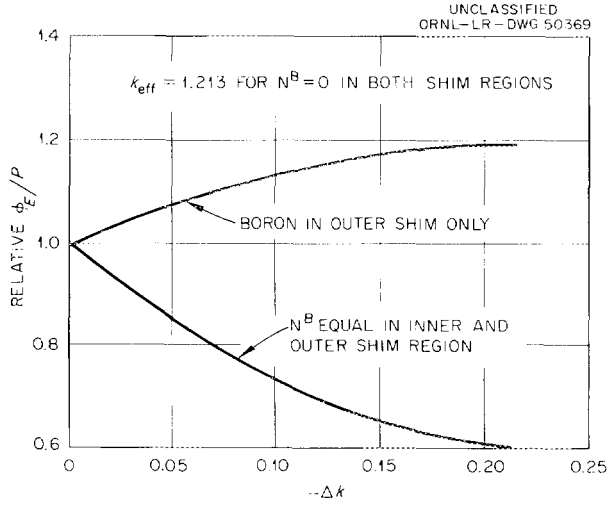

Fig. 69. Average Thermal Flux in the Central Experiment per Unit Power vs Change in Reactivity Caused by Boron Concentration Changes in a Single Outer Control Region and in a Combined Inner and Outer Control Region.

Based on the results reported herein, pertaining to the soluble-poison control systems, it was tentatively concluded that the most suitable version of the soluble-poison systems for the HFIR was that incorporating a separate annular poison region between the fuel annulus and the outer beryllium reflector. The poison region would provide shim control, while emergency shutdown and regulating control would be accomplished by mechanical means. In order to reduce the required poison concentration in the soluble shim region in accordance with solubility limitations, the use of a burnable poison was considered in the fuel plates or in plates adjacent to the shim region.

Mechanical Control Systems

In addition to the circumferential plate-type mechanical system selected for the HFIR, a horizontally split core and a movable side-reflector design were considered. A brief discussion of these two schemes follows.

Split core.--In the split-core design it was proposed that the bottom half of the core be moved relative to the fixed upper half. Two-dimensional, two-group calculations were made to obtain a curve of reactivity vs distance between the two halves and also to study the variations in power distribution and flux in the island region. As shown in Fig. 70, there is a slight increase in reactivity, when the core halves are

PREFACE TABLE FOR FIG. 70

Core calculation, PDQ (two-dimensional)
Cross-section set, No. 2
(GNU averaged two-group)
Thermal temperature, 80°C

Active core length, 30.6 cm
(no gap between halves)
Height of side reflector, 30.6 cm
(no gap between halves)
Height of H_2O end-reflector, 20 cm
(each end)

Region No.	Outer Radius, cm	Composition
1	7	H_2O
2	18	U-235 + Al + H_2O, M/W = 1, N^{25} = 59.4 x 10^{-5} atom/barn-cm
3	68	Be + 5% H_2O + Exp
1a	68	H_2O (end reflector)
1b	68	H_2O (gap between vertical halves)

Note: The thermal flux in Fig. 70 was averaged over a 31-cm length of the vertical centerline of the H_2O island for all core lengths.

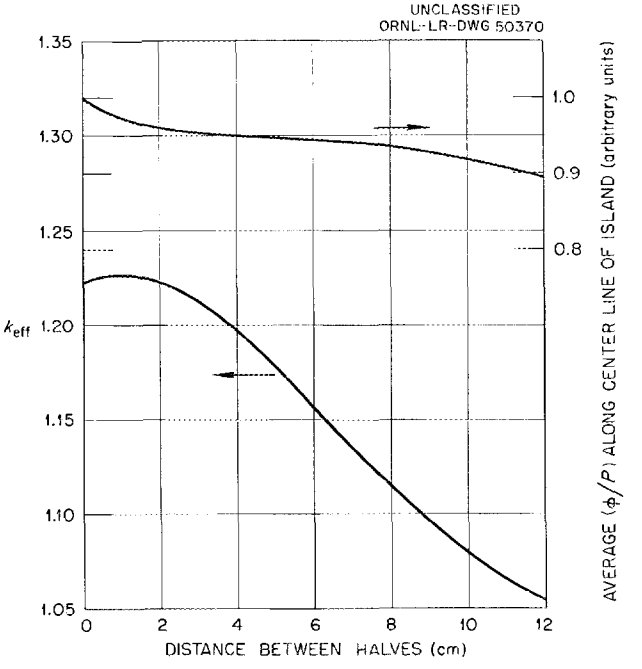

Fig. 70. Average Thermal Flux Along Center Line of Island per Unit Power, and Reactivity vs Distance Between Vertical Halves of Split Core.

first separated; this apparently results from increased moderation of the undermoderated core. After a separation of about 2 cm, the curve, by comparison to the usual S-curve for conventional control rods, is fairly straight for a change in reactivity of about 15%. Within this range the average change in k per centimeter of separation distance was about 1.5%. With the two halves separated, power peaking occurred at the fuel edges adjacent to the water gap between the two core halves. In order to reduce this peaking, poison could be added in an extension of the cladding beyond the meat. Such an extension plus a water space about 1 cm thick was also desired for establishing the coolant velocity profile. Therefore the fuel in the two halves would actually be separated by at least 2 cm so that the flat portion of the k vs distance curve as shown in Fig. 70 would not actually be used. Although the calculations associated with the curves in Fig. 70 did not account for variations caused by fuel burnup, it appears that control-wise the split-core design would be suitable for an HFIR core initially containing 13% reactivity with the core halves together.

In order to determine the variation of ϕ/P with distance between the two halves, it is necessary to study the fuel cycle. At the beginning of the cycle the core halves would be separated by about 10 cm. In comparing this core with a core controlled with circumferential control plates, it was observed that ϕ/P for the split core was about 25% less than for the nonsplit core (cf Figs. 69 and 70). As the fuel burned up, this difference was reduced to about 5%.

Further studies of the split-core design might possibly narrow the difference in ϕ/P between the two types of cores just mentioned. However, there is one outstanding disadvantage of the split core that was responsible for the termination of calculations: the cost of fabricating essentially two cores instead of one for each new loading. Irrespective of fuel cost, the cost of a core is determined more by the number of fuel plates than by the length of the plates. A split core requires twice as many plates as the one-piece core. Another disadvantage of the split core is the lack of multiplicity of control segments for emergency shutdown. Because of design and fabrication complications it was not desirable to divide the bottom core half into several independent sections. Thus an independent scram system would need to be provided.

Movable side reflector.--The possibility of moving segments of the beryllium outer reflector in the radial direction was considered, although such a system would introduce many problems associated with the installation of experiments in the outer reflector region. If experiments are neglected, complete removal of the beryllium reflector (leaving water in its place) will reduce k_{eff} by about 12% for a 30-cm-long core (possibly a little more for a 46-cm-long core because of the greater leakage from the longer core). Figure 71 indicates that as the inside diameter of the beryllium reflector is expanded reactivity changes in a nearly linear fashion until a water-gap thickness of about 6 cm is achieved. The decrease in reactivity resulting from the 6-cm movement is about 8%. (In actual operation the effective metal-to-water ratio of the annulus containing the beryllium would decrease as the wedge-shaped pieces of beryllium moved out radially; thus the decrease in reactivity would be somewhat greater than that given above. This effect and the effect of fuel burnup were not considered in the calculations.)

As the beryllium moves away from the fuel region and is replaced with water, there is an increase in power density at the outermost edge of the fuel region. This is indicated by the curve in Fig. 71 that represents the ratio of radial maximum-to-average power density. If radial grading of the fuel density is used, the maximum power density can be controlled by decreasing the fuel concentration near the outer edge. Nonuniform fuel burnup would also help, since the low fuel concentration in that area tends to accelerate burnup.

PREFACE TABLE FOR FIG. 71

Code calculation, Wanda
Cross-section set, No. 1 (two-group)
Thermal temperature, 80°C

Active core length, 30.5 cm
Axial buckling, 0.004568 cm^{-2}

Region No.	Outer Radius, cm	Composition	$N^{25} \times 10^{10}$ (atom/barn-cm)
1	2	100 g Pu-242 + Al + H_2O, M/W = 1	
2	7	H_2O	
3	9.2	U-235 + Al + H_2O + B^{10}, M/W = 1, N^{B-10}/N^{25} = 0.05	13.6
4	11.4		29.4
5	13.6		43.5
6	15.8		52.7
7	18		52.2
8		H_2O	
9	r_8 + 10	Be + 5% H_2O + Exp	
10	~68	H_2O	

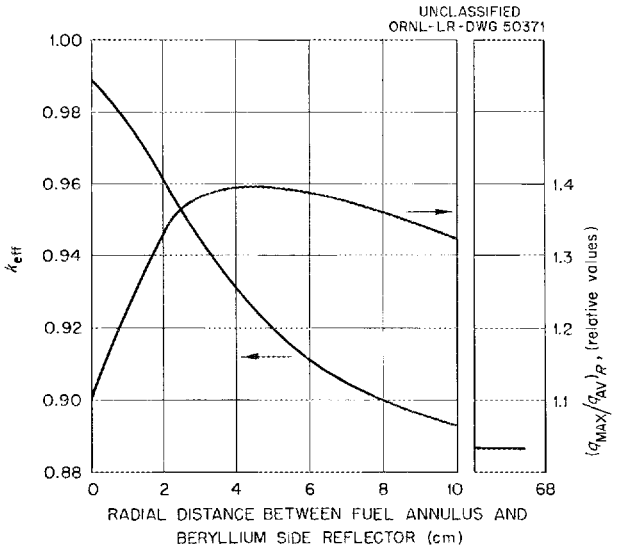

Fig. 71. Ratio of Maximum-to-Average Power Density in the Radial Direction, and Reactivity vs Radial Distance Between Fuel Annulus and Beryllium Side Reflector.

The water gaps between the beryllium wedges tend to cause a circumferential variation in power density near the outside edge of the fuel region. However, since the gaps are small when the beryllium is close, and since, as just described, the power density near the edge must initially be well below the maximum permissible, the circumferential variations would more than likely be insignificant.

The movement of the beryllium also changes the position of the peak thermal flux in the reflector. However, since the use of a movable reflector practically prohibits the incorporation of experiments in the beryllium portion of the reflector, the roaming flux would probably be of little consequence.

There is some question concerning the use of the movable reflector for safety control. Certainly a considerable amount of burnable poison would have to be used, since the total worth of the beryllium is only about 12%.

After this preliminary study, it was concluded that the movable-reflector control system should be discarded in favor of the vertical-plate system, primarily because of the lack of reactivity worth and the inability to install fixed-position experimental facilities in the beryllium.

Appendix 4

NUCLEAR CONSTANTS AND CALCULATIONAL PROCEDURE

As mentioned in the introduction, the majority of the calculations were made using two-group, one-dimensional multiregion diffusion-theory reactor codes in order to reduce to practical proportions the time and money required for the very extensive parameter study that was undertaken. At various times the results for particular cases were checked with more sophisticated methods such as two-group, two-dimensional multiregion diffusion theory (PDQ);[30] thirty-four-group, one-dimensional multiregion diffusion theory employing the Selengut-Goertzel term for neutron slowing-down by hydrogen (GNU-II);[31] thirty-four-group, one-dimensional multiregion consistent-P_1 theory employing the Selengut-Goertzel term for neutron slowing-down by hydrogen (Compone);[32] and multigroup, one-dimensional multiregion transport theory (SNG).[33] The two-group, one-dimensional codes used were Wanda,[34] for general calculations; Edna 1,[35] for obtaining adjoint fluxes; and Candle-2[36] for fuel-cycle-time calculations.

For all one-dimensional cases an axial buckling equal to 16 cm, 8 cm on each end, was used. This value appeared consistent with data from the MTR[37] and was later shown to give essentially the same value of k_{eff} as obtained from a two-group, two-dimensional calculation.

Several sets of cross sections were used in the process of calculating various HFIR cores. The original two-group cross sections, used with Wanda for a portion of the parameter study, were, with a few exceptions, extracted from a listing of Eyewash[38] cross sections, weighting the nonthermal constants with a 1/E slowing-down density in order to obtain the fast-group cross sections. The thermal diffusion coefficient was calculated from

$$D_2 = \frac{1}{3\left[\Sigma_{tr_2} + \Sigma_{a_2}\right]} ,$$

where $\Sigma_{tr_2}^{H_2O}$ was determined from values of λ_{tr} reported by Petrie et al.[39] The fast scattering removal cross section was calculated from

$$\Sigma_{R_1} = \frac{D_1}{\tau} ,$$

where both the fast diffusion coefficient and τ for water and water-aluminum mixtures were calculated by a numerical integration method[40] which assumed a 1/E flux, incorporated fission spectrum weighting, and included arbitrary weighting factors which were used to obtain agreement between calculated and experimental values of τ at a few points. Curves of D_1 and τ vs aluminum-to-water ratio are presented in Fig. 72. For beryllium τ was taken from ref. 41. To account for experiments and structural material in the outer beryllium reflector, a thermal absorption cross section of 0.002 cm^{-1} was added to the reflector for all cases.

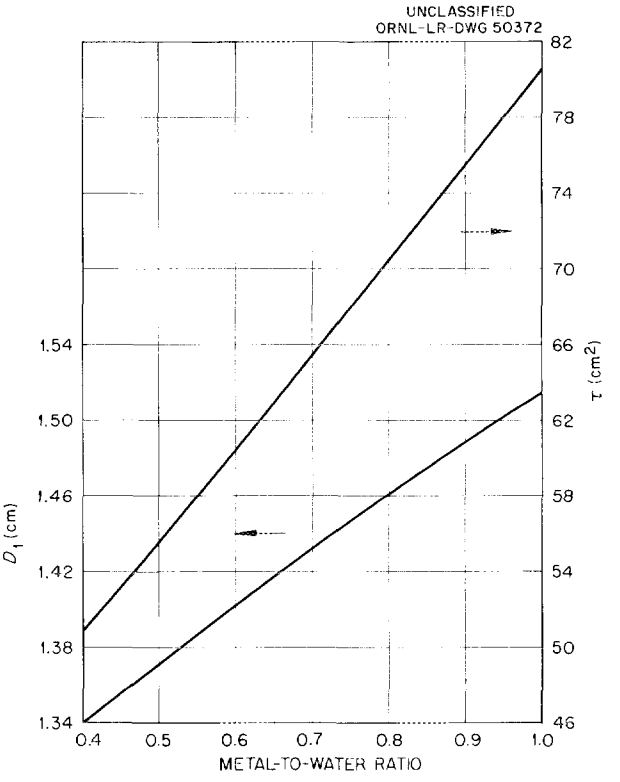

Fig. 72. Fast Diffusion Coefficient and Age for a Two-Group Cross-Section Set vs Volume Ratio of Aluminum to Water.

In addition to the n-2n reaction in beryllium there is an n-α reaction (with neutrons above 1 Mev) that leads to the formation of the comparatively-high-cross-section isotopes He^3 and Li^6. Depending on the energy spectrum in the beryllium, the "beryllium" cross section can increase significantly in a few months. Neither this effect nor the n-2n effect was considered in the parameter study reported herein. However, the subject has been investigated in connection with the HFIR, and the results, reported in ref. 42, indicate that the n-2n and n-α reactions in the beryllium side reflector would have no significant effect on the results of the parameter study and selection of a typical HFIR core.

For most of the calculations the experimental region in the center of the water island contained curium or plutonium and their irradiation products plus water and aluminum. The average thermal cross section of the target, as a function of time and excluding the water and aluminum, has been estimated by Claiborne[8] using the best available consistent set of cross sections and decay constants for the isotope chain starting with Pu^{242}. Averaged over a one-year period at an average thermal-neutron flux level of 3×10^{15}, the cross section was approximately 58 barns. Nuclearwise, it was assumed that the target cross section was all capture.

The aluminum in the island target served as the matrix material for the oxides of the prime feed material and also provided the necessary heat transfer surface area. It was initially estimated that the target heat, resulting from the fissioning of Cm^{245}, Cm^{247}, Cf^{249}, and Cf^{251}, could be adequately removed if there were 5 g of aluminum for each gram of plutonium oxide.

Table 13 lists the original set of two-group cross sections that were used. Throughout the parameter study there were some variations in cross sections because of different assumptions regarding temperatures. For some cases samarium and equilibrium xenon were taken into account by multiplying the uranium absorption cross section by 1.062.

Table 13. Cross-Section Set No. 1

Material	H	O	Al	B	Be	U^{235}	Target*	50% Al + 50% H_2O
σ_{a_2}	0.284	-	0.20	615	0.0087	569	58	-
σ_{f_2}	-	-	-	-	-	482	-	-
$3\sigma_{tr}$	179.3(H_2O)		3.95	-	2.08	24.59	-	-
σ_{a_1}	0.00887	-	0.024	36	0.0002	37.98	-	-
σ_{f_1}	-	-	-	-	-	27.13	-	-
D_1	1.20(H_2O)		-	-	-	-	-	1.5148
τ	33(H_2O)		-	-	-	-	-	80.6

*Average of all involved heavy isotopes for one year's irradiation at 3×10^{15} nv.

While preliminary parameter studies were being made with the cross sections in Table 13, an up-to-date and consistent set of thirty-four-group cross sections was being developed for use in GNU.[18] Upon the completion of this work, two-group constants were generated from multigroup calculations, the purpose being to obtain actual spectrum-averaged fast-group constants. The particular core used in the multigroup calculations contained a single fuel region; several calculations were made to cover the desired range of fuel concentrations. No attenpt was made to obtain a more accurate spectrum for each particular core. Table 14 lists the nuclear constants obtained from the multigroup results along with the characteristics of the core for which they were calculated. In all regions except the fuel region the fast-group cross sections were averaged over the specified fuel-concentration range.

When different length cores were calculated, only the target cross sections were changed. New target cross sections were obtained from GNU calculations using the same reactor described in Table 14, except that the length of the core and the metal-to-water ratio in the target were changed correspondingly. Table 15 lists the pertinent information and the target cross sections.

The fuel-cycle-time calculations required another set of cross sections since Candle-2 requires microscopic cross sections. These cross sections were calculated from a representative set of GNU-averaged two-group constants. Actually, Candle requires four-group cross sections, but the code can be used as a two-group code if for the two intermediate groups the transport cross sections are set equal to essentially infinity, the absorption and fission cross sections are set equal to zero, and the removal cross sections are set equal to each other and equal to the usual two-group

Table 14. Cross-Section Set No. 2

Actual length of all regions of cylindrical core = 30.5 cm

Target Region, R_1 = 2 cm, Temperature = 80°C

Material	H	O	Al	"Pu"
Atoms/barn-cm	0.0325	0.01625	0.0301	0.0006442

$\Sigma_{a_1} = 0.0005597$ $\quad \Sigma_{R_1} = 0.02324$ $\quad D_1 = 1.5351$

$\Sigma_{a_2} = 0.05291$ $\quad D_2 = 0.3261$

H_2O Region, R_2 = 7 cm, Temperature = 80°C

Material	H	O
Atoms/barn-cm	0.065	0.0325

$\Sigma_{a_1} = 0.0005419$ $\quad \Sigma_{R_1} = 0.04461$ $\quad D_1 = 1.40818$

$\Sigma_{a_2} = 0.01755$ $\quad D_2 = 0.1703$

Fuel Region, R_3 = 18 cm, Temperature = 80°C

Material	H	O	Al	U^{235}
Atoms/barn-cm	0.0325	0.01625	0.0301	(10 to 70) x 10^{-5}

$\Sigma_{a_1} = 17.59N^{25} + 0.00095; \quad 10 \times 10^{-5} \leq N^{25} \leq 40 \times 10^{-5}$

$= 15.55N^{25} + 0.01765; \quad 40 \times 10^{-5} \leq N^{25} \leq 70 \times 10^{-5}$

$\Sigma_{R_1} = 0.0221 - 1.5N^{25} \qquad D_1 = 27.5\ N^{25} + 1.5163$

$\nu\Sigma_{f_1} = 31.5N^{25} + 0.00037; \quad 10 \times 10^{-5} \leq N^{25} \leq 30 \times 10^{-5}$

$= 27.5N^{25} + 0.00158; \quad 30 \times 10^{-5} \leq N^{25} \leq 50 \times 10^{-5}$

$= 24.1N^{25} + 0.00330; \quad 50 \times 10^{-5} \leq N^{25} \leq 70 \times 10^{-5}$

$\Sigma_{a_2} = 537.3N^{25} + 0.01437 \quad D_2 = 0.3259 - 3.25N^{25} \quad \nu\Sigma_{f_2} = 1083\ 7N^{25}$*

Outer Beryllium-Reflector Region, R_4 = 48 cm, Temperature = 80°C

Material	H	O	Be	Exp.
Atoms/barn-cm	0.00325	0.001625	0.1174	0.1 (σ_{exp} = 0.02)

$\Sigma_{a_1} = 0.00008765$ $\quad \Sigma_{R_1} = 0.009546$ $\quad D_1 = 0.6591$

$\Sigma_{a_2} = 0.003818$ $\quad D_2 = 0.4576$

*After a large number of calculations had been completed, this value was found to be slightly in error. The revised value is $1108.4\ N^{25}$.

Table 15. Target Cross Sections for Different Length Cores; Cross-Section Set No. 2 Continued

N^{25} = 40 x 10^{-5} atoms/barn cm for all cores
Weight of feed material (Pu-242) = 100 g

	Core Length (cm)			
	30.48	45.72	60.96	91.44
M/W in target	1	0.5	0.33	0.20
N^H	0.0325	0.04333	0.04875	0.05418
N^O	0.01625	0.02167	0.02438	0.02709
N^{Al}	0.0301	0.0197	0.0148	0.0098
N^{Pu}	0.0006442	0.0004295	0.0003221	0.0002147
Σ_{a_1}	0.0005597	0.0005804	0.0005898	0.0006000
Σ_{R_1}	0.02324	0.03079	0.03455	0.03832
D_1	1.5351	1.4584	1.4360	1.4212
Σ_{a_2}	0.05291	0.04113	0.03523	0.02934
D_2	0.3261	0.2499	0.2237	0.2025

removal cross section. Also, all neutrons must be born in the top group. The top-group cross sections are equal to the usual fast, two-group constants. The validity of such a scheme from the standpoint of code operability is evident upon examination of the following four-group equations with the above substitutions introduced:

$$D_1 \nabla^2 \phi_1 - \Sigma_{a_1} \phi_1 - \Sigma_{R_1} \phi_1 + \nu_1 \Sigma_{f_1} \phi_1 + \nu_4 \Sigma_{f_4} \phi_4 = 0 \quad ,$$

$$\Sigma_{R_1} \phi_1 - \Sigma_{R_1} \phi_2 = 0 \quad ,$$

$$\Sigma_{R_1} \phi_2 - \Sigma_{R_1} \phi_3 = 0 \quad ,$$

$$D_4 \nabla^2 \phi_4 - \Sigma_{a_4} \phi_4 + \Sigma_{R_1} \phi_3 = 0 \quad .$$

Since $\phi_1 = \phi_2 = \phi_3$, the top and bottom equations are the usual two-group equations. In the two middle groups no neutrons are lost or gained by leakage or absorption; so $\Sigma_{R_1} \phi_1$ represents the neutrons transferred from the fast to the thermal group.

Four-group cross sections were not used in Candle, because at the time the fuel-cycle-time calculations were made, it appeared that the GNU code was not calculating four-group constants correctly.

The cross sections that were used in Candle are listed in Table 16. The use of these cross sections in Candle resulted in a k_{eff} about 1% less than obtained with Wanda using cross-section set No. 2.

The two-group constants used in the two-dimensional analysis of the temperature and void effects on reactivity were generated from one-dimensional, multigroup calculations (GNU). These latter calculations were made for each temperature and void fraction considered and for all combinations of region temperatures and all combinations of region voids. Because the resultant number of two-group cross-section sets was quite large, a listing has not been included herein.

Table 16. Two-Group* Cross Sections Used in Candle; Cross-Section Set No. 3

	σ_{tr}		σ_a		σ_R	$\nu\Sigma_f$	
	1	4	1	4	1	1	4
H_2O	7.086	60.59	0.01635	0.540	1.325	0	0
Al	3.476	1.462	0.006738	0.186	0.01043	0	0
Be	4.245	5.370	0.0003709	0.008050	0.05859	0	0
B	4	4	**	600	0	0	0
U^{235}	0	12.5	19.4	537.2	0	33.5	1083.7
X^{135}	0	0	2.16 x 10^4 ***	2.7 x 10^6	0	0	0
Sm^{149}	0	0	0	50,000	0	0	0
Pm^{149}	0	0	0	0	0	0	0
I^{135}	0	0	0	0	0	0	0
FP	0	0	11.2≠	52≠	0	0	0
U^{236}	0	0	0	6	0	0	0
Refl. exp.	0	0	0	0.02	0	0	0

*$\sigma_{tr_{2,3}} = \infty$, $\sigma_{a_{2,3}} = 0$, $\sigma_{f_{2,3}} = 0$, $\sigma_{R_1} = \sigma_{R_2} = \sigma_{R_3}$.

**Depends on boron concentration. See Fig. 37.

***Calculated from BNL-325 assuming $\sigma(0.15 \text{ ev} \rightarrow \infty) = 7.64E^{-2.56}$ and a 1/E flux.

≠N. J. Pattenden, ORNL-2778.

Appendix 5

COMPARISON OF CODE CALCULATION RESULTS

In an attempt to verify the methods of calculation for the flux-trap core design, comparison calculations were made[43] on an infinitely long HFIR core, using SNG (18 groups), GNU(18 groups), GNU(34 groups), and Cornpone(34 groups). The results showed good agreement between multigroup diffusion theory and transport theory, and since the GNU (34 groups) code was the most convenient to use, it was generally used to spot check the results obtained with Wanda. A typical comparison between the Wanda and GNU calculations, using the HFIR core as presently conceived, is presented in Figs. 73 and 74. For the core containing no control (Fig. 73), GNU predicted a 31% greater value of ϕ_m/P and a 5.9% lower value of k_{eff} than calculated with Wanda. It was also observed that the GNU results gave a lower average thermal flux in the fuel region and thus a greater percentage of nonthermal fissions. A possible explanation to all these differences is that the GNU-averaged scattering removal cross section used in Wanda was not consistent with the multigroup calculation. If it is assumed that $\Sigma_R = D_1/\tau$ and that D_1 as calculated for Wanda by GNU was correct, then τ for the fuel region, using the two-group GNU constants, calculates to be about 66 cm^2, as compared to an experimental value of 81 cm^2. This indicates that the two-group removal cross section used in Wanda was too large. A smaller removal cross section should increase the fast leakage, thus increasing the thermal flux in the island, increasing the percentage of fast fissions, and decreasing k_{eff}. To check the validity of this hypothesis, a smaller fuel-region removal cross section was calculated for Wanda using the experimental value of τ and the fast diffusion coefficient averaged with GNU. The results of Wanda and GNU calculations (for a slightly different core than that used for the comparison in Fig. 73) are presented in Table 17. For these particular cases the use of

Table 17. Comparison of Core Characteristics Using Different Codes and Different Scattering Removal Cross Sections

Code	Σ_R (cm^{-1})	k_{eff}	ϕ/P
Wanda	0.02173	1.2056	5.044×10^{13}
Wanda	0.01783	1.1589	5.688×10^{13}
GNU	-	1.1311	6.195×10^{13}

the smaller removal cross section reduced the differences in ϕ/P from 23% to 9% and reduced the differences in k_{eff} from 6% to 2%. These results indicate that the GNU-averaged, two-group removal cross sections were in error. Recently the GNU method of averaging was changed;* the two-group Σ_R now agrees reasonably well with the value used in the second Wanda calculation in Table 17.

*Change made by Betty Maskewitz (ORGDP), Jan. 14, 1960.

At the beginning of the fuel cycle the thermal-flux distribution is similar to that shown in Fig. 74. For both the Wanda and GNU cases k_{eff} was made very nearly equal to unity by including different amounts of boron poison in the control region. The Wanda calculation required about 2.5 times the boron concentration as GNU to compensate for 1.3 times as much excess reactivity. Increasing the fast-neutron leakage from the fuel so that more thermal neutrons must return through the control plates will increase the worth of the control plates. Thus the use of a smaller Σ_R in Wanda would decrease the calculated differences in control worth.

Even though the GNU multigroup calculations are generally considered to be more accurate than the Wanda two-group calculations, it was concluded that the latter calculations were satisfactory for the parameter studies and for establishing the so-called optimum core design. GNU calculations were then used to more accurately determine absolute values associated with the particular optimum core.

As a final check on the calculational methods, an extensive critical-experiment program is presently being conducted;[44] flux distributions, power distributions, critical mass, control-rod worth, and temperature and void coefficients are being determined or are scheduled to be determined, using experimental cores that approximate nuclearwise the proposed HFIR design.

PREFACE TABLE FOR FIGS. 73 AND 74

Code calculation, Wanda and GNU
Cross-section set, No. 2 (GNU averaged, two-group) and GNU 34 group (ORNL revised)

Thermal temperature, 80°C
Active core length, 45.72 cm
Axial buckling, 0.002591 cm^{-2}

Region No.	Outer Radius, cm	Composition	$N^{25} \times 10^{10}$ (atom/barn-cm)
1	7	H_2O	
2	7.5	U-235 + Al + H_2O, M/W = 1	15
3	8		18.0
4	8.5		21.6
5	9		25.5
6	9.5		29.9
7	10		34.4
8	11		39.1
9	12		47.8
10	13		54.5
11	15		60.0
12	16		57.7
13	17		50.9
14	17.5		46.0
15	18		41.1
16	18.5		36.0
17	19		31.1
18	21	Be + 5% H_2O + Exp + B*	
19	51	Be + 5% H_2O + Exp	

*For Fig. 73 region 18 did not contain boron. For Fig. 74 region 18 contained 200 x 10^{-5} atom/barn-cm ($\Sigma_{a_{th}} = 1.22\ cm^{-1}$) of natural boron for the GNU calculation; for the Wanda calculation enough poison was added to region 18 to make $\Sigma_{a_{th}} = 3.00\ cm^{-1}$.

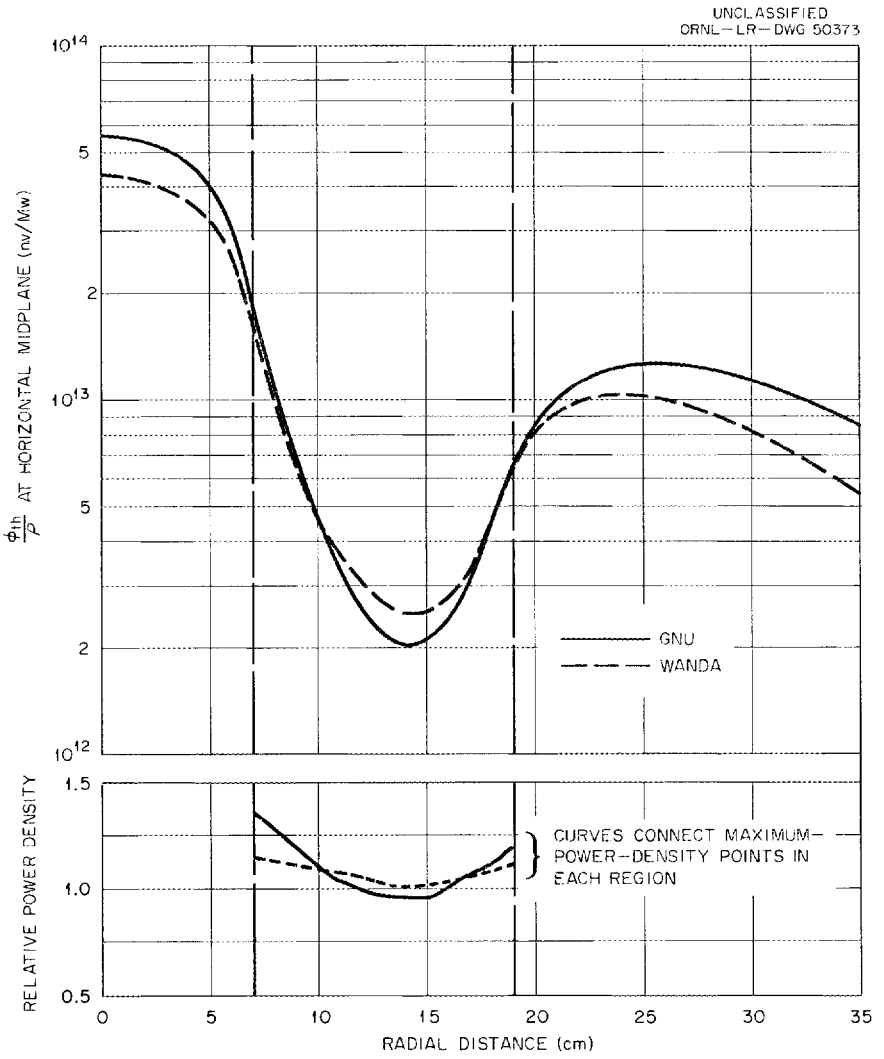

Fig. 73. Comparison of Reactor Characteristics Using Wanda and GNU Reactor Codes for a Core Containing No Controls.

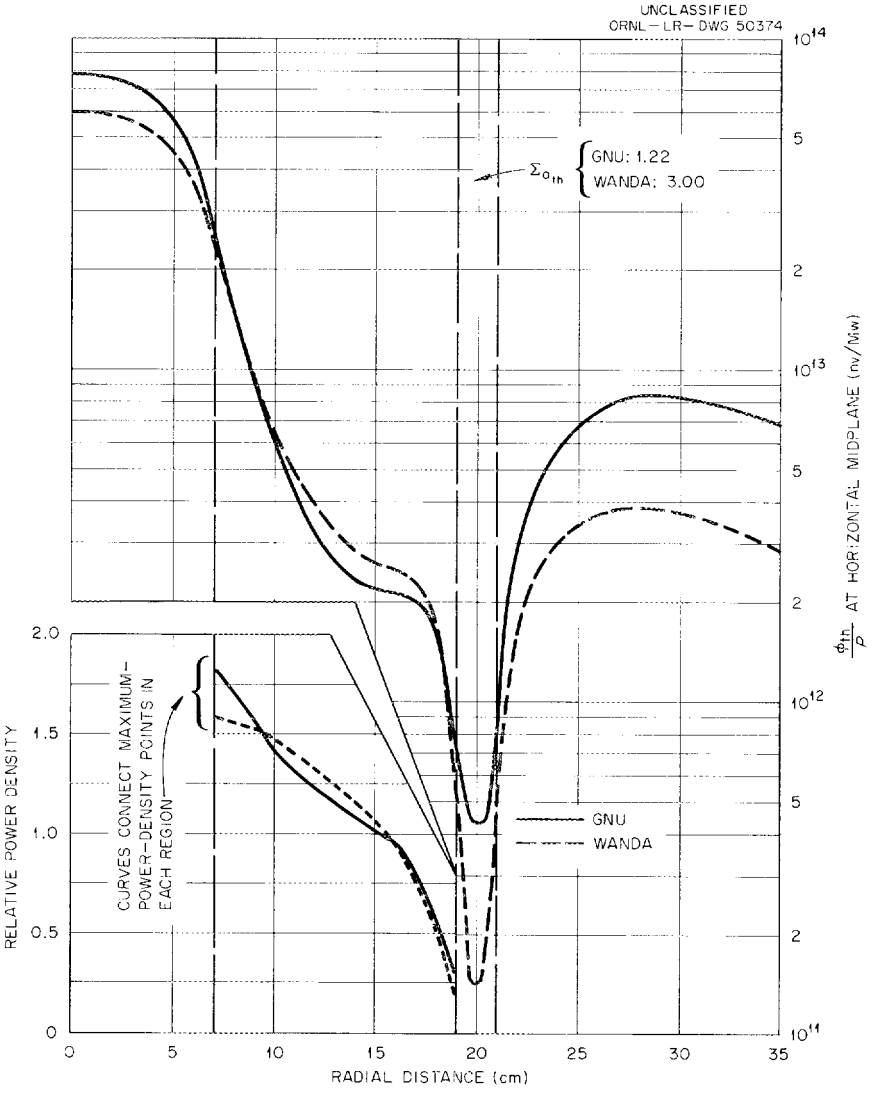

Fig. 74. Comparison of Reactor Characteristics Using Wanda and GNU Reactor Codes for a Core Containing an Annular Control Region.

REFERENCES

1. J. A. Lane et al., High Flux Isotope Reactor Preliminary Design Study, "Bibliography on Flux-Trap Reactors," ORNL-CF-59-2-65, pp 47-48.

2. R. D. Cheverton et al., High Flux Research Reactor (ORSORT study), ORNL-CF-56-8-206 (August 1956).

3. R. D. Cheverton, Further Calculations of a High Flux Research Reactor, ORNL, to be published.

4. L. E. Link et al., The Mighty Mouse Research Reactor, ANL-5688 (March 1957).

5. C. F. Leyse et al., High Flux Reactors for University Research, Internuc-22 (March 1958).

6. S. M. Feinberg et al., An Intermediate Reactor for Obtaining High Intensity Neutron Fluxes, Geneva Conference Paper 2142 (1958).

7. T. B. Fowler, Maximum Thermal Flux per Mw in Three-Region Homogeneous Reactors, ORNL CF-58-3-76.

8. H. C. Claiborne, Californium Production in the High Flux Isotope Reactor, ORNL CF-59-8-125.

9. H. C. Claiborne, Effect of Different Sets of Cross Sections on Cf^{252} Production in the HFIR, ORNL CF-59-10-19.

10. H. C. Claiborne, Effect of Non-Thermal Capture of Californium Production in the HFIR, ORNL CF-59-12-16.

11. W. K. Ergen, Transplutonium Elements, ORNL CF-59-11-109.

12. See pages 6 and 7 of Reference 1 (curves on pages 6 and 7 ascribed to A. Chetham-Strode.)

13. D. N. Dunning et al., "Boron Containing Control Rods," Nuclear Science and Engineering, Vol. 4, No. 3, Sept. 1958.

14. W. K. Barney et al., "The Use of Boron Carbide for Reactor Control," Nuclear Science and Engineering, Vol. 4, No. 3, Sept. 1958.

15. J. C. Griess, personal communication, ORNL, Feb. 1960.

16. J. L. English et al., A Series of Reports on Static and Dynamic Isothermal Aluminum Corrosion Tests, ORNL CF-59-7-72, 59-9-13, 59-10-17, 59-11-15, 59-12-50. 59-12-89, 60-2-15, 60-2-24, 60-2-52.

17. J. C. Griess et al., Effect of Heat Flux on the Corrosion of Aluminum by Water, Part I. Experimental Equipment and Preliminary Test Results, ORNL-2939.

18. C. W. Nestor, Multigroup Neutron Cross Sections, ORNL CF-60-3-35.

19. Personal Communication Between C. W. Nestor (ORNL) and M. L. Tobias (ORNL), March 1960.

20. J. C. Nance, Calibration of the ASTR, ANP Doc. No. NARF-57-48T, FZK-9-090, Nov. 1957.

21. Personal Communication, P. R. Kasten (ORNL), March 1959.

22. H. L. McMurry, Perturbation Theory and Application, 1. Theoretical, IDO-16252.

23. K. Donelion and J. Menke, MonP-379.

24. H. H. Clayton, Pile Instability due to Poison, TPI-41.

25. R. S. Stone, private communication, ORNL, 1959.

26. W. R. Gambill, Recommended Correlations for Thermal Design for HFIR Core Composed of Plate-Type Elements Without Spacers, memo to J. R. McWherter, ORNL, March 1, 1960.

27. J. C. Griess, personal communication, May 1960.

28. N. Hilvety, Preliminary Hot Spot Analysis of the HFIR, ORNL CF-60-3-12.

29. H. A. McLain, Status Report of the Soluble Poison Shim Control for the HFIR, ORNL CF-59-12-24.

30. G. G. Bilodeau et al., PDQ - An IBM-704 Code to Solve the Two-Dimensional Few-Group Neutron-Diffusion Equations, WAPD-TM-70, Aug. 1957.

31. C. L. Davis, GNU-II - A Multigroup, One-Dimensional Diffusion Program, CMR-101, 1957.

32. W. E. Kinney, ORNL, Unpublished ORACLE Program.

33. B. G. Carlson, The Sn Method and the SNG Code, LAMS-2201, 1959.

34. O. J. Marlowe et al., Wanda - A One-Dimensional Few-Group Diffusion Equation Code for the IBM-704, WAPD-TM-28, Nov. 1956.

35. C. J. Marlowe et al., Edna I: IBM-704 Code, report unpublished, Westinghouse Bettis Plant, May 1958.

36. C. J. Marlowe, P. A. Ombrellaro, Candle - A One-Dimensional Few-Group Depletion Code for the IBM-704, WAPD-TM-53 and Addendum.

37. M. L. Bott et al., Reflector Savings Due to the MTR Water Blanket, IDO-16075 (1953).

38. J. H. Alexander and N. D. Given, A Machine Multigroup Calculation, ORNL-1925.

39. C. D. Petrie et al., "Calculation of Thermal Group Constants for Mixtures Containing Hydrogen," Nuclear Science and Engineering, Vol. 2, No. 6, Nov. 1957.

40. M. L. Tobias, An ORACLE Code for the Calculation of Fermi Ages by Numerical Integration, ORNL CF-56-4-53.

41. H. L. McMurry, The Age in Beryllium-Water Mixtures, IDO-16067.

42. H. C. Claiborne, Effects of Fast Neutron Reactions in the Beryllium Reflector of the HFIR, ORNL CF-60-3-10.

43. H. C. Claiborne, A Comparison of Transport Theory and Diffusion Theory Calculations for the High Flux Isotope Reactor, ORNL CF-59-10-100.

44. A. D. Callihan, D. W. Magnuson, et al., ORNL, tests in progress.

ORNL-3006
UC-80 - Reactors-General
TID-4500 (15th ed.)

INTERNAL DISTRIBUTION

1. R. J. Beaver
2. D. S. Billington
3. F. T. Binford
4. E. P. Blizard
5. A. L. Boch
6. E. G. Bohlmann
7. E. S. Bomar
8. C. J. Borkowski
9. R. B. Briggs
10. R. D. Bundy
11. C. A. Burchsted
12. T. J. Burnett
13. C. D. Cagle
14. A. D. Callihan
15. W. R. Casto
16. C. E. Center
17. T. G. Chapman
18. R. A. Charpie
19. A. Chetham-Strode
20-24. R. D. Cheverton
25. H. C. Claiborne
26. F. W. Cooke
27-32. T. E. Cole
33. C. W. Collins
34. A. L. Colomb
35. J. A. Cox
36. J. H. Crawford, Jr.
37. F. L. Culler
38. J. E. Cunningham
39. J. W. T. Dabbs
40. E. P. Epler
41. W. K. Ergen
42. D. E. Ferguson
43. J. L. Fowler
44. A. P. Fraas
45. J. H. Frye
46. C. H. Gabbard
47. W. R. Gall
48. W. R. Gambill
49. E. H. Gift
50. J. P. Gill
51. J. H. Gillette
52. J. C. Griess
53. E. Guth
54. L. A. Haack
55. J. A. Harvey
56. N. Hilvety
57. H. W. Hoffman
58. L. B. Holland
59. D. K. Holmes
60. W. H. Jordan
61. P. R. Kasten
62. W. E. Kinney
63. W. C. Koehler
64. J. A. Lane
65. H. A. Levy
66. R. Livingston
67. M. I. Lundin
68. R. N. Lyon
69. H. G. MacPherson
70. R. E. Maerker
71. F. C. Maienschein
72. D. W. Magnuson
73. W. D. Manly
74. E. R. Mann
75. H. A. McLain
76. J. R. McWherter
77. E. C. Miller
78. K. Z. Morgan
79. W. L. Morgan
80. R. L. Moore
81. E. J. Murphy
82. L. C. Oakes
83. P. Patriarca
84. S. K. Penny
85. S. W. Peterson
86. M. E. Ramsey
87. W. D. Reel
88. P. M. Reyling
89. L. D. Roberts
90. M. W. Rosenthal
91. A. F. Rupp
92. H. C. Savage
93. R. E. Schappel
94. H. W. Schmitt
95. H. E. Seagren
96. M. J. Skinner
97. A. H. Snell
98. R. S. Stone
99. R. W. Stoughton
100. J. A. Swartout
101. A. Taboada
102. J. W. Tackett
103. E. H. Taylor
104. M. Tobias
105. D. B. Trauger
106. D. R. Vondy
107. D. W. Vroom
108. A. M. Weinberg
109. J. F. Wett

110. J. C. Wilson
111-113. C. E. Winters
114. E. O. Wollan
115-116. REED Library
117-118. ORNL-Y-12 Technical Library
119-120. Central Research Library
121-146. Laboratory Records Department
147. Laboratory Records, ORNL R.C.

EXTERNAL DISTRIBUTION

148. Division of Research and Development, AEC, ORO
149. National Bureau of Standards, Reactor Division (C. O. Muehlhouse)
150-151. Argonne National Laboratory (1 copy each to P. R. Fields and C. N. Kelber)
152-154. Lawrence Radiation Laboratory, Berkeley (1 copy each to S. Fried, A. Ghiorso, and G. T. Seaborg)
155. Lawrence Radiation Laboratory, Livermore (R. W. Hoff)
156-158. Los Alamos Scientific Laboratory (1 copy each to C. I. Brown, A. W. Charmatz, and R. A. Penneman)
159-160. Brookhaven National Laboratory (1 copy each to H. Kouts and P. Michael)
161. Phillips Petroleum Company, Atomic Energy Division, Idaho Falls (D. R. deBoisblanc)
162-745. Given distribution as shown in TID-4500 (15th ed.) under Reactors-General category (75 copies - OTS)